University of Southampton
Faculty of Social, Human and Mathematical Sciences
Mathematical Sciences

Time-domain metric reconstruction for self-force applications

by
Paco Giudice

A thesis presented for the degree of
Doctor of Philosophy

January 2018

UNIVERSITY OF SOUTHAMPTON

ABSTRACT

FACULTY OF SOCIAL, HUMAN AND MATHEMATICAL SCIENCES

Mathematical Sciences

Doctor of Philosophy

TIME-DOMAIN METRIC RECONSTRUCTION FOR SELF-FORCE APPLICATIONS

by Paco Giudice

We present a new method for calculation of the gravitational self-force (GSF) in Kerr geometry, based on a time-domain reconstruction of the metric perturbation from curvature scalars.

In our new approach, which relies on foundation work laid out by Pound *et al.* in [Phys. Rev. D **89**, 024009 (2014)], the GSF is computed directly from a scalar-like self-potential that satisfies the time-domain Teukolsky equation on the Kerr background. The metric perturbation from which the GSF is derived has a gauge discontinuity on a closed sphere $r = r_p(t)$, where $r_p(t)$ is the Boyer-Lindquist (possibly time-dependent) radial location of the particle. The crucial step in our method involves the formulation of suitable junction conditions for the metric perturbation at $r_p(t)$, which we do here for generic orbits in Kerr.

The new approach is computationally less intensive than existing time-domain methods, which rely on a direct integration of the linearised Einstein's equations and are impaired by mode instabilities. At the same time, it retains the utility and flexibility of a time-domain treatment, allowing calculations for any type of orbit (including highly eccentric or unbound ones) and the possibility of self-consistently evolving the orbit under the effect of the GSF.

For a first applications of our method, we consider circular geodesic orbits in Schwarzschild geometry, and then circular equatorial geodesic orbits in Kerr. For these cases we present a full numerical implementation, comparing results with those obtained using established frequency-domain methods, and also with analytical solutions where available. We finally lay out a roadmap for further applications of the method.

Contents

List of Figures

List of Tables

Declaration of authorship

I, Paco Giudice, declare that the thesis entitled:

Time-domain metric reconstruction for self-force applications

and the work presented in the thesis are both my own, and have been generated by me as the result of my own original research. I confirm that:

- This work was done wholly or mainly while in candidature for a research degree at this University;
- Where any part of this thesis has previously been submitted for a degree or any other qualification at this University or any other institution, this has been clearly stated;
- Where I have consulted the published work of others, this is always clearly attributed;
- Where I have quoted from the work of others, the source is always given. With the exception of such quotations, this thesis is entirely my own work;
- I have acknowledged all main sources of help;
- Where the thesis is based on work done by myself jointly with others, I have made clear exactly what was done by others and what I have contributed myself;
- Parts of this work have been published as:
  1. Leor Barack and Paco Giudice. Time-domain metric reconstruction for self-force applications. *Phys. Rev.*, D95(10):104033, 2017.

Signed:  Date: May 8, 2018

Acknowledgements

First, I would like to thank my supervisor, Prof. Leor Barack, for the opportunity to work with him and for his constant patience and guidance during this PhD project.

I would like to thank my examiners, Prof. Bernard Whiting and Prof. Nils Andersson, for taking the time to read through this thesis and all the useful comments.

I am grateful to my fellow self-force colleagues, Marta Colleoni, Cesar Antonio Merlin Gonzalez, Adam Pound, Maarten van De Meent, Abhay G. Shah and Charalampos Markakis, for the scientific and social support provided throughout this project.

I am thankful to my dear friend Leo for proof-reading this manuscript and Louiza and Dermot for hosting me before my Viva. They, together with the long list of people I met in the past 3 years, made my stay in Southampton all the more worthwhile.

As this thesis concludes my physics journey, I send my most sincere thanks to those physicists and friends who sticked with me thought the struggles of academia, in order of appearance: Tiziano Fulceri, Marco Piva, Giovanni Rabuffo, Andrea D'Amico, Markus Dierigl, Stanislav Schmidt.

List of acronyms

GW	Gravitational Waves
BH	Black Hole
GR	General Relativity
EFE	Einstein Field Equation
EMRI	Extreme Mass-Ratio Inspiral
(G)SF	(Gravitational) Self-Force
ISCO	Innermost Stable Circular Orbit
LIGO	Laser Interferometer Gravitational-Wave Observatory
LISA	Laser Interferometer Space Antenna
NR	Numerical-Relativistic
MST	Mino-Sasaki-Tanaka
FD	Frequency Domain
TD	Time Domain
ODE	Ordinary Differential Equation
IRG	Ingoing Radiation Gauges
ORG	Outgoing Radiation Gauges
CCK	Chrzanowski-Cohen-Kegeles
DW	Detweiler-Whiting

Chapter 1

Introduction

On September 14, 2015 the Laser Interferometer Gravitational-Wave Observatory (LIGO) [1] detected for the first time a Gravitational-Wave (GW) signal. The observed signal, designated GW150914, was consistent with the prediction of General Relativity (GR) for an inspiral and merger of a binary black-hole system (with initial masses $\sim 36M_\odot$ and $\sim 29M_\odot$) into a single black hole of mass $\sim 62M_\odot$, releasing $\sim 3M_\odot c^2$ in gravitational-radiation energy. This remarkable discovery represented the first direct detection of GWs, as well as the first direct observation of a black hole in nature, as well as a first direct observation of a merging pair of black holes.

More detections followed, including binary black-hole mergers GW151226 [2] and GW170104 [3], with final black-hole masses of $\sim 20.8M_\odot$ and $\sim 48.7M_\odot$, respectively. Altogether, LIGO has seen 6 black-hole mergers so far, with many more expected during the planned third scientific run (scheduled to begin in Autumn 2018). Then there was GW170817 [4]: the merger of two neutron stars of masses between $0.86 - 2.26M_\odot$, for which an electromagnetic counterpart has been identified. In recognising the importance of these events, The Nobel Prize in Physics 2017 was awarded to Rainer Weiss, Barry C. Barish and Kip S. Thorne, key contributors to the development of laser-interferometric GW detectors. To maximise science return of future observations it is essential to have accurate models of potential sources [5, 6, 7]. This work is concerned with the modelling of a particular type of binary source of GWs.

Specifically, we focus on the extreme mass-ratio regime. This is an astrophysically

relevant case of binary system and a key source for the European Space Agency's mission LISA (Laser Interferometer Space Antenna [8]). The detector will consist of three spacecraft, arranged in an equilateral triangle with sides $2.5 \cdot 10^6$km long, flying along an Earth-like heliocentric orbit trailing the Earth by 20 degrees, and with the orbital planes of the three spacecraft inclined relative to the ecliptic by about 0.33 degrees. The mean linear distance between the formation and the Earth will be 50 million kilometres. The detector should be able to detect GW signals (in the milliHertz band) from extreme-mass-ratio inspirals (EMRIs), a stellar-mass black hole or a neutron star slowly spiralling towards a massive black hole of mass $10^5 M_\odot - 10^7 M_\odot$. During the inspiral, the compact object typically emits $O(10^5)$ cycles of GWs in the LISA band, thus providing a detailed map of the strong-field region around the massive black hole. EMRIs are therefore excellent probes of fundamental aspects of GR and they can serve as extremely precise probes for strong-field gravity [9, 10]. The time-line for LISA mission is as follows: the project was originally proposed in 2008; LISA Pathfinder was launched in 2015 to test the necessary technology; the Phase-0 ground study has been performed and concluded in May 2017; the input for the industrial assessment Phase-A is planned for 2018; the expected launch is for 2034. The mission is planned for 4 years of duration.

The signals of typical EMRIs will be sufficiently weak to be buried in LISA's instrumental noise, extractable only using phase-coherent matched filtering [11]. Thus, accurate theoretical templates of EMRI waveforms will be needed to facilitate the very detection of EMRI signals, let alone enable their analysis of their physical and astrophysical properties. The scientific value of the observations will rely on the ability to compute accurate and faithful theoretical templates of the inspiral waveforms. It is therefore a necessity that a solid theoretical framework is set before the LISA launch.

Although a theoretical foundation of the extreme mass-ratio regime is in place, practical schemes to compute EMRI waveforms are still in development. This thesis introduces a new method to compute EMRI orbits and waveforms for use in LISA science. As we shall see, the new approach offers important advantages over existing methods.

1.1 The binary black-hole problem in GR

The concept of black holes has seen an interesting evolution over the past century, from a pure mathematical curiosity, through entities of potential physical reality, to central

players in contemporary high-energy astrophysics. One of the celebrated properties of astrophysical Black Holes (BHs), as described in GR, is their remarkable simplicity, owing itself to the no-hair theorems. Quoting from Chandrasekhar [12]: "*The black holes of nature are the most perfect macroscopic objects there are in the universe: the only elements in their construction are concepts of space and time.*"

However, put two such simple BHs in orbit around each other, and the ensuing dynamics becomes extremely complicated, due to the nonlinear nature of Einstein's gravity. Even though the binary BH problem, which is purely vacuum, may be said to constitute the simplest two-body problem in GR, still the description of the radiative inspiral and eventual merger remains a difficult theoretical problem, in general.

In Newtonian theory, a point-particle is usually represented as a delta-function, consistent with the linear equation of motion of the theory. In GR, this representation becomes inconsistent because of the non-linearity of Einstein Field Equation (EFE).

A direct approach to solve the EFE is to implement a full Numerical-Relativistic (NR) treatment. NR methods made an impressive advance in the past decade [13, 14, 15, 16] and they are now used to simulate the non-linear evolution of binary systems, at least for the final stages of a merger. When the separation between the two bodies is large or in case of a small mass ratio, the NR methods are less efficient [17] and other methodologies must be employed. For large separation between the two bodies, the post-Newtonian methods are best suited for solving the binary evolution. In this framework, the relativistic equation of motion is solved order by order in the separation of the two bodies (or in the velocities), introducing GR corrections for radiation reaction, internal structure, etc. The post-Newtonian formalism was the first approach to dynamics in GR [18] and it is today a thriving field or research [19, 20].

However, when the separation between the two bodies is of the order of their radii, the post-Newtonian approximation breaks down and a different strategy must be employed. An approximation scheme becomes possible when the mass ratio is very large (the "extreme mass ratio" regime). Black hole perturbation theory is a well suited framework to tackle the binary problem in this configuration. The system can be described as a particle of mass μ (the light black hole) moving around a black hole of mass $M \gg \mu$ with a background metric described by Schwarzschild or Kerr solutions. At the zeroth order in the mass ratio μ/M, the particle will follow a geodesic of the background metric.

At higher orders in the mass ratio, the particle motion will deviate from a background geodesic. At first-order in the mass ratio, the linear perturbations of the metric caused by the particle will back react as a gravitational self-force (SF) to the particle itself. A systematic expansion in the mass ratio can account, in principle, for all corrections coming from the finite mass of the small object and its internal structure.

A rigorously established formulation of self-forced motion through second gravitational SF order is now available, for general vacuum curved spacetimes (at least for non-spinning particles) [21, 22, 23, 24, 25]. Practical implementation of such formulation are still in development. This thesis focus on the first-order SF.

1.2 First-order gravitational self-force: an overview

The theory of gravitational SF in curved spacetime has a solid foundation. Recent foundational work on the SF problem [26, 27] has been inspired by classical work on the analogous electromagnetic SF problem in flat spacetime (Dirac, 1938 [28]) and curved spacetime (DeWitt and Brehme, 1960 [29]). The latter laid the mathematical foundation (i.e. covariant bi-tensors in curved spacetime) needed for the study of the gravitational problem. The gravitational SF problem has its first development with the independent derivations carried out by Quinn and Wald [26] and Mino, Sasaki and Tanaka (MST) [27]. The first group derived the SF via comparison between the singular self-field of the point particle and the one of a particle in a suitably constructed tangent flat space. The second group derived the same result using two different methods. In the first method they used local energy-momentum conservation argument, following the structure of DeWitt and Brehme's work. Both the Quinn and Wald derivation and the first MST derivation assumes the notion of a point particle and are therefore not entirely rigorous within a GR framework.

MST [27] have also for the first time derived the equation of motion using the method of matched asymptotic expansions, without assuming the notion of a point particle. The idea of matched asymptotic expansions builds upon the existence of two disparate length-scales of the system, $\mu \ll M$. The system can then be studied looking at two different regimes, the first where $r \ll M$ (where r is the distance from the small body) also referred to as "near zone" and the second where $r \gg \mu$ also referred to as "far zone". In the near zone regime, the metric is dominated by the field of the small body with

some tidal correction coming from the background metric. In the far-zone regime the small object will have the role of a "particle" and will weakly perturb the background metric. In their work MST showed that the expression for the gravitational SF is derived constraining the motion of the particle by matching the two approximations in a "buffer zone", $\mu \ll r \ll M$, where they both apply. The resulting equation of motion was later named as the MiSaTaQuWa formula, after the names of the five contributing authors. The formula is discussed and given explicitly in Chapter 2.

A more recent derivation by Gralla and Wald [21] relaxed the assumption of a Schwarzschild black hole "particle", so that the small body can be taken to be any sufficiently small black hole or a blob of ordinary matter. This derivation defines a one-parameter family of metrics and recovers the two length-scales via a suitable limiting procedure. Additionally, their work shows that in the far-zone limit the particle's energy-momentum is represented by the usual δ-function distribution, and the limit $\mu \to 0$ describes a particle moving along a geodesic of the background metric.

An alternative interpretation of the gravitational SF problem was introduced by Detweiler and Whiting [30]. They proposed a new decomposition of the full metric into regular (R-field) and singular (S-field) parts, and showed that the MiSaTaQuWa gravitational SF can also be expressed as the back-reaction force from the R-field, which is a smooth vacuum perturbation. This implies that the motion of the particle can now be seen as the geodesic motion on a certain smooth effective metric.

When dealing with the practical task of modelling the motion of a particle around a BH, one has to invoke methods that recast the formal equation of motion into practical regularisation schemes. In the case of orbits around a Kerr black hole the mode-sum regularisation [31] and the puncture method [32, 33] are two of the leading schemes. The mode-sum regularisation consists in decomposing the metric perturbation, needed for the MiSaTaQuWa formula, into modes and subtracting from each some analytical regularisation parameters. The latter are calculated from the singular form of the perturbation near the particle [34]. The procedure regularises each separate mode so that the sum of all modes converges to the desired regular value. High-order regularisation parameters are computed in [35, 36]. This method has been implemented successfully for the gravitational SF in Schwarzschild [37, 38] and more recently in Kerr [39, 40, 41]. The puncture method, on the other hand, relies on separating the full metric perturbation into an auxiliary *puncture* field and a *residual* field. The field equations are then

re-written for the residual field with an effective (non-singular) source. The method was implemented successfully for the scalar SF in Schwarzschild [42] and Kerr [32, 33], and in Schwarzschild for the gravitational SF [43]. For a review of both methods we refer to [44, 45].

There now exist a variety of computational strategies and working codes that implement the regularisation schemes numerically and calculate the Gravitational Self Force (GSF) for orbits in Schwarzschild or Kerr geometries (see, e.g., [41, 39] and references therein). Actual calculations have so far been restricted to 1-GSF order, but second-order results are expected soon [46, 47, 48, 49]. All GSF calculations require information about the local metric perturbation near the particle. The various strategies differ on the precise type of information required and on how it is obtained in practice. More concretely, schemes may be classified according to the regularization method (as described above: mode sum vs. puncture), the version of field equations that are being solved (e.g., linearised Einstein's equation vs. Teukolsky's equation), or, relatedly, the gauge in which the perturbation is computed. They can also be categorized according to whether the perturbation is solved for in the frequency domain (FD) [50], based on the expansion of the field equation in frequency modes, or in the time domain (TD) [51, 52], where the field equations are solved explicitly in time.

The FD decomposition is most suitable for periodic motion. One solves a single (or a coupled set of) ordinary differential equations (ODEs) for each frequency-harmonic mode of the perturbation. In TD methods one instead directly solves the partial differential equations (PDEs) that govern the time evolution of the perturbation, or of its individual multipole or azimuthal modes.

A choice of gauge will determine the version of field equations needed to be solved. The common choice in the past has been the Lorenz gauge, as the SF derivation was formulated in this particular gauge. This choice has some advantages, for instance the metric near the particle takes an isotropic form and the field equations take an hyperbolic form, admitting a well posed initial-value problem. Alternatively, in the Schwarzschild case, the Regge-Wheeler gauge [53] can be chosen to derive the metric perturbations [54, 55, 56] . But it is not clear how this may be extended to Kerr.

Recently, the SF has been formulated in a more general class of gauges [57, 21, 58, 59,

60]. This paves the way to a new approach, based on metric reconstruction from curvature scalars. Instead of tackling the complicated set of metric perturbation equations, one works within the elegant framework of the Newman-Penrose formalism, with the numerical task now reduced to solving the Teukolsky equation for either of the two Weyl scalars Ψ_0 or Ψ_4. Since this equation is fully separable into frequency-harmonic modes, even in the Kerr case, the problem further reduces to solving a set of ODEs in the FD. This approach has been gaining much momentum in the past few years, with the formulation of a metric reconstruction procedure suitable for GSF calculations [61, 59, 34], and with the derivation of a 1-GSF equation of motion based on a reconstructed metric [62]. Our work will also take advantage of this most recent development, proposing a new practical method of calculating GSF from a reconstructed metric.

Before reviewing our method, let us briefly describe the limitations of the existing approaches. A summary is given in Table 1.1.

Lorenz gauge in the frequency domain: This approach (used by Akcay *et al.* [63], Osburn *et al.* [64], [65] in Schwarzschild spacetime) is not directly suitable for evolving the orbit under radiation reaction, as it assumes strictly periodic motion. Secondly, high eccentricity or unbound orbits are problematic as strong contribution arises from high-frequency modes in the Fourier decomposition. Moreover, some near-static modes introduce additional problems arising from the inversion of a near-degenerate matrix during the numerical procedure [65].

Radiation Gauge in the frequency domain: this approach (developed by Shah *et al.*, van de Meent [40]) inherits the first two of the problems mentioned in the above case because of the frequency-domain treatment. Its main weaknesses are that its efficiency degrades quickly with increasing orbital eccentricity (see [41] for a detailed discussion of this point) and that its application to orbits that are not strictly periodic is more subtle. Though this method is free from the problem of near-static modes, the incorporation of gravitational SF back-reaction effects is less direct than in a time-domain treatment.

Lorenz gauge in the time domain: this method (developed by Barack, Sago [51], Dolan *et al.* [52]) avoids some of the problems related with the frequency-domain treatment. Nevertheless, the method has two significant disadvantages. First, it is computationally very expensive: It involves the numerical evolution of a set of 10 coupled PDEs for

Table 1.1: Weaknesses of computational approaches to the gravitational self-force, and advantages of our new method

	Lorenz Gauge	Radiation Gauge	Regge-Wheeler Gauge
FD	(Akcay, Osburn *et al.* [63, 64, 65]) • Hard to evolve orbit • Unsuited for high eccentricity • Problematic near-static modes	(Shah etal ,Van de Meent *et al.* [40]) • Hard to evolve orbit • Unsuited for high eccentricity	(Detweiler, Hopper *et al.* [55, 56]) • Hard to evolve orbit • Unsuited for high eccentricity • no Kerr case
TD	(Barack, Sago, Dolan [51, 52]) • computationally expansive • unstable modes	(Our New Method [67]) • suitable for any orbit • no unstable modes • no problem of near-static modes • suitable for self-consistent evolution of orbits	(Barack, Lousto [54]) • no obvious extension to Kerr

each multipole or azimuthal mode of the perturbation, over sufficiently long time to ensure that spurious radiation from imperfect initial conditions is sufficiently suppressed. Second, numerical evolutions have been shown [66] to be contaminated by certain non-physical Lorenz-gauge modes (which are associated with the low-multipole sector) that grow linearly in time, the elimination of which remains an open problem.

Regge-Wheeler gauge in Schwarzschild: This choice of gauge has been successfully implemented in TD for radial geodesics [54] and in FD for circular and eccentric orbits [55, 56]. The method is currently restricted to Schwarzschild spacetime. No clear extension to Kerr spacetime is currently available.

1.3 This thesis: A new approach for self-force calculations

This work aims to develop a new computational approach to the GSF, which combines the advantages of the Lorenz-gauge/TD and Teukolsky/FD methods, while avoiding some of their deficiencies. We introduce a new method [67], that is a *time-domain implementation of the radiation-gauge approach*. This would give us a way to evolve the orbit of the particle without recourse to a Fourier decomposition. Moreover, the gauge choice reduces the field equation to a single decoupled field equation (Teukolsky

equation). This will avoid the heavy numerics needed to solve the 10 coupled equation in Lorenz gauge.

The foundation of this work lies in the work of Pound *et al.* [62]. The authors have analysed the local form of the metric perturbations near a point particle in the class of completed radiation gauges. As a result, they obtained a rigorous formulation of the SF, complete with a practical mode-sum calculation formula, starting from a reconstructed metric perturbation in a radiation gauge. This method has been applied already in the frequency domain [68, 40, 41]. Here we are going to apply it in the time domain for the first time. Instead of reconstructing the metric perturbation from a sum over frequency-harmonic modes, as is traditional, we obtain it directly from a certain time-dependent Hertz potential, which, in turn, is obtained by numerically solving the Teukolsky equation in the TD. Our approach thus retains the utility and flexibility of a TD treatment, but offers a much more computationally efficient platform compared to the Lorenz-gauge/TD approach: one solves a single scalarlike equation instead of a coupled set of ten, and the problem of unstable modes is altogether avoided.

TD evolution of the Teukolsky equation has long been used in studies of black hole perturbations, notably by G. Khanna and collaborators [69]. Applications include the study of late-time behaviour of vacuum perturbations outside a Kerr black hole [70], investigations into the Cauchy horizon singularity inside black holes [71], and the modelling of gravitational radiation from particle orbits [72]. In these studies, the Teukolsky equation is numerically solved for the Weyl scalar Ψ_0 (or Ψ_4) via time evolution in 2+1 dimensions (2+1D), and the relevant physics (e.g., asymptotic behaviour at null or timelike infinity) is directly read off that curvature scalar. In our approach, a time evolution of the Teukolsky equation is used only as a first step in a procedure for reconstructing the local metric perturbation at the particle. Such a direct TD reconstruction has not been attempted so far, to the best of our knowledge.

Furthermore, in our method we do not solve the Teukolsky equation for the physical Weyl scalar Ψ_0 (or Ψ_4), as in existing codes. Rather, we solve it for a certain Hertz potential Φ that is *not* the Weyl scalar corresponding to the physical perturbation. The field Φ satisfies the TD Teukolsky equation in vacuum (with boundary conditions similar to those of the Weyl scalar), but the source term in that equation differs from that of Ψ_0 (or Ψ_4). A key ingredient of the formulation work to be presented in this work is a

derivation of the point-particle source function for the Hertz potential.[1]

In practice, our method is designed with a 1+1D implementation in mind, that is a numerical evolution (either Cauchy or characteristic) on a 2D grid with one temporal dimension and one spatial dimension. In the case of a Schwarzschild background, the Teukolsky equation naturally separates into decoupled 1+1D evolution equations for each multipole (spin-weighted spherical harmonic) mode of Φ. Not so in the Kerr case, where different multipoles (ℓ modes) remain coupled. Nonetheless, a 1+1D implementation is still a viable route even in the Kerr case, as demonstrated in [73], at least in situations where mode coupling is relatively weak. In a 1+1D treatment, the particle's worldline splits the numerical grid into two disjoint domains. The formulation of a source term for Φ then translates into the prescription of *junction* conditions that the field Φ must satisfy on the interface between the two domains—specifically, the jumps in the value of Φ and a sufficient number of its derivatives across the particle's worldline. The bulk of the formulation work will be devoted to deriving these junction conditions.

To recap, our goal here is to formulate a TD evolution problem for a certain Hertz potential Φ, from which the physical metric perturbation and the GSF can be derived directly by taking derivatives. We will formulate our method for arbitrary particle orbits in Kerr spacetime, and then, as a proof of principle, we shall present a full numerical implementation for the case of circular geodesic orbits in Schwarzschild spacetime, and then for circular equatorial orbits in Kerr. We leave the full numerical implementation of our method in Kerr to future work.

1.4 Layout

The structure of this thesis is as follows. Chapter 2 reviews the SF formalism. The notion of "gravitational force" is introduced, followed by the notion of GSF, and the MiSaTaQuWa formula is provided. Additionally, the interpretation of SF via the Detweiler-Whiting formulation is described. The gauge dependence of SF is also discussed. The basics of the Newman-Penrose null-tetrad formalism are given in the context of black-hole perturbation theory. With the relevant foundation at hand, we describe the metric reconstruction procedure. The reconstruction procedure for vacuum perturbations

[1] In related literature, the Hertz potential is usually denoted by Ψ, with a lowercase ψ denoting the Weyl scalars: ψ_0 and ψ_4. Here, to avoid potential confusion, we use Φ for the Hertz potential; lowercase ϕ and ψ_0/ψ_4 will be reserved for the 1+1D projections of Φ and Ψ_0/Ψ_4, respectively.

developed by Chrzanowski, Cohen and Kegeles is described. Finally, the metric reconstruction for a particle is given and we introduce the derivation of the GSF from such reconstructed metric, as proposed by Pound *et al.* in [62].

In chapter 3, we describe our new time-domain evolution scheme for the Hertz potential. The chapter analyses the procedure by discussing the three necessary components: the field equation, the boundary conditions and the junction conditions at the particle. We provide the field equation for the Hertz field, namely the Teukolsky equation. The boundary conditions at the horizon and at null-infinity are analysed. Finally, we develop a procedure to derive junction conditions at the particle for the Hertz potential.

In chapter 4, the procedure proposed is applied to the specific case of circular orbits in Schwarzschild spacetime. Both field equation and junction conditions are given explicitly. We also provide the analytical solution for static modes of the Hertz potential, to be compared with the numerical results.

In Chapter 5, the methodology of our numerical computation is described in detail. The necessary finite-difference-scheme terms are derived. Our numerical results are then provided. We show comparison with the frequency domain computation as well as for the analytical solutions described in Chapter 4.

Chapter 6 extends the computation to the case of circular orbits in Kerr spacetime and propose an iterative scheme to compute the junction conditions. Similarly to the Schwarzschild case, the analytical solution for static modes for Kerr background is provided.

In chapter 7, the methodology of the numerical computation for the Kerr case is described in detail. The field equation presents couplings between neighbouring modes, thus we introduce the needed finite difference scheme terms necessary for the numerical computation. Finally, the numerical results are provided. Firstly, a vacuum tests for the field evolution is provided. Secondly, we tested the convergence of our proposed iteration scheme as well as the convergence of partial sum over ℓ-mode contributions. Moreover, we show the agreement with the analytical solution for static modes given in chapter 6. To conclude, the numerical results for non-static modes are presented.

In Chapter 8, the content of this work is summarised and the possible applications and extension of our method are discussed.

1.4.1 Notation

Throughout this work we use standard geometrized units, in which $G = 1 = c$. We adopt the metric signature $(-+++)$. Greek letters are used for spacetime indices, and a comma denotes a partial derivative, as in $A_{,\alpha} := \partial A/\partial x^{\alpha}$. Bracketed indices, as in $e^{\alpha}_{(a)}$, run over $1, \ldots, 4$ and identify tetrad legs. Complex conjugation is denoted by an overbar, as in $\bar{m}^{\alpha}$. Parenthetical indices are symmetrized, as in $A_{(\alpha\beta)} = (A_{\alpha\beta} + A_{\beta\alpha})/2$. We will consider a Kerr background with metric $g^{K}_{\alpha\beta}$, mass parameter M and angular-momentum parameter a. This work adopts standard Boyer-Lindquist coordinates (t, r, θ, φ). The sign conventions for the Weyl scalars, the spin coefficients of the Newman-Penrose formalism, and the Hertz potential, are consistent with those of [34] (as summarized in Appendix A therein).

Chapter 2

Review of relevant background: self-force and metric reconstruction

This section reviews the relevant background, while setting up notation and conventions. We define what we mean by SF and provide the MiSaTaQuWa formula. The alternative description of motion in a perturbed spacetime proposed by Detweiler and Whiting is also summarised. Once the foundation work is laid out, we proceed by describing the practical scheme for calculating the GSF from a reconstructed metric perturbation. We start by introducing the Newman-Penrose approach to BH perturbation theory. Then, we present the (TD version of the) reconstruction of the vacuum metric perturbations in vacuum for Kerr spacetime. The case of perturbations sourced by an orbiting point particle is then reviewed. To conclude, we summarise the method by Pound *et al.* [62] for computing the GSF experienced by the particle, using the reconstructed metric as input.

2.1 "Gravitational force" and the self-force

It is commonly stated in introductory material on GR that a particle moves on a geodesic trajectory of the background metric. This statement becomes inaccurate when one takes into account the finite mass and size of the object represented by the particle. The motion beyond the geodesic approximation can be described using the SF approach, in

which back-reaction from the finite mass and size of the object is interpreted in terms of an effective "self-force" that drives the motion away from being purely geodesic from the perspective of a certain fixed background geometry. To describe this physical effect, let us start by introducing the notion of "gravitational force" in the simplest case of a smooth external metric perturbation.

2.1.1 "Gravitational force"

Consider a background metric g and some smooth perturbation h. A particle of mass μ will follow a geodesic trajectory of the perturbed spacetime $g+h$, described, in a given coordinate system x^α, by

$$\frac{d^2x^\alpha}{d\tau'^2} + \Gamma'^{\alpha}_{\mu\nu}\frac{dx^\mu}{d\tau'}\frac{dx^\nu}{d\tau'} = 0, \tag{2.1}$$

where τ' is an affine parameter along the trajectory and $\Gamma'^{\alpha}_{\mu\nu}$ are the connection coefficients associated with the perturbed metric $g+h$. The trajectory, defined on the perturbed metric, can be projected to the background g (with the same coordinate system x^α). If we interpret this new trajectory as a deviation from a geodesic of g we can write an equation for the force experienced by the particle as

$$F^\alpha_{\rm grav} = \mu\left(\frac{d^2x^\alpha}{d\tau^2} + \Gamma^\alpha_{\mu\nu}\frac{dx^\mu}{d\tau}\frac{dx^\nu}{d\tau}\right), \tag{2.2}$$

where τ is an affine parameter in the background metric g, and $\Gamma^\mu_{\alpha\beta}$ are the connection coefficients associated with g. The tensorial indices of all these quantities in the background metric are raised and lowered using $g_{\mu\nu}$. We intend to write an equation for the force in terms of the metric perturbation h. To do so, we write the difference between the connections $\Gamma'^{\alpha}_{\mu\nu}$ and $\Gamma^\alpha_{\mu\nu}$ in terms of linear terms in h only. Explicitly one finds

$$F^\alpha_{\rm grav} = -\frac{1}{2}\mu(g^{\alpha\lambda}+u^\alpha u^\lambda)\left(\nabla_\nu h_{\lambda\mu}+\nabla_\mu h_{\lambda\nu}-\nabla_\lambda h_{\mu\nu}\right)u^\mu u^\nu := \mu\nabla^{\alpha\beta\gamma}h_{\beta\gamma}, \tag{2.3}$$

where $u^\alpha = dx^\alpha/d\tau$ and ∇_α denotes covariant differentiation with respect to the background metric g. The differential operator $\nabla^{\alpha\beta\gamma}$, often called*force operator*, determines the (entirely fictitious) "gravitational force" exerted by an external perturbation h (at the linear order). This is given explicitly by

$$\nabla^{\alpha\beta\gamma} = \frac{1}{2}\left(g^{\alpha\delta}u^\beta - 2g^{\alpha\beta}u^\delta - u^\alpha u^\beta u^\delta\right)u^\gamma\nabla_\delta. \tag{2.4}$$

The metric perturbations are often written in a trace-reversed form, that is

$$\bar{h}_{\alpha\beta} = h_{\alpha\beta} - \frac{1}{2} g_{\alpha\beta} g^{\mu\nu} h_{\mu\nu}. \tag{2.5}$$

In terms of $\bar{h}_{\alpha\beta}$, Eq. (2.3) becomes

$$F^{\alpha}_{\text{grav}} = \mu \bar{\nabla}^{\alpha\beta\gamma} \bar{h}_{\beta\gamma}, \tag{2.6}$$

with

$$\bar{\nabla}^{\alpha\beta\gamma} = \frac{1}{4} \left(2g^{\alpha\delta} u^{\beta} u^{\gamma} - 4g^{\alpha\beta} u^{\gamma} u^{\delta} - 2u^{\alpha} u^{\beta} u^{\gamma} u^{\delta} + u^{\alpha} g^{\beta\gamma} u^{\delta} + g^{\alpha\delta} g^{\beta\gamma} \right) \nabla_{\delta}. \tag{2.7}$$

Different choices of the coordinates in the two spacetimes will in general give different values for the gravitational force. This is a manifestation of the gauge dependence of the gravitational force. In general, the gravitational force as defined above will be pure gauge and have no invariant physical content.

2.1.2 Self-force and MiSaTaQuWa formula

In the case of metric perturbations produced by the particle, the above description falls apart as the field h is singular at the particle location and equation (2.6) cannot be employed. This problem was studied by Quinn and Wald [26] and Mino, Sasaki and Tanaka [27] leading to the so called MiSaTaQuWa formula. The authors originally derived the formula in Lorenz gauge, that is under the condition

$$\nabla^{\beta} \bar{h}_{\alpha\beta} = 0, \tag{2.8}$$

but their formula was later shown to be valid in a broader range of gauges [57].

To start, the physical (retarded) metric perturbation h, at any point x, is decomposed as a direct and tail part, that is

$$\bar{h}_{\alpha\beta} = \bar{h}^{\text{dir}}_{\alpha\beta} + \bar{h}^{\text{tail}}_{\alpha\beta}. \tag{2.9}$$

The direct term represents the perturbation coming from the intersection of the past light-cone of x with the particle trajectory. The tail term accounts for the perturbations

coming from the particle motion *inside* the past light-cone of x. This latter contribution can be viewed as resulting from the scattering of waves off the spacetime curvature. Both $\bar{h}_{\alpha\beta}$ and $\bar{h}^{\rm dir}_{\alpha\beta}$ diverge when evaluated on the particle. However, $\bar{h}^{\rm tail}_{\alpha\beta}$ is continuous and differentiable on the worldline (though it is generally it is not twice differentiable on the worldline, and it is not a vacuum solution of the linearized Einstein equations). The MiSaTaQuWa formula states that the physical gravitational SF on a point x of the particle's trajectory results from the back reaction of the tail field, namely

$$F^{\alpha}_{\rm self}(x) = \mu \bar{\nabla}^{\alpha\beta\gamma} \bar{h}^{\rm tail}_{\beta\gamma}(x). \tag{2.10}$$

2.1.3 Detweiler-Whiting formulation

The decomposition into direct and tail field is not the only route to deriving a useful formula for the SF. Indeed Detweiler and Whiting (DW) [30] proposed a different formulation, decomposing the retarded metric perturbation in the form

$$\bar{h}_{\alpha\beta} = \bar{h}^{\rm S}_{\alpha\beta} + \bar{h}^{\rm R}_{\alpha\beta}. \tag{2.11}$$

Here the R-field $\bar{h}^{\rm R}_{\alpha\beta}$ is a certain smooth, vacuum solution of the perturbation equations. The S-field $\bar{h}^{\rm S}_{\alpha\beta}$ captures the full singular part of the perturbation near the particle. The authors show that the SF can be also computed as

$$F^{\alpha}_{\rm self}(x) = \mu \bar{\nabla}^{\alpha\beta\gamma} \bar{h}^{\rm R}_{\beta\gamma}(x), \tag{2.12}$$

which they showed to be equal to the MiSaTaQuWa force. Hence, The DW formula is a statement of the fact that a suitably identified singular field h^S does not contribute to the SF. The practical prescription for constructing the R and S fields is described in the review [74].

The above gives us a new way to interpret the SF. The particle effectively moves freely along a geodesic of a smooth perturbed spacetime with metric $g_{\alpha\beta} + h^R_{\alpha\beta}$. However, it is important to not mistake the effective metric $g_{\alpha\beta} + h^R_{\alpha\beta}$ with the actual physical metric $g + h$. Note that the R-field itself is a-causal: The value of the R-field at an event x depends not only on events in the the causal past of x but also on events *outside* the light-cone of x [74].

The MiSaTaQuWa and DW formulas represent two equivalent interpretations of the same physical SF. This has been demonstrated in, e.g., Ref. [75] with an explicit calculation of a certain gauge-invariant SF effect using both approaches.

2.1.4 Gauge dependence

The SF is a gauge dependent quantity. The original derivation of the MiSaTaQuWa formula (2.10) was carried out in Lorenz gauge. Further work has extended the notion of SF to a wider range of gauges. The first extension of the SF in a gauge other than Lorenz was carried out by Barack and Ori in [57], where gauges related to Lorenz gauge by a continuous gauge transformation are considered. By studying the transformation of Eq. (2.10) under the gauge transformation $x^\alpha \to x^\alpha - \xi^\alpha$ they derived the change δF^α, explicitly

$$\delta F^\alpha = -\mu(g^{\alpha\lambda} + u^\alpha u^\lambda)(\xi_{\lambda;\mu\nu} + \xi_\varrho R^\varrho{}_{\mu\lambda\nu})u^\mu u^\nu. \tag{2.13}$$

Here ξ^α is continuos and δF^α result to be finite. They concluded that any gauge transformation of this kind will simply shift the centre of mass.

Further work by Gralla and Wald [21, 76] extended to gauges related to Lorenz via transformation that may be discontinuous but bounded. Gralla later [58], and for the first time, reformulated the GSF without a direct reference to the Lorenz gauge, using a certain spatial averaging around the particle and demanding continuity as well as a certain parity condition for the perturbation near the particle. Finally, in [62], the authors extended to a class of gauges beyond the Gralla or Gralla-Wald class as discussed in Sec. 2.6.

It is important to clarify the following, potentially confusing point. The GSF itself can always be nullified with a suitable choice of gauge. In that case, however, the physical information about the SF motion will be encoded in the gauge-transformed metric perturbation [55]. *It is the combination of the GSF and the associated metric perturbation that carries the gauge-invariant physical content.*

2.2 The Newman-Penrose null-tetrad formalism

The goal of this thesis is to develop a new method to compute the metric perturbation $h_{\alpha\beta}$ in order to derive the associated SF via equation (2.12). It is then necessary to

introduce perturbation theory in GR. We choose to make use of the Newman-Penrose (NP) description. This will be used extensively throughout this work. Here we review the method following the discussion in [12].

In [77], Newman and Penrose suggested the introduction of a null basis. Such a choice is motivated by its effectiveness in making explicit the symmetries of black hole solution in general relativity. As it will be shown, the perturbation equations in these spacetimes can be reduced to a simple form, at least for some choice of gauge.

We define a tetrad basis over a spacetime (with a metric $g_{\mu\nu}$) as a basis of contravariant vectors $e^{\mu}_{(a)}$ chosen suitably to the spacetime in consideration (here the index μ runs over the 4 spacetime coordinates and the parenthetical index runs over the 4 basis vectors). The associated covariant vectors are given by:

$$e_{(a)\nu} = g_{\mu\nu} e^{\mu}_{(a)}. \tag{2.14}$$

We normalize $e^{\mu}_{(a)}$ as

$$e_{(a)\mu} e^{\mu}_{(b)} = \eta_{(a)(b)}, \tag{2.15}$$

where $\eta_{(a)(b)}$ may be chosen as convenient. The choice of $\eta_{(a)(b)}$ in this work is of a constant symmetric matrix given in (2.19) below. We also define the *Ricci rotation coefficients* using the tetrad as

$$\gamma_{(a)(b)(c)} = e^{\nu}_{(a)} e_{(b)\nu;\mu} e^{\mu}_{(c)}, \tag{2.16}$$

where the semicolon indicates a covariant derivative with respect to the spacetime metric. Using this definition it is easy to see that for an $\eta_{(a)(b)}$ with constant coefficients the rotation coefficients are antisymmetric in the first pair of indices ($\gamma_{(a)(b)(c)} = -\gamma_{(b)(a)(c)}$). The rotation coefficients feature, for example, in the derivative of a projected component of a tensor A_i with respect to a tetrad component:

$$A_{(a),(b)} = e^{\nu}_{(a)} A_{\mu;\nu} e^{\mu}_{(b)} + \gamma_{(a)(b)(c)} A^{(c)}. \tag{2.17}$$

When working in a Petrov type D spacetime (see Sec. 2.2.1), the NP choice of a tetrad is a tetrad of (complex-valued) null vectors $(l, n, m, \bar{m})$, where (l, m) are real and $\bar{m}$ is the complex conjugate of m. These null vectors are taken to be all mutually orthogonal,

except for

$$l \cdot n = 1, \qquad m \cdot \bar{m} = -1. \tag{2.18}$$

With these choices for the tetrad, $\eta_{(a)(b)}$ takes the form

$$\eta_{(a)(b)} = \begin{bmatrix} 0 & 1 & 0 & 0 \\ 1 & 0 & 0 & 0 \\ 0 & 0 & 0 & -1 \\ 0 & 0 & -1 & 0 \end{bmatrix}. \tag{2.19}$$

The directional derivatives corresponding to the basis vectors will be denoted by the following symbols:

$$\boldsymbol{D} := l^\mu \partial_\mu, \qquad \boldsymbol{\Delta} := n^\mu \partial_\mu, \qquad \delta := m^\mu \partial_\mu, \qquad \delta^* := \bar{m}^\mu \partial_\mu. \tag{2.20}$$

The Ricci rotation coefficients, when choosing the NP tetrad, are called *spin coefficients* and are denoted by

$$\begin{aligned} &\alpha = \frac{1}{2}(\gamma_{214} + \gamma_{344}), \quad \beta = \frac{1}{2}(\gamma_{213} + \gamma_{343}), \quad \gamma = \frac{1}{2}(\gamma_{212} + \gamma_{342}), \quad \varepsilon = \frac{1}{2}(\gamma_{211} + \gamma_{341}), \\ &\pi = \gamma_{241}, \quad \tau = \gamma_{312}, \quad \mu = \gamma_{243}, \quad \varrho = \gamma_{314}, \\ &\nu = \gamma_{242}, \quad \lambda = \gamma_{244}, \quad \sigma = \gamma_{313}, \quad \kappa = \gamma_{311}. \end{aligned} \tag{2.21}$$

We recall that the Weyl tensor $C_{\alpha\beta\gamma\delta}$ is the traceless part of the Riemann tensor, satisfying

$$R_{\alpha\beta\gamma\delta} = C_{\alpha\beta\gamma\delta} - \frac{1}{2}(\eta_{\alpha\gamma}R_{\beta\delta} - \eta_{\beta\gamma}R_{\alpha\delta} - \eta_{\alpha\delta}R_{\beta\gamma} + \eta_{\beta\delta}R_{\alpha\gamma}) + \frac{1}{6}(\eta_{\alpha\gamma}\eta_{\beta\delta} - \eta_{\alpha\delta}\eta_{\beta\gamma})R, \tag{2.22}$$

where R is the Ricci scalar and $R_{\alpha\beta}$ the Ricci tensor. This tensor has ten independent components that can be written using the tetrad basis as five complex scalars (named

Weyl scalars)

$$\begin{aligned}
\Psi_0 &= -C_{1313} = -C_{\alpha\beta\gamma\delta} l^\alpha m^\beta l^\gamma m^\delta, \\
\Psi_1 &= -C_{1213} = -C_{\alpha\beta\gamma\delta} l^\alpha n^\beta l^\gamma m^\delta, \\
\Psi_2 &= -C_{1342} = -C_{\alpha\beta\gamma\delta} l^\alpha m^\beta \bar{m}^\gamma n^\delta, \\
\Psi_3 &= -C_{1242} = -C_{\alpha\beta\gamma\delta} l^\alpha n^\beta \bar{m}^\gamma n^\delta, \\
\Psi_4 &= -C_{2424} = -C_{\alpha\beta\gamma\delta} n^\alpha \bar{m}^\beta n^\gamma \bar{m}^\delta.
\end{aligned} \tag{2.23}$$

It will be shown in the following subsection that, in the (unperturbed) Kerr background, all Weyl scalars but Ψ_2 vanish. In the framework of a linear perturbation analysis, the symbols Ψ_0, Ψ_1, $\delta\Psi_2$, Ψ_3, Ψ_4 are thus used to represent first-order perturbations of the corresponding fields (with $\delta\Psi_2 = \Psi_2 - \Psi_{2(background)}$). One can show that Ψ_0 and Ψ_4 are invariant under gauge transformations (namely, under infinitesimal rotations of the null basis and infinitesimal coordinate transformations). The scalars Ψ_1 and Ψ_3 are not gauge invariant, and may be nullified by a suitable rotation of the null frame. Moreover, $\delta\Psi_2$ (which represent perturbations of the "Coulomb-like", non-radiative, part of the fields) can also be nullified by a suitable infinitesimal coordinate transformation (additionally, the $Im(\delta\Psi_2)$ is a gauge invariant quantity). It is therefore only the scalars (Ψ_0, Ψ_4) which carry gauge-invariant information about the radiative part of the fields.

2.2.1 Tetrad transformations and type D spacetimes

After we defined our tetrad frame on the spacetime, for a reason that will become clear shortly, let us consider three types of tetrad rotations (we follow the discussion in [12])

1) rotations that leave l_α unchanged;

2) rotations that leave n_α unchanged;

3) rotations of m_α into $m_\alpha e^{i\theta}$ or $\bar{m}_\alpha$ into $\bar{m}_\alpha e^{-i\theta}$,

where θ is a real function on the manifold. For (1) and (2) the other basis component will mix, while 3 leaves l and n unchanged. These transformations imply certain transformation properties for the spin coefficients and the Weyl scalars. These transformation properties determine the so-called *Petrov classification* of the spacetime, as follows.

Let's take, for instance, $\Psi_4 \neq 0$. In the case of $\Psi_4 = 0$ this scalar can be made non-null by a transformation of type 1 (except for the case of flat spacetime where all Weyl scalars vanish). Now applying a transformation of type 2 we find the following [12]

$$\begin{aligned}
\Psi_0 &\to \Psi_0 + 4b\Psi_1 + 6b^2\Psi_2 + 4b^3\Psi_3 + b^4\Psi_4, \\
\Psi_1 &\to \Psi_1 + 3b\Psi_2 + 3b^2\Psi_3 + b^3\Psi_4, \\
\Psi_2 &\to \Psi_2 + 2b\Psi_3 + b^2\Psi_4, \\
\Psi_3 &\to \Psi_3 + b\Psi_4, \\
\Psi_4 &\to \Psi_4,
\end{aligned} \tag{2.24}$$

where b is the rotation parameter. The Petrov classification is based on identifying the number of roots of the equation that nullifies Ψ_0. In this work, we will only be interested in the group called type D that has two distinct roots for the equation.

It can be shown that all the scalars but Ψ_2 can be nullified in type D spacetimes [12]. As assumed, we have two roots of the transformation equation for Ψ_0 so we can write

$$\Psi_0 = \Psi_4(b - b_1)^2(b - b_2)^2, \tag{2.25}$$

where (b_1, b_2) are the two (complex) roots. Then, we substitute this form into the other scalar transformations in (2.24) and normalise, at each stage, in order to have the same coefficient Ψ_4 for the highest power of b. We can make (Ψ_1, Ψ_0) vanish taking $b = b_1$. Moreover, we take an additional type 1 transformation with rotational coefficient d. The latter will leave the first two scalars unchanged and for a rotation coefficient $d = (b_2 - b_1)^{-1}$ the new scalars (Ψ_3, Ψ_4) will vanish. The last standing scalar Ψ_2 is invariant under type 3 transformations, so it is the only non vanishing scalar for these type of spaces.

The black-hole solutions (Schwarzschild, Reissner-Nordstrom and Kerr) of general relativity happen to be type D spacetimes under Petrov classification. This will be very useful when looking at perturbations around Schwarzschild or Kerr spacetimes.

2.3 Vacuum Kerr perturbations in the Newman–Penrose formalism

The Kerr metric, in Boyer-Lindquist coordinates, is given by

$$ds^2 = -\frac{\Delta}{\Sigma}(dt - a\sin^2\theta d\varphi)^2 + \frac{\Sigma}{\Delta}dr^2 + \frac{\sin^2\theta}{\Sigma}((r^2+a^2)d\varphi - adt)^2 + \Sigma d\theta^2, \tag{2.26}$$

where a is the spin parameter, $\Delta := r^2 - 2Mr + a^2$ and $\Sigma := r^2 + a^2\cos^2\theta$. There exists a class of null geodesics in Kerr described by

$$\frac{dt}{d\tau} = \frac{r^2+a^2}{\Delta}C, \qquad \frac{dr}{d\tau} = \pm C, \qquad \frac{d\varphi}{d\tau} = \frac{a}{\Delta}C, \qquad \frac{d\theta}{d\tau} = 0, \tag{2.27}$$

where C is a constant. This suggests a choice for our tetrad basis. The Kinnersley's null tetrad is accordingly defined, in Boyer-Lindquist coordinates, by

$$e^\alpha_{\mathbf{1}} =: l^\alpha = \frac{1}{\Delta}\left(r^2+a^2, \Delta, 0, a\right), \tag{2.28a}$$

$$e^\alpha_{\mathbf{2}} =: n^\alpha = \frac{1}{2\Sigma}\left(r^2+a^2, -\Delta, 0, a\right), \tag{2.28b}$$

$$e^\alpha_{\mathbf{3}} =: m^\alpha = -\frac{\bar{\varrho}}{\sqrt{2}}\left(ia\sin\theta, 0, 1, \frac{i}{\sin\theta}\right), \tag{2.28c}$$

$$e^\alpha_{\mathbf{4}} =: \bar{m}^\alpha = \frac{\varrho}{\sqrt{2}}\left(ia\sin\theta, 0, -1, \frac{i}{\sin\theta}\right), \tag{2.28d}$$

where

$$\varrho \;:=\; -1/(r - ia\cos\theta). \tag{2.29}$$

The legs $e^\alpha_{\mathbf{n}}$ are all null and mutually orthogonal, except for the products given in equations 2.18.

As mentioned in Sec. 2.2.1, on the Kerr geometry all Weyl scalars vanish, except Ψ_2. This is explicitly given by

$$\Psi_2 = -\frac{M}{(r - ia\cos\theta)^3}. \tag{2.30}$$

The only non-vanishing spin coefficients are

$$\begin{aligned}
&\varrho = -\frac{1}{(r - ia\cos\theta)}, \quad \beta = \frac{\cot\theta}{2\sqrt{2}(r + ia\cos\theta)}, \quad \pi = \frac{ia\sin\theta}{\sqrt{2}(r - ia\cos\theta)^2}, \\
&\tau = -\frac{ia\sin\theta}{\sqrt{2}(r^2 + a^2\sin^2\theta)}, \quad \mu = -\frac{\Delta}{2(r^2 + a^2\sin^2\theta)(r - ia\cos\theta)}, \\
&\gamma = \mu + \frac{r - M}{2(r^2 + a^2\sin^2\theta)}, \quad \alpha = \pi - \bar{\beta}.
\end{aligned} \tag{2.31}$$

Now consider a generic vacuum perturbation of Kerr. For a generic choice of gauge, three of the Bianchi identities take the form [78]

$$(\delta^* - 4\alpha + \pi)\Psi_0 - (\boldsymbol{D} - 4\varrho - 2\varepsilon)\Psi_1 - 3\kappa\Psi_2 = 0, \tag{2.32}$$

$$(\boldsymbol{\Delta} - 4\gamma + \mu)\Psi_0 - (\delta - 4\tau - 2\beta)\Psi_1 - 3\sigma\Psi_2 = 0, \tag{2.33}$$

$$(\boldsymbol{D} - \varrho - \varrho^* - 3\varepsilon + \varepsilon)\sigma - (\delta - \tau + \pi^* - \alpha^* - 3\beta)\kappa - \Psi_0 = 0. \tag{2.34}$$

In order to derive two master equations for (Ψ_0, Ψ_4) we need to take out Ψ_1 from these equations. This can be done by using the following commutation rule, valid on any type-D spaces [78, 12]:

$$\begin{aligned}
&(\boldsymbol{D} - (p+1)\varepsilon + q\varrho - \varrho^* + \varepsilon^*)(\delta - p\beta + q\tau) \\
&- (\delta - (p+1)\beta + q\tau - \alpha^* + \pi^*)(\boldsymbol{D} - p\varepsilon + q\varrho) = 0,
\end{aligned} \tag{2.35}$$

with (p, q) any two constants. Here we will use the case $p = 2$ and $q = -4$. We apply the two operators $(\delta + \pi^* - \alpha^* - 3\beta - 4\tau)$ and $(\boldsymbol{D} - 3\varepsilon + \varepsilon^* - 4\varrho - \varrho^*)$ to (2.32) and (2.33) respectively. Now, subtracting one from the other we find that the Ψ_1 term vanishes. Moreover, the σ and κ terms resulting from this subtraction have identical coefficients to the ones in (2.34), thus we can substitute them with Ψ_0 and obtain

$$\begin{aligned}
&[(\boldsymbol{D} - 3\varepsilon + \varepsilon^* - 4\varrho - \varrho^*)(\boldsymbol{\Delta} - 4\gamma + \mu) \\
&- (\delta + \pi^* - \alpha^* - 3\beta - 4\tau)(\delta^* + \pi - 4\alpha) - 3\Psi_2]\Psi_0 = 0.
\end{aligned} \tag{2.36}$$

This gives the decoupled equation for Ψ_0.

In order to derive the equation for the second complex scalar Ψ_4 we interchange $l^\alpha \to n^\alpha$ and $m^\alpha \to \bar{m}^\alpha$, as the full set of NP equations is invariant under this switch of

basis vectors. This interchange implies the following substitutions

$$\boldsymbol{D} \to \boldsymbol{\Delta}, \quad \varepsilon \to -\gamma, \quad \varrho \to -\mu, \quad \pi \to -\tau, \quad \beta \to -\alpha, \quad \delta \to \delta^*, \quad \Psi_0 \to \Psi_4. \tag{2.37}$$

So we find for Ψ_4 the following field equation:

$$\begin{aligned}&[(\boldsymbol{\Delta} + 3\gamma - \gamma^* + 4\mu + \mu^*)(\boldsymbol{D} + 4\varepsilon - \varrho) \\ &- (\delta^* - \tau^* + \beta^* + 3\alpha + 4\pi)(\delta - \tau + 4\beta) - 3\Psi_2]\Psi_4 = 0.\end{aligned} \tag{2.38}$$

Eqs.(2.36) and (2.38) can be expressed explicitly in terms of Boyer-Lindquist coordinates by the single equation

$$\begin{aligned}\hat{T}(\psi^s) := &\left[\frac{(r^2+a^2)^2}{\Delta} - a^2\sin^2\theta\right]\psi^s_{,tt} - \Delta^{-s}(\Delta^{s+1}\psi^s_{,r})_{,r} + \frac{4Mar}{\Delta}\psi^s_{,t\varphi} + \left(\frac{a^2}{\Delta} - \frac{1}{\sin^2\theta}\right)\psi^s_{,\varphi\varphi} \\ &- \frac{1}{\sin\theta}(\psi^s_{,\theta}\sin\theta)_{,\theta} - 2s\left[\frac{a(r-M)}{\Delta} + \frac{i\cos\theta}{\sin^2\theta}\right]\psi^s_{,\varphi} - 2s\left[\frac{M(r^2-a^2)}{\Delta} - r - ia\cos\theta\right]\psi^s_{,t} \\ &+ (s^2\cot^2\theta - s)\,\psi^s = 0,\end{aligned} \tag{2.39}$$

with $\Psi_0 = \psi^{s=+2}$ and $\Psi_4 = \rho^4\psi^{s=-2}$. This is known as the *Master Teukoslky Equation*. The sourced Teukolsky equation can be derived in a similar manner as done explicitly in [78], and the source is given in Sec. 2.5.2. In Eq. (2.39), the angular dependence of ψ^s is separable through a decomposition in (frequency dependent) *spin-weighted spheroidal harmonics* when working in the frequency domain [78]. Because of the frequency dependence of the spheroidal harmonics, separation of the θ dependence is not possible in the time domain (namely, without first decomposing the field into its Fourier components).

2.4 Metric Reconstruction in vacuum

In order to compute the value of the SF on a particle orbiting a Kerr Black hole we need the metric perturbations near the particle. In our approach we will reconstruct the metric perturbation from the Weyl curvature scalars. A reconstruction procedure for vacuum perturbations was developed by Chrzanowski [79] and Cohen and Kegeles [80], with later contributions from Wald [81], Stewart [82], Lousto and Whiting [83] and others. As it is common, we shall refer to it here as the CCK procedure.

Considering a vacuum perturbation $h_{\alpha\beta}$ of a Kerr black hole geometry, with corresponding Weyl scalars Ψ_0 and Ψ_4, the CCK method prescribes the reconstruction of $h_{\alpha\beta}$ from either Ψ_0 or Ψ_4. More precisely, the reconstruction procedure returns a perturbation $h^{\rm rec}_{\alpha\beta}$ that is equal to $h_{\alpha\beta}$ up to (i) some gauge perturbation $h^{\rm gauge}_{\alpha\beta}$, and (ii) a "completion" piece $h^{\rm comp}_{\alpha\beta}$ representing a four-parameter family of simple, stationary and axisymmetric vacuum solutions: mass and angular momentum perturbations of Kerr, and perturbations away from Kerr into Kerr-NUT or C-metric geometries [84]. Thus, the original perturbation is given by

$$h_{\alpha\beta} = h^{\rm rec}_{\alpha\beta} + h^{\rm comp}_{\alpha\beta} + h^{\rm gauge}_{\alpha\beta}, \tag{2.40}$$

where $h^{\rm comp}_{\alpha\beta}$ and $h^{\rm gauge}_{\alpha\beta}$ are not fixed within the CCK procedure, and must be determined separately.

In the case of gravitational perturbations, Wald [85, 86] showed elegantly how to derive the reconstruction formulas via the use of the so called Hertz potential. Here we will give a summary of the derivation.

2.4.1 Derivation

We introduce the notion of *adjoint*. For a linear partial differential operator L taking scalar fields into scalar fields, the adjoint $L^\dagger$ is defined as any operator satisfying

$$\psi(L\phi) - (L^\dagger\psi)\phi = \nabla_\mu s^\mu, \tag{2.41}$$

where ψ and ϕ are scalar fields and s^μ is any vector field. This notion can be extended to n-index tensor fields. We say that an operator is self-adjoint if $L = L^\dagger$ (and the two operators have the same domain).

Define $\hat{E}$ to be the linearised Einstein describing perturbations in vacuum spacetime with metric $g_{\mu\nu}$. This operator is a self-adjoint operator [86], which will come to play at the end of the construction. We now specialize to the case of a Kerr metric. Let's denote the Teukolsky operator by $\hat{T}$ as in Eq. (2.39) and define a field Φ (Hertz potential) satisfying the adjoint vacuum equation

$$\hat{T}^\dagger\Phi = [(\boldsymbol{\Delta}+3\gamma-\gamma^*+\mu^*)(\boldsymbol{D}+3\varrho)-(\delta^*-\tau^*+\beta^*+3\alpha)(\delta+3\tau+4\beta)-3\Psi_2]\Phi = 0. \tag{2.42}$$

We also introduce an operator $\hat{O}$ such that $\hat{O}[h_{\mu\nu}] = \Psi_0$, where Ψ_0 is the Weyl scalar field associated with the perturbation $h_{\mu\nu}$.

The Teukoslky procedure derives an equation for a complex scalar field starting from the Ricci tensor operator. This is equivalent to defining the operator $\hat{S}$ such that

$$\hat{S}\hat{E}(h_{\mu\nu}) = \hat{T}(\Psi_0) = \hat{T}\hat{O}(h_{\mu\nu}), \tag{2.43}$$

for all vacuum perturbations $h_{\mu\nu}$. In practice, the operator $\hat{S}$ describes the manipulations that must be performed on the Einstein equations to derive Teukolsky equations. Then the equation $\hat{E}(h_{\mu\nu}) = 0$ implies $\hat{T}(\Psi_0) = 0$.

Now Wald gives a simply proven theorem:

Theorem: If $\hat{S}\hat{E} = \hat{T}\hat{O}$, for $(\hat{S}, \hat{E}, \hat{T}, \hat{O})$ linear partial differential operators, and Φ (Hertz potential) satisfies $\hat{T}^\dagger\Phi = 0$ (adjoint Teukolsky equation), then $\hat{S}^\dagger\Phi$ (reconstruction formula) satisfies $\hat{E}^\dagger(\hat{S}^\dagger\Phi) = 0$. In particular, if $\hat{E}$ is self-adjoint then $\hat{S}^\dagger\Phi$ is a solution of $\hat{E}(f) = 0$.

Thus using the theorem, we obtain that $\hat{S}^\dagger\Phi$ is a solution of $\hat{E}[h_{\mu\nu}] = 0$. Notice that $\hat{O}\hat{S}^\dagger$ maps solutions of $\hat{T}^\dagger\Phi = 0$ into solutions of $\hat{T}\Phi = 0$: indeed, applying $\hat{S}\hat{O}^\dagger$ to $\hat{T}^\dagger(\Phi) = 0$ we find:

$$\hat{S}(\hat{O}^\dagger\hat{T}^\dagger(\Phi)) = 0 \quad \Rightarrow \quad \hat{S}\hat{E}^\dagger\hat{S}^\dagger\Phi = 0 \quad \Rightarrow \quad (\hat{S}\hat{E})\hat{S}^\dagger\Phi = 0 \quad \Rightarrow \quad \hat{T}(\hat{O}\hat{S}^\dagger\Phi) = 0. \tag{2.44}$$

Here we used that $\hat{E}$ is self-adjoint. In order for the reconstructed metric to be the physical metric of our system we impose the inversion relation to map the Hertz potential to the Weyl scalar Ψ_0, that is

$$\Psi_0 = \hat{O}Re[\hat{S}^\dagger\Phi]. \tag{2.45}$$

Wald gives the operators defined above explicitly in the electromagnetic case [85].

2.4.2 Explicit reconstruction formula

There are two variants of the reconstruction procedure, returning $h^{\text{rec}}_{\alpha\beta}$ in two different gauges, known as the "ingoing" and "outgoing" traceless radiation gauges (IRG and

ORG, respectively). The corresponding gauge conditions are

$$l^\alpha h^{\rm rec}_{\alpha\beta} = 0 \quad \text{(IRG)}, \qquad n^\alpha h^{\rm rec}_{\alpha\beta} = 0 \quad \text{(ORG)}, \tag{2.46}$$

along with the trace-free condition

$$g^{\alpha\beta} h^{\rm rec}_{\alpha\beta} = 0, \tag{2.47}$$

where $g^{\alpha\beta}$ is the inverse of the background Kerr metric $g_{\alpha\beta}$. Notice that in vacuum the trace condition (2.47) can be imposed consistently with 2.46) [87, 88].

The CCK procedure starts with the derivation of a suitable *Hertz potential* Φ (one such potential for ORG and another for IRG—call them $\Phi^{\rm ORG}$ and $\Phi^{\rm IRG}$, respectively). This Hertz potential is required to satisfy two differential equations. The first is the master (source-free) Teukolsky equation [as in Eq. (2.39)],

$$\begin{aligned}
&\left(\frac{(r^2+a^2)^2}{\Delta} - a^2\sin^2\theta\right)\frac{\partial^2\Phi}{\partial t^2} + \frac{4Mar}{\Delta}\frac{\partial^2\Phi}{\partial t\partial\varphi} + \left(\frac{a^2}{\Delta} - \frac{1}{\sin^2\theta}\right)\frac{\partial^2\Phi}{\partial\varphi^2} - \Delta^{-s}\frac{\partial}{\partial r}\left(\Delta^{s+1}\frac{\partial\Phi}{\partial r}\right) \\
&- \frac{1}{\sin\theta}\frac{\partial}{\partial\theta}\left(\sin\theta\frac{\partial\Phi}{\partial\theta}\right) + (s^2\cot^2\theta - s)\Phi - 2s\left(\frac{M(r^2-a^2)}{\Delta} - r - ia\cos\theta\right)\frac{\partial\Phi}{\partial t} \\
&\qquad - 2s\left(\frac{a(r-M)}{\Delta} + \frac{i\cos\theta}{\sin^2\theta}\right)\frac{\partial\Phi}{\partial\varphi} = 0,
\end{aligned} \tag{2.48}$$

with $s = +2$ for $\Phi^{\rm ORG}$ and $s = -2$ for $\Phi^{\rm IRG}$. The second equation (derived from 2.45) links Φ to one of the given Weyl-scalar perturbations Ψ_0 or Ψ_4:

$$\boldsymbol{D}^4\bar{\Phi}^{\rm IRG} = 2\Psi_0, \tag{2.49}$$

$$\Delta^2\tilde{\boldsymbol{\Delta}}^4\Delta^2\bar{\Phi}^{\rm ORG} = 32\varrho^{-4}\Psi_4, \tag{2.50}$$

where

$$\begin{aligned}
\boldsymbol{D} &:= l^\alpha\partial_\alpha = \frac{r^2+a^2}{\Delta}\partial_t + \partial_r + \frac{a}{\Delta}\partial_\varphi, \\
\tilde{\boldsymbol{\Delta}} &:= -\frac{2\Sigma}{\Delta}n^\alpha\partial_\alpha = -\frac{r^2+a^2}{\Delta}\partial_t + \partial_r - \frac{a}{\Delta}\partial_\varphi,
\end{aligned} \tag{2.51}$$

and $\boldsymbol{D}^4 := \boldsymbol{DDDD}$, etc. Alternatively, instead of (2.49) or (2.50), one can require

$$\begin{aligned}
\tilde{\mathcal{L}}_{-1}\tilde{\mathcal{L}}_0\tilde{\mathcal{L}}_1\tilde{\mathcal{L}}_2\bar{\Phi}^{\mathrm{IRG}} - 12M\Phi^{\mathrm{IRG}}_{,t} &= 8\varrho^{-4}\Psi_4, \qquad (2.52)\\
\mathcal{L}_1\mathcal{L}_0\mathcal{L}_{-1}\mathcal{L}_{-2}\bar{\Phi}^{\mathrm{ORG}} + 12M\Phi^{\mathrm{ORG}}_{,t} &= 8\Psi_0, \qquad (2.53)
\end{aligned}$$

where

$$\begin{aligned}
\mathcal{L}_s &:= -(\partial_\theta - s\cot\theta + i\csc\theta\partial_\varphi) - ia\sin\theta\partial_t,\\
\tilde{\mathcal{L}}_s &:= -(\partial_\theta + s\cot\theta - i\csc\theta\partial_\varphi) + ia\sin\theta\partial_t. \qquad (2.54)
\end{aligned}$$

It can be shown [89] that the combination of (2.48) and (2.49) [or (2.48) and (2.52)] determines Φ^{IRG} uniquely, and similarly the combination of (2.48) and (2.50) [or (2.48) and (2.53)] determines Φ^{ORG} uniquely.

Given Φ, the vacuum perturbation $h^{\mathrm{rec}}_{\alpha\beta}$ is obtained via

$$h^{\mathrm{rec}}_{\alpha\beta} = \mathrm{Re}\left(e_{\mathbf{a}(\alpha}e_{\mathbf{b}\beta)}\mathcal{D}^{\mathbf{ab}}\Phi\right), \qquad (2.55)$$

where the symmetrization is over the tensorial indices $\alpha\beta$, and $\mathcal{D}^{\mathbf{ab}}$ are certain second-order differential operators. Explicitly, the nonvanishing operators $\mathcal{D}^{\mathbf{ab}}$ are given by

$$\begin{aligned}
\mathcal{D}^{\mathbf{11}} &= -2(\delta + \bar{\alpha} + 3\beta - \tau)(\delta + 4\beta + 3\tau),\\
\mathcal{D}^{\mathbf{33}} &= -2(\boldsymbol{D} - \varrho)(\boldsymbol{D} + 3\varrho),\\
\mathcal{D}^{\mathbf{13}} &= \mathcal{D}^{\mathbf{31}} = (\delta - 2\bar{\alpha} + 2\beta - \tau)(\boldsymbol{D} + 3\varrho)\\
&\quad + (\boldsymbol{D} + \bar{\varrho} - \varrho)(\delta + 4\beta + 3\tau) \qquad (2.56)
\end{aligned}$$

for the IRG, and by

$$\begin{aligned}
\mathcal{D}^{\mathbf{22}} &= -2\varrho^{-4}(\delta^* + 2\alpha + 4\bar{\beta} - \tau)(\delta^* - 3\alpha + \bar{\beta}),\\
\mathcal{D}^{\mathbf{44}} &= -2\varrho^{-4}(\boldsymbol{\Delta} + 5\mu - 3\gamma + \bar{\gamma})(\boldsymbol{\Delta} + \mu - 4\gamma),\\
\mathcal{D}^{\mathbf{24}} &= \mathcal{D}^{\mathbf{42}} = \varrho^{-4}\Big[(\delta^* + 2\alpha + 4\bar{\beta} + \bar{\tau})(\boldsymbol{\Delta} + \mu - 4\gamma)\\
&\quad + (\boldsymbol{\Delta} + 5\mu - \bar{\mu} - 3\gamma - \bar{\gamma})(\delta^* - 3\alpha + \bar{\beta})\Big] \qquad (2.57)
\end{aligned}$$

for the ORG. Here we have for the directional derivatives

$$\begin{aligned}
\boldsymbol{\Delta} &:= n^\alpha \partial_\alpha = \frac{1}{2\Sigma}\left[(r^2+a^2)\partial_t - \Delta\partial_r + a\partial_\varphi\right], \\
\delta &:= m^\alpha \partial_\alpha = -\frac{\bar{\varrho}}{\sqrt{2}}\left(ia\sin\theta\partial_t + \partial_\theta + i\csc\theta\partial_\varphi\right), \\
\delta^* &:= \bar{m}^\alpha \partial_\alpha = \frac{\varrho}{\sqrt{2}}\left(ia\sin\theta\partial_t - \partial_\theta + i\csc\theta\partial_\varphi\right),
\end{aligned} \tag{2.58}$$

where the spin coefficients are as in (2.31) and $\boldsymbol{D}$ as in (2.51).

In this work we will use the IRG (the choice is dictated by numerical stability of the corresponding Teukolsky equation, as we shall discuss in Chapter 5). For this choice, the non-vanishing tetrad components of the metric are reconstructed via

$$\begin{aligned}
h_{nn}^{IRG} &= -\{(\delta+\overline{\alpha}+3\beta-\tau)(\delta+4\beta+3\tau)\} \\
&\quad \Phi^{IRG} + c.c., && \text{(2.59a)} \\
h_{\overline{m}\overline{m}}^{IRG} &= -\{(\boldsymbol{D}-\varrho)(\boldsymbol{D}+3\varrho)\}\Phi^{IRG} + c.c., && \text{(2.59b)} \\
h_{(n\overline{m})}^{IRG} &= -\frac{1}{2}\{(\delta-\overline{\alpha}+3\beta-\overline{\pi}-\tau)(\boldsymbol{D}+3\varrho) + \\
&\quad (\boldsymbol{D}+\overline{\varrho}-\varrho)(\delta+4\beta+3\tau)\}\Phi^{IRG} + c.c., && \text{(2.59c)}
\end{aligned}$$

where *c.c.* stands for the complex conjugate part of the whole expression. Similar expressions hold for the ORG case.

2.5 Particle source

The formalism described in the previous section can be extended to the particle case. In particular, the metric reconstruction in radiation gauge have been carefully studied in [57, 62]. Here, some basics of geodesic motion in Kerr are described, including the source terms for Teukolsky equation needed for our implementation. A summary of the metric reconstruction for a particle in Kerr is then given is Sec. 2.6.

2.5.1 Geodesic motion

The geodesic equations that govern Kerr black hole orbits are:

$$\Sigma^2\left(\frac{dr}{d\tau}\right)^2 = \Big[E(r^2+a^2)-aL\Big]^2 - \Delta\left[r^2+(L-aE)^2+Q\right], \tag{2.60}$$

$$\Sigma^2\left(\frac{d\theta}{d\tau}\right)^2 = Q-\cot^2\theta L^2 - a^2\cos^2\theta\left(1-E^2\right), \tag{2.61}$$

$$\Sigma^2\left(\frac{d\phi}{d\tau}\right)^2 = \csc^2\theta L_z + aE\left(\frac{r^2+a^2}{\Delta}-1\right) - \frac{a^2L}{\Delta}, \tag{2.62}$$

$$\Sigma^2\left(\frac{dt}{d\tau}\right)^2 = E\left[\frac{(r^2+a^2)^2}{\Delta} - a^2\sin^2\theta\right] + aL\left(1-\frac{r^2+a^2}{\Delta}\right), \tag{2.63}$$

where τ is proper time measured along the orbit. Up to initial conditions, orbits are specified by the quantities E, L, and Q ("specific energy", "specific z-component of angular momentum", and "Carter constant"); E and L are associated with the two Killing vectors in Kerr spacetime $(\xi^\mu_{(t)}, \xi^\mu_{(\phi)})$ and Q with the Killing tensor $Q^{\mu\nu}$, explicitly

$$E = \xi^\mu_{(t)}u_\mu, \quad L = -\xi^\mu_{(\phi)}u_\mu, \quad Q = Q^{\mu\nu}u_\mu u_\nu. \tag{2.64}$$

Thus, these are conserved quantities. In the case of circular and equatorial motion in Kerr these quantities are explicitly (taking $\theta_0 = \pi/2$ and $dr_0/d\tau = d^2r_0/d\tau^2 = 0$)

$$E = \frac{1-2v^2+\tilde{a}v^3}{\sqrt{1-3v^2+2\tilde{a}v^3}}, \qquad L = r_0 v\,\frac{1-2\tilde{a}v^3+\tilde{a}^2v^4}{\sqrt{1-3v^2+2\tilde{a}v^3}}, \tag{2.65}$$

where $v := \sqrt{M/r_0}$ and $\tilde{a} := a/M$. The Carter constant is given explicitly (for any orbit) by

$$Q = u_\theta^2 + \cos^2\theta_0[a^2(1-E^2)+\csc^2\theta_0 L^2]). \tag{2.66}$$

Notice that in Eqs. (2.60) and (2.61), the RHS is only r and θ dependent, respectively. This fact means that the orbits will have two specific frequencies associated with radial and longitudinal motion. The orbits are then bi-periodic.

2.5.2 Energy-momentum

The stress-energy tensor for the orbiting particle is modelled as a δ-function distribution along the worldline (as previously mentioned, this representation is suitable at linear

order in the perturbation theory). Thus, we write explicitly

$$\begin{aligned} T^{\alpha\beta} &= \mu \int u^\alpha u^\beta \delta^{(4)}(x^\alpha - x_0^\alpha(\tau))(-g)^{-1/2} d\tau \\ &= \mu \int \frac{u^\alpha u^\beta}{\Sigma \sin\theta} \delta(r - r_0(\tau))\delta(\cos\theta - \cos\theta_0(\tau))\delta(\varphi - \varphi_0(\tau))\delta(t - t_0(\tau)) d\tau \\ &= \frac{\mu}{u^t r_0^2} u^\alpha u^\beta \delta(r - r_0)\delta(\cos\theta - \cos\theta_0)\delta(\varphi - \varphi_0) \end{aligned} \tag{2.67}$$

where the particle of mass μ is located at the point x_0^α with Boyer-Lindquist coordinates $(t_0, r_0, \theta_0, \varphi_0)$, $u^\alpha = dx_0^\alpha/d\tau$ and $g = \det(g^{\mu\nu}) = -(\Sigma \sin\theta)^2$. The third line specialize to circular orbits and it is obtained by changing the integration variable from τ to t and integrating in a time-t interval containing t_0. In the abouve u^t is the t component of the four-velocity, given explicitly by [in the notation of Eq. (2.65)]

$$u^t = \frac{1 + \tilde{a}v^3}{\sqrt{1 - 3v^2 + 2\tilde{a}v^3}} \tag{2.68}$$

The corresponding source of the Teukolsky equation can be obtained in terms of the components of $T^{\alpha\beta}$ projected along the Newman-Penrose tetrad. For $s = \pm 2$, the relations are explicitly [78]

$$\begin{aligned} T_{+2} =& 8\pi\Sigma\Big[(\boldsymbol{\delta} - 2\beta - 4\tau)(\boldsymbol{\delta} - \bar{\varpi})T_{\mathbf{11}} - (\boldsymbol{D} - 4\varrho - \bar{\varrho})(\boldsymbol{\delta} + 2\bar{\alpha})T_{\mathbf{13}} \\ & - (\boldsymbol{\delta} - 2\beta - 4\tau)(\boldsymbol{D} - 2\bar{\varrho})T_{\mathbf{13}} + (\boldsymbol{D} - 4\varrho - \bar{\varrho})(\boldsymbol{D} - \bar{\varrho})T_{\mathbf{33}}\Big], \end{aligned} \tag{2.69}$$

$$\begin{aligned} T_{-2} =& \frac{8\pi\Sigma}{\varrho^4}\Big[(\bar{\boldsymbol{\delta}} + 2\alpha + 5\varpi - \bar{\tau})(\bar{\boldsymbol{\delta}} + 2\varpi - \bar{\tau})T_{\mathbf{22}} - (\boldsymbol{\Delta} + 3\gamma - \bar{\gamma} + 4\mu + \bar{\mu})(\bar{\boldsymbol{\delta}} + 2\alpha - 2\bar{\tau})T_{\mathbf{24}} \\ & - (\bar{\boldsymbol{\delta}} + 2\alpha + 5\varpi - \bar{\tau})(\boldsymbol{\Delta} + 2\gamma + 2\bar{\mu})T_{\mathbf{24}} + (\boldsymbol{\Delta} + 3\gamma - \bar{\gamma} + 4\mu + \bar{\mu})(\boldsymbol{\Delta} + 2\gamma - 2\bar{\gamma} + \bar{\mu})T_{\mathbf{44}}\Big], \end{aligned} \tag{2.70}$$

where $T_{\boldsymbol{ij}} = T_{\alpha\beta} e_i^\alpha e_j^\beta$. In Appendix A we explicitly compute and re-write in a convenient form the Teukolsky source for the case $s = 2$. The latter will be needed in our later discussed numerical implementation.

2.6 Metric reconstruction for a particle source

The vacuum reconstruction procedure is guaranteed to return a valid vacuum solution $h^{\rm rec}_{\alpha\beta}$ whenever the Weyl scalar one starts with (Ψ_4 or Ψ_0) is a solution to the source-free Teukolsky equation. But when matter sources are present, the procedure can fail to return a valid solution even at vacuum points away from any sources. This is true even in the simplest example of a static particle in flat space, in either the IRG or the ORG. As shown first in [57], the reconstructed perturbation develops a stringlike singularity, which emanates from the particle in the radial null direction, either outward or inward, or in both directions (depending on the specific choice of gauge within each of the IRG or ORG classes). Reference [62] introduced a categorization of reconstructed perturbations based on the form of singularity—the two "half-string" classes and the "full string" class—and showed that any reconstructed metric belongs to one of the classes (assuming continuity away from the string). A "no-string" gauge may be formed by joining together the two "regular sides" of two opposite half-string perturbations along a closed surface $\mathcal{S}$ through the particle as shown in Fig. 2.1. Such a construction was first introduced by Friedman and collaborators in [61, 59]. The no-string perturbation is free from stringlike singularities, but has a gauge discontinuity (and also delta-function distributions [62]) on the interface $\mathcal{S}$.

Specializing to a particle in a bound orbit around a Kerr black hole, we let the particle's worldline be represented (in Boyer-Lindquist coordinates) by $x_{\rm p} = \{t, r_{\rm p}(t), \theta_{\rm p}(t), \varphi_{\rm p}(t)\}$, where the radius $r_{\rm p}(t)$ is compactly supported outside the Black hole's event horizon. It is convenient to choose the interface $\mathcal{S}$ to be the surface $r = r_{\rm p}(t)$, and we denote the interior of $\mathcal{S}$ [i.e., $r < r_{\rm p}(t)$] by $\mathcal{S}^-$ and its exterior [i.e., $r > r_0(t)$] by $\mathcal{S}^+$. Then a half-string reconstructed metric has a string singularity in either $\mathcal{S}^-$ or $\mathcal{S}^+$ (and is smooth elsewhere off the particle), and a full-string metric has a string singularity in both. A no-string reconstructed metric is smooth anywhere in both vacuum domains $\mathcal{S}^-$ and $\mathcal{S}^+$ but has a discontinuity across the interface $\mathcal{S}$ between them.

Our time-domain metric reconstruction prescription in this work will yield the no-string vacuum perturbations $h^{\rm rec\pm}_{\alpha\beta}$, where $\pm$ denotes values in the corresponding vacuum domains $\mathcal{S}^\pm$. We denote the corresponding total, completed perturbations in $\mathcal{S}^\pm$ by

$$h^{\pm}_{\alpha\beta} = h^{\rm rec\pm}_{\alpha\beta} + h^{\rm comp\pm}_{\alpha\beta} + h^{\rm gauge\pm}_{\alpha\beta}, \tag{2.71}$$

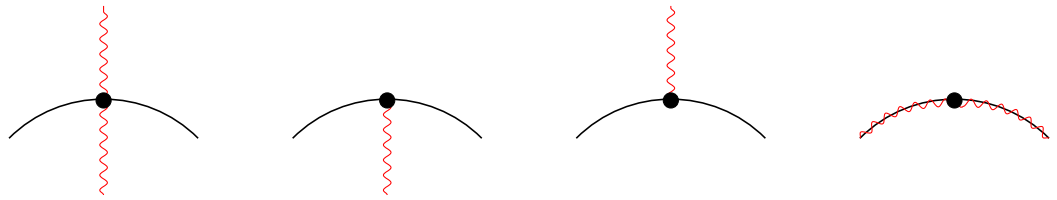

Figure 2.1: Types of gauge singularities [1].

where $h^{\rm comp\pm}_{\alpha\beta}$ and $h^{\rm gauge\pm}_{\alpha\beta}$ are the contributions from the "completion" and "gauge" perturbations in the corresponding domains [recall Eq. (2.40)].

The completion piece $h^{\rm comp\pm}_{\alpha\beta}$ has been derived recently in Refs. [34, 90] (for arbitrary bound geodesic motion in Kerr spacetime). Their main result is that (in a no-string radiation gauge)

$$h^{\rm comp\pm}_{\alpha\beta} = \begin{cases} \mu E h^{(\delta M)}_{\alpha\beta} + \mu L h^{(\delta J)}_{\alpha\beta} & \mathcal{S}^+, \\ 0 & \mathcal{S}^-, \end{cases} \tag{2.72}$$

Here E and L are the specific energy and specific angular momentum associated with the geodesic orbit (see Sec. 2.5.1) and $h^{(\delta M)}_{\alpha\beta}$ and $h^{(\delta J)}_{\alpha\beta}$ are the vacuum perturbations given explicitly by [91]

$$\begin{aligned}
h^{(\delta M)}_{tt} &= \frac{2r}{\Sigma^2}\left(r^2 + 3a^2\cos^2\theta\right), \\
h^{(\delta M)}_{t\varphi} &= -\frac{ra^3\sin^2 2\theta}{\Sigma^2}, \\
h^{(\delta M)}_{rr} &= \frac{2r}{M\Delta^2}\left[Mr^2 + 3a^2M + a^2(r-3M)\sin^2\theta)\right], \\
h^{(\delta M)}_{\theta\theta} &= -(2/M)a^2\cos^2\theta, \\
h^{(\delta M)}_{\varphi\varphi} &= -\frac{2a^2\sin^2\theta}{M\Sigma^2}\left[\Sigma^2 + Mr(r^2 - a^2\cos^2\theta)\sin^2\theta\right],
\end{aligned} \tag{2.73}$$

$$\begin{aligned}
h^{(\delta J)}_{tt} &= -\frac{4ar\cos^2\theta}{\Sigma^2}, \\
h^{(\delta J)}_{t\varphi} &= -\frac{2r\sin^2\theta}{\Sigma^2}\left(r^2 - a^2\cos^2\theta\right), \\
h^{(\delta J)}_{rr} &= -\frac{ar}{M\Delta^2}\left[r + 2M - (r-2M)\cos 2\theta\right], \\
h^{(\delta J)}_{\theta\theta} &= (2/M)a\cos^2\theta, \\
h^{(\delta J)}_{\varphi\varphi} &= \frac{2a^2\sin^2\theta}{M\Sigma^2}\left(\Sigma^2 + 2Mr^3\sin^2\theta\right),
\end{aligned} \tag{2.74}$$

[1] The Illustration is provided through the courtesy of C. Merlin

with all other components vanishing.

A gauge adjustment $h^{\text{gauge}\pm}_{\alpha\beta}$ may need to be included in certain applications (see Refs. [92] or [93] for examples), but in this work we will set $h^{\text{gauge}\pm}_{\alpha\beta} := 0$ for simplicity. Since $h^{\text{rec}\pm}_{\alpha\beta}$ are each a vacuum solution in its corresponding vacuum domain ($\mathcal{S}^{\pm}$), they can be reconstructed from suitable Hertz potentials $\Phi^{\pm}$ by applying the vacuum reconstruction formula (2.55) in each of the domains:

$$h^{\text{rec}\pm}_{\alpha\beta} = \text{Re}\left(e_{\mathbf{a}(\alpha}e_{\mathbf{b}\beta)}\mathcal{D}^{\mathbf{ab}}\Phi^{\pm}\right). \tag{2.75}$$

2.6.1 Self-force from a reconstructed metric

In Ref. [62], Pound *et al.* obtained a formulation of the GSF starting from a reconstructed metric (in either the IRG or the ORG), complete with practical mode-sum formulas. Two different schemes were described, one based on (either of the two) half-string gauges, and another based on the no-string gauge. The prescription for calculating the GSF in the no-string scheme is as follows. First, given the reconstructed (and completed) perturbations $h^{\pm}_{\alpha\beta}$, introduce the one-sided "force" fields [recall Eq. (2.3)]

$$F^{\pm}_{\alpha} := -\frac{1}{2}\mu(\delta^{\beta}_{\alpha} + u_{\alpha}u^{\beta})(2\nabla_{\nu}h^{\pm}_{\beta\mu} - \nabla_{\beta}h^{\pm}_{\mu\nu})u^{\mu}u^{\nu}, \tag{2.76}$$

defined on $\mathcal{S}^{\pm}$, respectively, where μ is the mass of the particle, ∇_{α} is a covariant derivative compatible with the background (Kerr) geometry, and u^{α} is any smooth extension of the particle's four-velocity to form a vector field in spacetime. Next, expand each coordinate component of the fields $F^{\pm}_{\alpha}$ in spherical harmonics $Y_{\ell m}(\theta,\varphi)$ on spheres of constant r, t, and for each multipole contribution (summed over azimuthal number m) take the one-sided radial limits to the particle:

$$F^{\ell\pm}_{\alpha} := \lim_{r\to r^{\pm}_{\text{p}}} \sum_{m=-\ell}^{\ell} Y_{\ell m}(\theta_{\text{p}},\varphi_{\text{p}}) \int F^{\pm}_{\alpha}\bar{Y}_{\ell m}(\theta,\varphi)d\Omega, \tag{2.77}$$

where $d\Omega := \sin\theta d\theta d\varphi$. These one-sided ℓ-mode force contributions are each finite (bounded), and generally grow in amplitude as $\sim \ell$ for large ℓ. According to [62], given $F^{\ell\pm}_{\alpha}$, the physical GSF is calculated via

$$F_{\alpha} = \sum_{\ell=0}^{\infty}\left[\frac{1}{2}(F^{\ell+}_{\alpha} + F^{\ell-}_{\alpha}) - B_{\alpha}\right], \tag{2.78}$$

where B_α is the standard, Lorenz-gauge regularization parameter (which depends on the details of the orbit, but not on ℓ). An analytical expression for B_α, for generic orbits in Kerr, was first derived in [94] and it is given explicitly in Appendix B as in [44].

The mode-sum formula (2.78) can be implemented in either the IRG or the ORG. While $F^{\ell\pm} \sim \ell$ at large ℓ, the average $\frac{1}{2}(F_\alpha^{\ell+}+F_\alpha^{\ell-})$ approaches a constant (ℓ-independent) value, and the entire summand in (2.78) is guaranteed to fall off at least as $\sim \ell^{-2}$. Hence, the mode sum converges at least as $\sim 1/\ell$.

In conclusion, we see that knowledge of the "no-string" perturbations $h_{\alpha\beta}^{\mathrm{rec}\pm}$ (and their derivatives at the particle) provides sufficient input for calculating the physical GSF.

In the next chapter we will lay out our proposed method for deriving the appropriate potentials $\Phi^\pm$, via a direct time-domain evolution of the Teukolsky equation. Once $\Phi^\pm$ are at hand, the GSF is obtained (in a completed no-string gauge) by substituting for $\Phi^\pm$ in Eq. (2.75), then consequently for $h_{\alpha\beta}^{\mathrm{rec}\pm}$ in Eq. (2.71) (where the (analytical) completion part of the perturbation $h_{\alpha\beta}^{\mathrm{comp}\pm}$ is added), for $h_{\alpha\beta}^{\pm}$ in Eq. (2.76), for $F_\alpha^\pm$ in Eq. (2.77), and finally for $F_\alpha^{\ell\pm}$ in the mode-sum formula (2.78).

Chapter 3

Time-domain evolution scheme for the Hertz potentials $\Phi^{\pm}$

Our goal here is to formulate a practical evolution scheme for $\Phi^{\pm}$, suitable for numerical integration in 1+1D. Such a formulation requires three components. First, starting from the master Teukolsky equation (2.48), we need to introduce a suitable decomposition of $\Phi^{\pm}$ into multipole modes and obtain a time-evolution equation for the "time-radial" piece of each of the modes. Second, we need to derive the physical boundary conditions for the fields $\Phi^{\pm}$ and for their multipole modes. Third, we need to formulate junction conditions for the multipole modes on the surface $\mathcal{S}$ [i.e., $r = r_{\rm p}(t)$]. These three components of the problem are dealt with, each in turn, in the next subsections.

We aim here to give a full formulation for both $\Phi^{\rm IRG}$ and $\Phi^{\rm ORG}$. Since the former is a solution of the master equation (2.48) with $s = -2$, and the latter is a solution of that equation with $s = +2$, we shall use the notation

$$\Phi_{-2} := \Phi^{\rm IRG}, \qquad \Phi_{+2} := \Phi^{\rm ORG}, \tag{3.1}$$

which will allow us to unify the treatment of both gauges. Correspondingly, the vacuum potentials in the regions $\mathcal{S}^+$ [i.e., $r > r_{\rm p}(t)$] and $\mathcal{S}^-$ [i.e., $r < r_{\rm p}(t)$] will be denoted by $\Phi^{\pm}_s$, with $s = -2$ for IRG and $s = +2$ for ORG.

3.1 The Teukolsky equation in a 1+1D form

As far as we know, in general, the master Teukolsky equation (2.48) cannot be separated in the time domain, i.e. without first decomposing Φ_s into frequency modes $\sim e^{i\omega t}$; only the azimuthal dependence can be separated, using $\Phi_s = \sum_m \Phi_{sm} e^{im\varphi}$. A full separation of the angular dependence becomes possible in the special case of $a = 0$ (Schwarzschild background), or for t-independent perturbations. In both special cases, separation is achieved using a basis of *spin-weighted spherical harmonic* functions ${}_sY_{\ell m}(\theta, \varphi)$ [95]. For spins $s = \pm 2$, relevant here, these functions are derived from the standard spherical harmonics $Y_{\ell m}(\theta, \varphi)$ via

$$ {}_{\pm 2}Y_{\ell m} = \sqrt{\frac{(\ell-2)!}{(\ell+2)!}} \left[\frac{\partial^2 Y_{\ell m}}{\partial \theta^2} - \left(\frac{\cos\theta \pm 2m}{\sin\theta} \right) \frac{\partial Y_{\ell m}}{\partial \theta} + \left(\frac{m^2 \pm 2m\cos\theta}{\sin^2\theta} \right) Y_{\ell m} \right], \tag{3.2} $$

and they satisfy the differential equation

$$ \frac{1}{\sin\theta} \frac{\partial}{\partial\theta} \left(\sin\theta \frac{\partial {}_sY_{\ell m}}{\partial\theta} \right) + \left(-\frac{m^2 + 2ms\cos\theta}{\sin^2\theta} - s^2\cot^2\theta + s + (\ell - s)(\ell + s + 1) \right) {}_sY_{\ell m} = 0. \tag{3.3} $$

Since the spherical harmonics satisfy $\bar{Y}_{\ell m} \equiv (-1)^m Y_{\ell,-m}$ (where the sign factor is conventional), it is easy to see that we have the symmetry relation

$$ {}_{\pm 2}\bar{Y}_{\ell m} \equiv (-1)^m {}_{\mp 2}Y_{\ell,-m}. \tag{3.4} $$

Our strategy here will be to expand $\Phi_s^{\pm}$ in ${}_sY_{\ell m}(\theta, \varphi)$ even in the Kerr case. The resulting field equations for the time-radial modes will exhibit coupling between modes of different ℓ (though modes of different m will remain decoupled). We will then formulate our evolution problem for that mode-coupled set.

We thus expand the fields $\Phi_s^{\pm}$ in the form

$$ \Phi_s^{\pm} = (r\Delta^s)^{-1} \sum_{\ell=2}^{\infty} \sum_{m=-\ell}^{\ell} \phi^{\pm}_{s\ell m}(t, r) {}_sY_{\ell m}(\theta, \tilde{\varphi}). \tag{3.5} $$

Here, the radial factor $(r\Delta^s)^{-1}$ is introduced to regulate the behavior of $\phi^{\pm}_{s\ell m}$ at infinity and on the event horizon; its particular form will be explained in Sec. 3.2 below. The azimuthal coordinate $\tilde{\varphi}$ is a horizon-regularized version of the Boyer-Lindquist φ, defined

through

$$\tilde{\varphi} = \varphi + \frac{a}{r_+ - r_-} \ln\left(\frac{r - r_+}{r - r_-}\right), \tag{3.6}$$

where

$$r_\pm = M \pm (M^2 - a^2)^{1/2}; \tag{3.7}$$

it satisfies $\partial\tilde{\varphi}/\partial r = a/\Delta$. Had we instead used the standard φ in Eq. (3.5), the field $\phi^-_{s\ell m}$ would exhibit irregular oscillations $\sim e^{\pm im\Omega_{\rm H} r_*}$ near the event horizon [96]. Here $\Omega_{\rm H} = a/(2Mr_+)$ is the horizon's angular velocity, and r_* is the standard "tortoise" coordinate, satisfying

$$\frac{dr_*}{dr} = \frac{r^2 + a^2}{\Delta}. \tag{3.8}$$

Note that $\tilde{\varphi} = \varphi + O(a/r)$, and hence $\tilde{\varphi}$ approaches the standard φ at large r.

Inserting the expansion (3.5) into the master equation (2.48), and using Eq. (3.3), we obtain

$$\sum_{\ell m} {}_sY_{\ell m}(\theta, \tilde{\varphi}) \left[\tilde{D}\phi^\pm_{s\ell m} - a^2 \sin^2\theta \, (\phi^\pm_{s\ell m})_{,tt} + 2ias\cos\theta \, (\phi^\pm_{s\ell m})_{,t}\right] = 0, \tag{3.9}$$

where $\tilde{D}$ is a certain partial differential operator independent of θ, φ. Note how the two terms $\propto \sin^2\theta$ and $\propto \cos\theta$ prevent a full separation of variables when $a \neq 0$ and the field is t dependent. Following the treatment (and notation) of Ref. [97], we proceed by re-expanding the angular functions ${}_sY_{\ell m}\cos\theta$ and ${}_sY_{\ell m}\sin^2\theta$ in spin-weighted harmonics:

$${}_sY_\ell \cos\theta = c^{\ell+1}_- \, {}_sY_{\ell+1} + c^\ell_0 \, {}_sY_\ell + c^{\ell-1}_+ \, {}_sY_{\ell-1}, \tag{3.10}$$

$${}_sY_\ell \sin^2\theta = C^{\ell+2}_{--} \, {}_sY_{\ell+2} + C^{\ell+1}_- \, {}_sY_{\ell+1} + C^\ell_0 \, {}_sY_\ell + C^{\ell-1}_+ \, {}_sY_{\ell-1} + C^{\ell-2}_{++} \, {}_sY_{\ell-2}. \tag{3.11}$$

Here we have dropped the index m for clarity, and the coefficients are

$$\begin{aligned} c^\ell_- &= \left[\frac{(\ell^2 - s^2)(\ell^2 - m^2)}{\ell^2(2\ell - 1)(2\ell + 1)}\right]^{1/2}, \\ c^\ell_0 &= -\frac{ms}{\ell(\ell+1)}, \\ c^\ell_+ &= c^{\ell+1}_-, \end{aligned} \tag{3.12}$$

and

$$\begin{aligned} C^\ell_{++} &= -c_+^{\ell+1}c_+^\ell, \\ C^\ell_{+} &= -c_+^{\ell}(c_0^{\ell+1}+c_0^\ell), \\ C^\ell_{0} &= 1-(c_-^\ell)^2-(c_+^\ell)^2-(c_0^\ell)^2, \\ C^\ell_{-} &= -c_-^{\ell}(c_0^{\ell}+c_0^{\ell-1}), \\ C^\ell_{--} &= -c_-^{\ell-1}c_-^\ell. \end{aligned} \tag{3.13}$$

Substituting back into (3.9) and using the orthogonality property of the functions ${}_sY_{lm}$, we finally separate out the angular dependence, arriving at a mode-coupled set of equations for the time-radial part. For each s, ℓ, m (with $s = \pm 2$, $\ell \geq 2$ and $|m| \leq \ell$), it has the form

$$\hat{D}\phi^\ell_{sm} + \mathcal{I}(\phi^{\ell\pm1}_{sm}, \phi^{\ell\pm2}_{sm}) = 0, \tag{3.14}$$

where, to avoid confusion, we have omitted the label $\pm$ associated with the domains $\mathcal{S}^\pm$, and used superscript for the multipole label ℓ. In this equation, $\hat{D}$ is yet another time-radial differential operator (independent of θ, φ), and $\mathcal{I}$ is a functional describing *coupling* between each of the ℓ-modes and their nearest and next-to-nearest neighbours:

$$\mathcal{I} = -a^2\left(C^\ell_{++}\phi^{\ell+2}_{sm} + C^\ell_{+}\phi^{\ell+1}_{sm} + C^\ell_{-}\phi^{\ell-1}_{sm} + C^\ell_{--}\phi^{\ell-2}_{sm}\right)_{,tt} + 2ias\left(c^\ell_+\phi^{\ell+1}_{sm} + c^\ell_-\phi^{\ell-1}_{sm}\right)_{,t}. \tag{3.15}$$

The coupling disappears when $a = 0$ or the perturbation is t independent.

To write Eq. (3.14) explicitly in a convenient form, we introduce the advanced and retarded time coordinates,

$$v := t + r_* \quad \text{and} \quad u := t - r_*, \tag{3.16}$$

respectively (which reduce to the standard double-null Eddington-Finkelstein coordinates in the Schwarzschild case). Then the 1+1D modal Teukolsky equation (3.14) takes the explicit form

$$\phi^\ell_{,uv} + U(r)\phi^\ell_{,u} + V(r)\phi^\ell_{,v} + W(r)\phi^\ell + K(r)\left[-a^2C^\ell_0\,\phi^\ell_{,tt} + \mathcal{I}(\phi^{\ell\pm1}, \phi^{\ell\pm2})\right] = 0, \tag{3.17}$$

where ∂_u, ∂_v and ∂_t are taken with fixed v, u and r, respectively, and we have dropped the indices s, m for improved readability. The radial functions in this equation read

$$K(r) = \frac{\Delta}{4(r^2+a^2)^2}, \tag{3.18}$$

$$U(r) = 2K(r)\left[2sM + ia(sc_0^\ell + m) - a^2/r \; +4Mr(sM - sr + iam)/\Delta\right], \tag{3.19}$$

$$V(r) = 2K(r)\left[2sr + ia(sc_0^\ell - m) + a^2/r\right], \tag{3.20}$$

$$W(r) = K(r)\left[(\ell - s)(\ell + s + 1) + 2(s+1)M/r \; +2iam/r - 2a^2/r^2\right]. \tag{3.21}$$

It is important to reiterate that, even in the Kerr case, the 1+1D Teukolsky equation (3.17) exhibits only a *finite* coupling between spherical-harmonic modes: each ℓ mode couples only to its nearest and next-to-nearest neighbors. This is a remarkable property that can bring much simplification in practice (see below). We also note that the coupling terms contained in $\mathcal{I}$ in Eq. (3.17) are expected to be subdominant (compared to, e.g., the term $\propto W$ in that equation) in the problem of interest to us here: these terms are relatively suppressed by factors of orders $(a\omega)^2$ or $a\omega$, where ω is a characteristic frequency of the perturbation, which, in most relevant scenarios (and for relevant values of m) is considerably smaller than $1/M$, giving suppression factors considerably smaller than unity.[1] This can be used to one's advantage in numerical implementations, as we further discuss in Sec. 3.3 below.

The term $\propto \phi^\ell_{,tt}$ may be eliminated from Eq. (3.17) by introducing a modified (ℓ, m, s-dependent) radial coordinate $\tilde{r}_*$, satisfying

$$\frac{d\tilde{r}_*}{dr_*} = \sqrt{1 - 4K(r)a^2 C_0^\ell} =: \beta_{\ell m}(r)\,. \tag{3.22}$$

The expression under the square root here is positive definite, and smaller than 1, since $0 < 4Ka^2 < 1$ and also (it can be shown) $0 < C_0^\ell < 1$ for all relevant ℓ, m, s. We note that $\beta \to 1$ in both limits $r \to \infty$ and $r \to r_+$, meaning the modified coordinate $\tilde{r}_*$

[1] The situation is less clear for strongly bound orbits around a near-extremal black hole, where one may expect $\omega \sim 1/M$. This case will require further investigation. We suspect that coupling between modes remains subdominant even in that case, thanks to the time-delay effect noted in [98] (recalling that coupling terms all involve t derivatives).

coincides with the usual r_* in both limits. Introducing also the modified advanced and retarded times $\tilde{v} := t + \tilde{r}_*$ and $\tilde{u} := t - \tilde{r}_*$, Eq. (3.17) becomes

$$\phi^\ell_{,\tilde{u}\tilde{v}} + \tilde{U}(r)\phi^\ell_{,\tilde{u}} + \tilde{V}(r)\phi^\ell_{,\tilde{v}} + \tilde{W}(r)\phi^\ell + \tilde{K}(r)\mathcal{I}(\phi^{\ell\pm1}, \phi^{\ell\pm2}) = 0, \tag{3.23}$$

with

$$\tilde{K}(r) := K(r)/\beta^2, \qquad \tilde{W}(r) := W(r)/\beta^2, \tag{3.24}$$

$$\tilde{U} := \frac{1}{2\beta^2}\left[(1+\beta)U + (1-\beta)V + \frac{1}{2}\frac{d\beta}{dr_*}\right], \tag{3.25}$$

$$\tilde{V} := \frac{1}{2\beta^2}\left[(1+\beta)V + (1-\beta)U - \frac{1}{2}\frac{d\beta}{dr_*}\right]. \tag{3.26}$$

The form (3.23) (without a $\phi^\ell_{,tt}$ term) is more conveniently amenable to a finite-difference representation, especially in double-null-type coordinates.

We envisage a numerical implementation of Eq. (3.23) using a finite-difference scheme based on $\tilde{u}, \tilde{v}$ coordinates. For stationary modes of the perturbation, and in the Schwarzschild case, the coupling terms in (3.23) vanish, and the equation takes a simple form, ready for numerical implementation ℓ by ℓ. In the general Kerr case, the equation can first be recast in a matrix form, introducing the vector variable $\vec{\phi} := \{\phi^{\ell=1}, \phi^{\ell=2}, \ldots, \phi^{\ell_{\rm max}}\}$, where $\ell_{\rm max}$ is a suitable cutoff; in many problems, including the GSF problem, the large-ℓ truncation error may be controlled and made sufficiently small. The matrix equation can then be discretized and solved as in the Schwarzschild case, this time obtaining all ℓ modes at once. Since the coupling between modes is finite and "weak" (modes couple only to nearest and next-to-nearest neighbors), the matrices involved are band diagonal and hence comfortably amenable to numerical manipulation.

3.2 Boundary conditions for $\phi^\pm_{s\ell m}$

Typically, and in the GSF problem in particular, we require the physical, "retarded" solution for the metric perturbation, i.e., the one for which there is no radiation coming in from past null infinity, and no radiation coming out of the past event horizon. In frequency-domain implementations, and also in Cauchy-type time evolutions, this requirement is imposed via a choice of boundary conditions on suitable timelike boundaries. In a characteristic-type 1+1D evolution of the kind we have in mind here, the numerical domain has no timelike boundaries, and the solution is completely determined

once initial data are specified on two initial characteristic rays. In principle, one should be able to select the retarded solution via a suitable choice of characteristic initial data (though in practice we shall adopt a much simpler approach, described below). But even though boundary conditions are not actively imposed at each time step, knowledge of the form of physical boundary conditions is still important, for a number of reasons. First, as we shall see, such knowledge informs our choice of regulator functions [specifically, the factor $(r\Delta^s)^{-1}$ in Eq. (3.5)] that control the behavior of the numerical field at large retarded and advanced times. Our choice of regulator will be such that the physical solution is globally bounded in magnitude. Second, once a numerical solution is obtained, it is important to check that it is indeed the desired physical solution. Third, there are cases where pieces of the physical field may be determined analytically (see Sec. 4.1 for an example), and in such cases the choice of a particular solution requires knowledge of the physical boundary conditions.

Our goal now, therefore, is to prescribe physical boundary conditions for the time-radial fields $\phi^{\pm}_{s\ell m}(t,r)$. In Sec. 3.2.1 we will consider the behavior at null infinity, and in Sec. 3.2.2 the behavior at the event horizon. In Sec. 3.2.3 we will discuss the special case of stationary modes. In all cases we will base our analysis on a study of the asymptotic form of solutions to the 1+1D time-domain Teukolsky equation (3.23). We recall the coordinates $(\tilde{u},\tilde{v})$ are interchangeable with the standard (u,v) in both asymptotic limits.

3.2.1 Behavior at null infinity

Consider solutions of (3.23) that for $r \gg M$ have the asymptotic forms $\sim r^{\alpha}e^{-i\omega u}$ ("outgoing waves") or $\sim r^{\beta}e^{-i\omega v}$ ("incoming waves"), for some frequency $\omega \neq 0$ (the case $\omega = 0$ will be considered separately below). We determine the powers α and β by substituting each of these asymptotic-form *Ansätze* in Eq. (3.23). When expanding in powers of $1/r$ (at fixed t) we find

$$\tilde{V}(r) = s/r + O(1/r^2), \qquad \tilde{K}(r), \tilde{U}(r), \tilde{W}(r) = O(1/r^2). \tag{3.27}$$

Thus Eq. (3.23) takes the asymptotic form

$$\phi^{+}_{s,uv} + \frac{s}{r}\phi^{+}_{s,v} = 0. \tag{3.28}$$

where we suppress the ℓ, m indexes to improve readability. Substituting the ingoing/outgoing *Ansätze* into the equation, the leading-order terms are

$$\begin{aligned} -\frac{1}{2}i\alpha\omega r^{\alpha-1}e^{-iu\omega} + O(r^{\alpha-2}) = 0, \\ (\frac{1}{2}\beta - s)r^{\beta-1}e^{-iv\omega} + O(r^{\beta-2}) = 0, \end{aligned} \tag{3.29}$$

giving $\alpha = 0$ and $\beta = 2s$. Thus we have the two asymptotic solutions

$$\begin{aligned} \phi^+_{s\omega} &\sim e^{-i\omega u} \quad \text{(physical)}, \\ \phi^+_{s\omega} &\sim r^{2s}e^{-i\omega v} \quad \text{(nonphysical)}. \end{aligned} \tag{3.30}$$

It is easy to check, using (3.5) and the reconstruction formula (2.75), that the first solution yields a reconstructed metric with a large-r asymptotic form $h^{\text{rec}+}_{\alpha\beta} \sim e^{-i\omega u}/r$ (in suitable Cartesian coordinates), representing a purely outgoing wave—hence the designation "physical". The second solution yields a perturbation $h^{\text{rec}+}_{\alpha\beta} \sim e^{-i\omega v}$ (multiplied by some factor of r), which does not represent a purely outgoing wave—hence "nonphysical".

We note that, for the physical solution, the magnitude of ϕ^+_s approaches a constant, generally nonzero value at future null infinity ($v \to \infty$ for any fixed u). This behavior, which is computationally desirable, was achieved by introducing the factor $(r\Delta^s)^{-1} \sim r^{-2s-1}$ in Eq. (3.5). Without this factor, the physical solution would blow up as $\sim r^3$ for $s = -2$ (IRG), or would fall off rapidly, as $\sim r^{-5}$, for $s = +2$ (ORG), both types of behavior being computationally problematic.

Note also that, for $s = +2$, any nonphysical solution blows up rapidly (as $\sim r^4$) at infinity. This means that, in an ORG implementation, a numerical solution ϕ^+_s that can be demonstrated to remain bounded at infinity (even as the finite-difference step size tends to zero) is automatically guaranteed to be the physical solution, i.e., the one satisfying the correct, outgoing boundary conditions. An IRG calculation does not share this convenient feature: for $s = -2$, nonphysical modes decay rapidly (as $\sim r^{-4}$) at infinity and would be hard to identify in the data. In this sense, it is computationally advantageous to calculate the external field ϕ^+_s in the ORG.

3.2.2 Behavior at the event horizon

Moving on to consider the behavior along the horizon, examine the form of (3.23) for small Δ. Noting $\tilde{K}(r), \tilde{V}(r), \tilde{W}(r) = O(\Delta)$ while $\tilde{U}(r) = O(\Delta^0)$, we find that, at leading order in Δ, the equation reduces to

$$\phi^-_{s,uv} + \left(\frac{s(M-r_+)}{2Mr_+} + im\Omega_{\rm H}\right)\phi^-_{s,u} = 0. \tag{3.31}$$

This equation admits the two pure-mode asymptotic solutions

$$\begin{aligned} \phi^-_{s\ell m\omega} &\sim e^{-i\omega v} \quad \text{(physical)}, \\ \phi^-_{s\ell m\omega} &\sim \Delta^s e^{-i\omega u} e^{-2im\Omega_{\rm H} r_*} \quad \text{(nonphysical)}. \end{aligned} \tag{3.32}$$

where we reintroduced the ℓ, m indexes as the asymptotic solutions depend explicitly on m. It can be checked that the first solution yields a reconstructed perturbation that (in suitable, horizon-regular coordinates such as $\{v, r, \theta, \tilde{\varphi}\}$) has the asymptotic form $h^{{\rm rec}-}_{\alpha\beta} \sim e^{-i\omega v}$, representing a purely ingoing wave at the future event horizon. This is therefore the "physical" solution.[2] For the physical solution, $\phi^-_{s\ell m\omega}$ approaches a finite, generally nonzero value at the horizon ($u \to \infty$ for any fixed v), which is computationally desirable. Indeed, to achieve this was the purpose of our introduction of a regulator factor Δ^{-s} in Eq. (3.5).

It can also be checked that the second solution in (3.32) produces a reconstructed perturbation that, in coordinates regular on the past event horizon, has the asymptotic behavior $h^{{\rm rec}-}_{\alpha\beta} \sim e^{-i\omega u}$ there.[3] This solution thus represents nonphysical outgoing waves at the past horizon. Note that for $s = -2$ the nonphysical modes blow up as $\sim \Delta^{-2}$ at the horizon. Hence, in an IRG reconstruction it is sufficient to demonstrate the boundedness of the internal numerical solution $\phi^-_{s\ell m\omega}$ at the horizon in order to establish that it represents the true, physical solution (up to numerical error). In the ORG, on the other hand, nonphysical modes decay rapidly (as $\sim \Delta^2$) near the horizon and would be hard

[2] From Eq. (3.5) we see that, for the physical solution, the Hertz potential Φ^-_s itself is $\propto \Delta^{-s}$ at the horizon. This apparent irregular behavior owes itself simply to the irregularity of the Kinnersley tetrad at the horizon; see, e.g., Sec. V of [99].

[3] Note that our coordinate $\tilde{\varphi}$ is *not* regular on the past horizon, and it is this coordinate irregularity that gives rise to the singular factor $e^{-2im\Omega_{\rm H} r_*}$ in the "nonphysical" solution in (3.32). When we say that this solution is nonphysical we do not refer to this coordinate irregularity but to the fact that the solution represents outgoing waves at the past horizon.

to identify there if they existed in the numerical data. Thus, there is a computational advantage in calculating the internal field $\phi^-_{s\ell m}$ in the IRG.

3.2.3 Stationary modes

Finally, let us consider the asymptotic behavior of stationary, t-independent (or, equivalently, $\omega = 0$) modes. Substituting the *Ansatz* $\phi \sim r^\alpha$ in Eq. (3.23) and considering the leading-order beavior at $r \gg M$, one obtains $\alpha = s - \ell$ or $\ell + s + 1$, and hence the two asymptotic solutions

$$\begin{aligned} \phi^+_{s\ell m} &\sim r^{-\ell+s} \quad \text{(physical)}, \\ \phi^+_{s\ell m} &\sim r^{\ell+s+1} \quad \text{(nonphysical)}. \end{aligned} \tag{3.33}$$

The designations 'physical' and 'nonphysical' here come from examining the behavior of the physical perturbation associated with each solution. To eliminate gauge dependence, it is instructive to consider, for example, the corresponding Weyl scalars Ψ_0 or Ψ_4. Using Eq. (3.5) with (2.49) and (2.50) [or with (2.52) and 2.53)] shows $\Psi_0, \Psi_4 \sim r^{-\ell-3}$ for the first solution in (3.33), and $\Psi_0, \Psi_4 \sim r^{\ell-2}$ for the second, in both the IRG and ORG cases. Thus, the first solution corresponds to a perturbation whose curvature decays at infinity (hence 'physical'), while the second solution ('nonphysical') corresponds to a perturbation whose curvature does not decay at infinity (and, for $\ell > 2$, it actually blows up there).

We move on to consider the behavior on the event horizon. Two stationary asymptotic solutions there are

$$\begin{aligned} \phi^-_{s\ell m} &\sim \text{const} \quad \text{(physical)}, \\ \phi^-_{s\ell m} &\sim \Delta^s \quad \text{(nonphysical)}, \end{aligned} \tag{3.34}$$

where, importantly, the first solution has a regular Taylor expansion on the horizon, while the second solution also contains a high-order contribution of the form $(\log \Delta) \times$ a Taylor series in Δ. It can be checked that the corresponding Weyl scalars have the behavior $\Psi_s \sim \Delta^{-s}$ for the first solution, and $\Psi_s \sim \Delta^0$ (plus higher-order log terms) for the second solution. As explained (e.g.) in Sec. V of Ref. [99], carefully taking into account the irregularity of the Kinnersley tetrad at the horizon, for a smooth physical

perturbation it is not the Weyl scalars themselves that are regular (smooth) at the horizon, but rather the product $\Delta^s\Psi_s$. Applying this criterion to our solutions, we have that $\Delta^s\Psi_s$ is perfectly smooth for the first solution ("physical"), but non-smooth for the second solution ("nonphysical"). In the latter case, $\Delta^s\Psi_s$ blows up like Δ^{-2} for $s=-2$, while for $s=+2$ the differentiability is spoiled by the $\log\Delta$ term.

We note that, in terms of our variable $\phi^{\pm}(t,r)$, the stationary piece of the physical perturbation is bounded everywhere, just like the rest of the perturbation. For nonphysical stationary perturbations, ϕ^- blows up on the horizon in the IRG case, and ϕ^+ blows up at infinity in both the IRG and ORG cases. This is true for all relevant values of ℓ, i.e. $\ell \geq 2$.

3.2.4 Summary

In summary, our choice of time-radial fields $\phi^{\pm}_{s\ell m}(t,r)$ is such that, in terms of these variables, the physical, retarded solution is bounded both at infinity and on the horizon—and, in fact, anywhere else in the computation domain. This is a convenient feature, computationally. Furthermore, we have noted that all nonphysical ORG solutions $\phi^+_{s\ell m}$ blow up at infinity, while all nonphysical IRG solutions $\phi^-_{s\ell m}$ blow up at the horizon. Thus, boundedness of an ORG solution at infinity implies that the correct outgoing boundary conditions are satisfied at infinity, and boundedness of an IRG solution at the horizon implies that the correct ingoing boundary conditions are satisfied on the horizon.

Unfortunately, we cannot make a stronger statement: In the ORG case, boundedness of the solution on the horizon does *not* necessarily mean that boundary conditions are satisfied there, because nonphysical ORG modes are subdominant on the horizon. Similarly, in the IRG case, boundedness of the solution at infinity does *not* necessarily imply, in general, that boundary conditions are satisfied there, because nonphysical IRG modes are subdominant at infinity (with the exception of stationary modes, which blow up there). This situation suggests that, at least from a computational point of view, it would be convenient to work with a mixed-gauge field composed of the ORG $\phi^+_{s\ell m}$ and the IRG $\phi^-_{s\ell m}$. However, the formulation of jump conditions on the orbit (see below) would then be harder, and one would also need to generalize the SF formulation to accommodate the possibility of such a mixed-gauge perturbation. It would be worth

exploring the mixed-gauge idea in future work, but here we shall stick with the more straightforward single-gauge approach.

3.3 Jump conditions for $\phi^{\pm}$ across $\mathcal{S}$

Finally, we need a set of rules that relate the fields $\phi^{+}_{s\ell m}$ and $\phi^{-}_{s\ell m}$ along the particle's timelike trajectory in the 1+1D domain. Specifically, we need the "jumps"

$$[\phi] := \lim_{\epsilon\to 0}\left[\phi^{+}(t, r_p(t)+\epsilon) - \phi^{-}(t, r_p(t)-\epsilon)\right], \tag{3.35}$$

as well as the jumps in the first derivatives—say, $[\phi_{,\tilde{u}}]$ and $[\phi_{,\tilde{v}}]$. (In this subsection we occasionally, where possible, omit the indices $s\ell m$ for brevity.) The jumps in higher-order derivatives may also be required, depending on the particular numerical method implemented and on the order of numerical convergence sought. Our goal now is to describe a method for determining these jumps, as functions along the particle's world-line. We will assume that the jumps $[\psi_{\pm 2}]$ in the physical Weyl scalars, and in their derivatives, are already known. These jumps may be deduced directly, in analytic form, from the source term of the (1+1D version of the) Teukolsky equation, without needing to solve the equation for the Weyl scalars themselves—a specific example will be worked out explicitly in Appendix A. Thus, we will be seeking to determine the jumps in the Hertz potential and its derivatives in terms of the jumps in the physical Weyl scalars and their derivatives.

Our starting point are Eqs. (2.49), (2.50), (2.52) and (2.53), as applied to the vacuum solutions $\Phi^{\pm}_{s}$. Recall these are relations that the vacuum Hertz potential must satisfy given the physical Weyl scalars Ψ_0 or Ψ_4. First, we need to obtain the 1+1D version of these equations. To this end, we substitute the expansion (3.5) for $\Phi^{\pm}_{s}$ on the left-hand side of each of these relations, and on the right-hand side we substitute for $\Psi_4 =: \varrho^4\Psi_{s=-2}$ and $\Psi_0 =: \Psi_{s=+2}$ using the analogous expansions

$$\Psi^{\pm}_{s} = (r\Delta^{s})^{-1}\sum_{\ell=2}^{\infty}\sum_{m=-\ell}^{\ell}\psi^{\pm}_{s\ell m}(t,r)\,{}_{s}Y_{\ell m}(\theta,\tilde{\varphi}) \tag{3.36}$$

for $s = \pm 2$.

Considering first the relations (2.49) and (2.50) (whose frequency-domain versions are often referred to as "radial inversion formulas"), we observe that the differential operators on the left-hand side do not couple between different ℓ modes: the equations relate each (spin-weighted spherical-harmonic) ℓ mode of the Hertz potentials $\bar{\Phi}^{\pm}_{s}$ and their derivatives to the same ℓ mode of the Weyl scalars $\Psi^{\pm}_{-s}$ (with m opposite in sign). Using (3.4) and the orthogonality of ${}_{s}Y_{\ell m}$ we obtain, for each ℓ, m,

$$8r\Delta^2\mathcal{D}_l^4\left(\Delta^2\bar{\phi}^{\mathrm{IRG}\pm}_{\ell m}/r\right) = (-1)^m\psi^{\pm}_{2,\ell,-m}, \tag{3.37}$$

$$\frac{1}{2}r\tilde{\mathcal{D}}_n^4\left(\bar{\phi}^{\mathrm{ORG}\pm}_{\ell m}/r\right) = (-1)^m\psi^{\pm}_{-2,\ell,-m}, \tag{3.38}$$

where the differential operators are

$$\begin{aligned} \mathcal{D}_l &:= \Delta^{-1}\left(\Sigma\partial_v - ima\right), \\ \tilde{\mathcal{D}}_n &:= -(\Sigma/\Delta)\partial_u; \end{aligned} \tag{3.39}$$

here ∂_v is taken with fixed u, and ∂_u is taken with fixed v. We observe that (3.37) and (3.38) are effectively *ordinary* differential equations for $\bar{\phi}^{\mathrm{IRG}\pm}_{\ell m}$ and $\bar{\phi}^{\mathrm{ORG}\pm}_{\ell m}$, with independent variables v and u, respectively.

In general, the alternative relations (2.52) and (2.53) ("angular inversion formulas") are less useful here, because they feature operators that *do* mix between different ℓ modes, giving rise to mode-coupled relations; even worse, the equations relate each ℓ mode of $\Phi^{\pm}$ to an *infinite* number of ℓ modes of $\Psi^{\pm}_{s}$. The coupling disappears only in the Schwarzschild case, $a = 0$, where, in fact, the angular inversion formulas become extremely simple (since the operators $\tilde{\mathcal{L}}_s$ and $\mathcal{L}_s$ reduce to, respectively, spin-lowering and spin-raising operators when they act on spin-weighted spherical harmonics). This simplicity was noted previously by Lousto and Whiting in [83], where they considered 1+1D metric reconstruction in Schwarzschild. Here, however, our ambition is to treat the more general Kerr case, so we will utilize the "radial" inversion equations—even as (in the next two sections) we consider a Schwarzschild example.

Focusing thus on the 1+1D inversion formulas (3.37) and (3.38), we first note that the *general* solution for each of these two ODEs can be written down in a simple closed form (involving four nested integrals with respect to v or u, respectively). Based on the form of these general solutions it is straightforward to show (in analogy with Ori's analysis in

[89]) that $\phi^{\rm IRG\pm}_{\ell m}$ and $\phi^{\rm ORG\pm}_{\ell m}$ each admits a *unique* particular solution that also satisfies the vacuum Teukolsky equation (3.23), as required. This confirms the uniqueness of the Hertz potential in the reconstruction procedure.

However, the above closed-form particular solutions for $\phi^{\rm IRG\pm}_{\ell m}$ and $\phi^{\rm ORG\pm}_{\ell m}$ involve integrals of the Weyl scalars ($\psi^{\pm}_{2}$ and $\psi^{\pm}_{-2}$, respectively) along rays extending to infinity and down to the event horizon, and to evaluate them in practice would require solving the appropriate sourced Teukolsky equations as a preliminary step. In our method we wish to bypass this preliminary step, and work directly with the Hertz potential; we wish to have no recourse to knowledge of the Weyl scalars themselves (except the values of their jumps across the particle, which, as mentioned, are accessible directly from the source of the Teukolsky equation). Our goal, therefore, is to express the jumps in ϕ (and its derivatives) in terms of the *jumps* in ψ (and its derivatives) alone. In what follows we describe a procedure that achieves that.

Let us start with the IRG case (the ORG case will follow analogously). Evaluating the difference between the '+' and '−' versions of Eq. (3.37) at $r = r_{\rm p}(t)$ yields a relation of the form

$$\sum_{n=0}^{4} f_n(r_p)[\partial_{\tilde v}^n \phi^{\rm IRG}_{\ell m}] = (-1)^m \left[\bar\psi_{2,\ell,-m}\right], \tag{3.40}$$

in which $f_n(r_{\rm p})$ are some smooth functions along the orbit, and the jumps on the right-hand side are assumed known. For a reason that will become clear shortly, we also need the $\tilde v$ derivative of (3.37), which yields

$$\sum_{n=0}^{5} \tilde f_n(r_p)[\partial_{\tilde v}^n \phi^{\rm IRG}_{\ell m}] = (-1)^m \left[(\bar\psi_{2,\ell,-m})_{,\tilde v}\right], \tag{3.41}$$

where $\tilde f_n(r_{\rm p})$ are some other smooth functions, and the jumps on the right-hand side are also known. Our goal is to determine the jumps $[\phi]$ and $[\phi_{,\tilde v}]$, as well as $[\phi_{,\tilde u}]$, as functions along the orbit (here and in the following discussion we omit the labels ℓ, m and IRG for brevity).

Using an overdot to denote $d/d\tau$, where τ is proper time along the orbit, we write

$$[\dot\phi] = \dot{\tilde u}_{\rm p}\,[\phi_{,\tilde u}] + \dot{\tilde v}_{\rm p}\,[\phi_{,\tilde v}]\,, \tag{3.42}$$

$$[\dot\phi_{,\tilde v}] = \dot{\tilde u}_{\rm p}\,[\phi_{,\tilde v\tilde u}] + \dot{\tilde v}_{\rm p}\,[\phi_{,\tilde v\tilde v}]\,, \tag{3.43}$$

where $\tilde u_{\rm p}(\tau)$ and $\tilde v_{\rm p}(\tau)$ are the values of $\tilde u$ and $\tilde v$ at a worldline point with proper time

τ. Equation (3.42) gives $[\phi_{,\tilde{u}}]$ in terms of $[\dot{\phi}]$ and $[\phi_{,\tilde{v}}]$. In Eq. (3.43) we replace $[\phi_{,\tilde{v}\tilde{u}}]$ in favor of $[\phi]$, $[\phi_{,\tilde{v}}]$ and $[\phi_{,\tilde{u}}]$ using the Teukolsky equation (3.23), and hence express $[\phi_{,\tilde{v}\tilde{v}}]$ in terms of $[\phi]$ and $[\phi_{,\tilde{v}}]$ (and their τ derivatives) alone. (For $a \neq 0$ this relation will involve also the jump in the coupling terms $\mathcal{I}$. Let us ignore these terms for a moment to simplify the discussion; we shall return to them momentarily.) Next, we write

$$[\ddot{\phi}] = \ddot{\tilde{v}}_{\rm p}\,[\phi_{,\tilde{v}}] + \ddot{\tilde{u}}_{\rm p}\,[\phi_{,\tilde{u}}] + \dot{\tilde{u}}^2_{\rm p}\,[\phi_{,\tilde{u}\tilde{u}}] + \dot{\tilde{v}}^2_{\rm p}\,[\phi_{,\tilde{v}\tilde{v}}] + 2\dot{\tilde{v}}_{\rm p}\dot{\tilde{u}}_{\rm p}\,[\phi_{,\tilde{v}\tilde{u}}]\,, \tag{3.44}$$

$$[\ddot{\phi}_{,\tilde{v}}] = \ddot{\tilde{v}}_{\rm p}\,[\phi_{,\tilde{v}\tilde{v}}] + \ddot{\tilde{u}}_{\rm p}\,[\phi_{,\tilde{v}\tilde{u}}] + \dot{\tilde{u}}^2_{\rm p}\,[\phi_{,\tilde{v}\tilde{u}\tilde{u}}] + \dot{\tilde{v}}^2_{\rm p}\,[\phi_{,\tilde{v}\tilde{v}\tilde{v}}] + 2\dot{\tilde{v}}_{\rm p}\dot{\tilde{u}}_{\rm p}\,[\phi_{,\tilde{v}\tilde{v}\tilde{u}}]\,, \tag{3.45}$$

and use (3.23) again to replace all mixed-derivative jumps with lower-order-derivative jumps. We thus express $[\phi_{,\tilde{u}\tilde{u}}]$ and (in turn) $[\phi_{,\tilde{v}\tilde{v}\tilde{v}}]$ in terms of $[\phi]$ and $[\phi_{,\tilde{v}}]$ (and their first and second τ derivatives) alone.

Proceeding in a similar way, we can determine $[\phi_{,\tilde{u}\tilde{u}\tilde{u}}]$ and $[\phi_{,\tilde{v}\tilde{v}\tilde{v}\tilde{v}}]$ in terms of $[\phi]$, $[\phi_{,\tilde{v}}]$ and their first, second and third τ derivatives; and finally we can determine $[\phi_{,\tilde{u}\tilde{u}\tilde{u}\tilde{u}}]$ and $[\phi_{,\tilde{v}\tilde{v}\tilde{v}\tilde{v}\tilde{v}}]$ in terms of $[\phi]$, $[\phi_{,\tilde{v}}]$ and their first, second, third and fourth τ derivatives. Equations (3.40) and (3.41) can thus be written as a coupled set of ODEs for $[\phi]$ and $[\phi_{,\tilde{v}}]$:

$$\sum_{n=0}^{3}\left(a_n(\tau)\frac{d^n\,[\phi]}{d\tau^n} + b_n(\tau)\frac{d^n\,[\phi_{,\tilde{v}}]}{d\tau^n}\right) + \mathcal{I}\text{-terms} = (-1)^m\left[\bar{\psi}_{2,\ell,-m}\right], \tag{3.46}$$

$$\sum_{n=0}^{4}\left(c_n(\tau)\frac{d^n\,[\phi]}{d\tau^n} + d_n(\tau)\frac{d^n\,[\phi_{,\tilde{v}}]}{d\tau^n}\right) + \mathcal{I}\text{-terms} = (-1)^m\left[(\bar{\psi}_{2,\ell,-m})_{,\tilde{v}}\right], \tag{3.47}$$

where $a_n(\tau),\ldots,d_n(\tau)$ are certain smooth functions along the worldline (depending only on $r_{\rm p}, \dot{r}_{\rm p}, \ldots, d^4 r_{\rm p}/d\tau^4$, as well as on ℓ). The terms collected under '$\mathcal{I}$-terms' are certain linear combinations of the coupling term $\mathcal{I}(\phi^{\ell\pm1}, \phi^{\ell\pm2})$ and its $\tilde{v}$ and $\tilde{u}$ derivatives (up to third derivatives), which have entered the relations via our use of the Teukolsky equation (3.23). Unfortunately, the general explicit form of Eqs. (3.46) and (3.47) is too unwieldy to be presented here in any meaningful way, but it can be straightforwardly obtained using computer algebra tools, following the procedure described above. In Chapter 4 we will present explicit expressions for the special case of circular geodesic orbits in Schwarzschild spacetime [where all $\mathcal{I}$-terms drop, and the coefficients $a_n,\ldots,d_n$ depend only on $r_{\rm p}$(=const)].

Let us for the moment ignore the coupling terms in Eqs. (3.46) and (3.47). Then these equations constitute a coupled set of fourth-order ODEs for the jumps $[\phi_{\ell m}]$ and $[\phi_{\ell m,\tilde{v}}]$ as functions along the orbit. How to solve these equations depends on the particular problem under consideration. If the perturbation is sourced by a particle on a fixed bound geodesic orbit, then the jumps may be assumed to exhibit the same periodicity as the orbit (two fundamental frequencies, in general), and the ODEs (3.46) and (3.47) can then be conveniently recast as a set of algebraic equations, one for each frequency (the assumption of periodicity then effectively selects a particular solution of the ODEs).[4] If the perturbation is sourced by a slowly evolving orbit (e.g., under the effect of the SF), then one should still be able to obtain a frequency-by-frequency algebraic solution at some initial point along the orbit, then solve the set (3.46) and (3.47) as ODEs, starting from these initial conditions. For nonperiodic (parabolic- or hyperbolic-type) orbits, initial conditions may be formulated at infinity, using an asymptotic analysis. In Chapter 4 we give the explicit physical solution of Eqs. (3.46) and (3.47) for the special case of circular geodesic orbits in Schwarzschild spacetime.

How should the ℓ-mode coupling terms in Eqs. (3.46) and (3.47) be dealt with, in the Kerr case? As already mentioned, we expect the $\mathcal{I}$-term in the field equation (3.17) to be small, in general, in a certain relative sense. The coupling terms in the jump equations (3.46) and (3.47) will be small in the same sense. One could then incorporate these terms perturbatively, using an iterative scheme: In the first iteration, Eqs. (3.46) and (3.47) are solved for each ℓ, m with the coupling terms dropped. The solutions are then used to calculate the $\mathcal{I}$-terms in Eqs. (3.46) and (3.47), and the equations are solved again, with these $\mathcal{I}$-terms as sources. One keeps iterating in this manner until a sufficiently convergent solution is achieved; the smaller the coupling terms are in relative magnitude, the less iterations should be required. How computationally tasking this procedure may prove to be would depend on the number of iterations required and on whether the jump equations are solved as ODEs or via a mode decomposition. Yet we expect the computational cost of calculating the jumps to be negligible compared with the cost of solving the field equation in the time domain.

At any rate, once the jumps $[\phi]$ and $[\phi_{,\tilde{v}}]$ have been computed as functions along the

[4] By solving the jump equations (3.46) and (3.47) frequency by frequency we would *not* be reverting to the standard frequency-domain approach to metric reconstruction: the field equation (3.17) would still be solved in the time domain. In Appendix C we follow this procedure and calculate the jumps for any bound geodesic orbit in Schwarzschild

orbit, the jumps in any higher $\tilde{v}$ and $\tilde{u}$ derivatives of ϕ are calculable algebraically using the order-reduction procedure described a couple of paragraphs above: $[\phi_{,\tilde{u}}]$ is obtained from (3.42), then $[\phi_{,\tilde{v}\tilde{v}}]$ is obtained from (3.43), and so on.

Finally, the ORG version of the problem is dealt with in a completely analogous manner, this time starting with Eq. (3.38). The procedure again yields ODEs of the form (3.46)-(3.47), but now with $[\phi_{,\tilde{v}}]$ replaced with $[\phi_{,\tilde{u}}]$ and, on the right-hand side, $\bar{\psi}_{2,\ell,-m}$ replaced with $\bar{\psi}_{-2,\ell,-m}$. The explicit form of the coefficients $a_n(\tau), \ldots, d_n(\tau)$ and of the $\mathcal{I}$-terms will also differ.

3.3.1 An illustrative example: static particle in flat space

Let us illuminate the construction of junction conditions using the simple case of a static particle in flat space. This toy model will provide a clear idea of the method that will be applied later on to more relevant cases. The Teukolsky equation and the inversion relation reduce to

$$\partial_r^2 \phi^*_{\ell m} = -\frac{6}{r}\partial_r \phi^*_{\ell m} + \frac{\lambda_0}{r^2}\phi^*_{\ell m}, \tag{3.48}$$

$$\partial_r^4 \phi^*_{\ell m} = \psi_{2,\ell-m}, \tag{3.49}$$

where we defined $\lambda_0 = (\ell+3)(\ell-2)$. With the first equation we are able to write the second derivative $\partial_r^2 \phi^*_{\ell m}$ in terms of $\partial_r \phi^*_{\ell m}$ and $\phi^*_{\ell m}$. By taking derivatives of the same equation we can write higher derivatives of $\phi^*_{\ell m}$ in terms of $\partial_r \phi^*_{\ell m}$ and $\phi^*_{\ell m}$ by substituting again from Eq. (3.48). In this manner we obtain

$$\begin{aligned}
\partial_r^3 \phi^*_{\ell m} &= \frac{(\lambda_0+42)\partial_r \phi^*_{\ell m}}{r^2} - \frac{8\lambda_0 \phi^*_{\ell m}}{r^3}, \\
\partial_r^4 \phi^*_{\ell m} &= \frac{\lambda_0(\lambda_0+66)\phi^*_{\ell m}}{r^4} - \frac{16(\lambda_0+21)\partial_r \phi^*_{\ell m}}{r^3}, \\
\partial_r^5 \phi^*_{\ell m} &= \frac{(\lambda_0^2+210\lambda_0+3024)\,\partial_r \phi^*_{\ell m}}{r^4} - \frac{20\lambda_0(\lambda_0+30)\phi^*_{\ell m}}{r^5}.
\end{aligned} \tag{3.50}$$

Substituting the above into the inversion relation and its r derivative, and taking the difference across the particle, we find

$$\begin{aligned}
&\frac{\lambda_0(\lambda_0+66)[\phi^*_{\ell m}]}{r^4} - \frac{16(\lambda_0+21)[\partial_r\phi^*_{\ell m}]}{r^3} = [\psi_{2,\ell-m}],\\
&\frac{(\lambda_0^2+210\lambda_0+3024)\,[\partial_r\phi^*_{\ell m}]}{r^4} - \frac{20\lambda_0(\lambda_0+30)[\phi^*_{\ell m}]}{r^5} = [\partial_r\psi_{2,\ell-m}].
\end{aligned} \tag{3.51}$$

This set can be inverted algebraically to derive $[\phi_{\ell m}]$ and $[\phi_{\ell m,r}]$ in terms of $[\psi_{2,\ell-m}]$ and $[\psi_{2,\ell-m,r}]$. Explicitly,

$$[\phi_{\ell m}] = \left(\frac{[\psi^*_{2,\ell-m}]}{B} - \frac{[\partial_r\psi^*_{2,\ell-m}]}{\tilde{B}}\right)\left(\frac{A}{B} - \frac{\tilde{A}}{\tilde{B}}\right)^{-1}, \tag{3.52}$$

$$[\partial_r\phi_{\ell m}] = \left(\frac{[\psi^*_{2,\ell-m}]}{A} - \frac{[\partial_r\psi^*_{2,\ell-m}]}{\tilde{A}}\right)\left(\frac{B}{A} - \frac{\tilde{B}}{\tilde{A}}\right)^{-1}. \tag{3.53}$$

where we defined

$$A := \frac{\lambda_0(\lambda_0+66)}{r^4}, \quad B := -\frac{16(\lambda_0+21)}{r^3}, \tag{3.54}$$

$$\tilde{A} := -\frac{20\lambda_0(\lambda_0+30)}{r^5}, \quad \tilde{B} := \frac{(\lambda_0^2+210\lambda_0+3024)}{r^4}. \tag{3.55}$$

In these equations, the jumps $[\psi^*_{2,\ell-m}]$ and $[\partial_r\psi^*_{2,\ell-m}]$ on the right-hand side are readily obtained from the source of the Teukolsky equations, as explained in Appendix A, where explicit expressions for these jumps are given in the case of circular orbits in Schwarzschild .

3.4 Summary of proposed evolution scheme

In summary, our evolution scheme for the Hertz potential consists of the 1+1D evolution equation (3.23), the asymptotic boundary conditions (3.30) and (3.32) ("physical"), and jump conditions across the particle's orbits, given as solutions to Eqs. (3.46) and (3.47). We have sketched how the actual jump conditions for the modes of the Hertz potential may be obtained in practice, depending on the orbital configuration.

In the next Chapters we will illustrate the application of our method with the concrete example of a particle moving in a fixed circular geodesic orbit around Schwarzschild and Kerr black holes. We formulate the evolution problem as applied to this case, including explicit expressions for the jumps across the particle. A full numerical implementation

will be presented in Chapter 5 for Schwarzschild and in Chapter 7 for Kerr. In our implementation, we will choose the IRG.

Chapter 4

Circular orbits in Schwarzschild (formulation)

As a first example, in this chapter we apply our new method to the case of circular geodesic orbits in Schwarzschild spacetime. An important simplification arises, since the individual (l, m) modes decouple from each other in the Schwarzschild case. Still, the example is useful in illustrating the applicability of some of the key novel features of our method, and in starting to build the necessary computational tools for a Kerr implementation.

In this Chapter we present the formulation of the problem, specializing the equations of the previous chapter to the case of circular geodesic orbits in Schwarzschild, and giving all relevant equations in explicit form. We also derive explicit analytical solutions for the axially-symmetric modes of the Hertz potential. A full numerical implementation will be presented in the Chapter 5.

Specialized to $a = 0$ (Schwarzschild case) and $s = -2$ (IRG), the 1+1D Teukolsky equation (3.23) becomes

$$\phi^{\ell}_{,uv} + U(r)\phi^{\ell}_{,u} + V(r)\phi^{\ell}_{,v} + W(r)\phi^{\ell} = 0, \tag{4.1}$$

with

$$U(r) = \frac{2M}{r^2}, \qquad V(r) = -\frac{2f}{r}, \tag{4.2}$$

$$W(r) = \frac{f}{4}\left(\frac{\lambda}{r^2} - \frac{2M}{r^3}\right), \tag{4.3}$$

where we have introduced

$$f(r) := 1 - 2M/r, \qquad \lambda := (\ell+2)(\ell-1). \tag{4.4}$$

Note that, in the Schwarzschild case, (i) the 1+1D Teukolsky equation does not couple between ℓ modes, so individual modes evolve independently of each other; (ii) the equation has no reference to the azimuthal number m (as expected, by virtue of the background's spherical symmetry); and (iii) the modified coordinates $\tilde{u}, \tilde{v}$ reduce to the standard coordinates u, v.

Next consider the jump equations (3.46)-(3.47). For $a = 0$, the coupling terms drop. Specializing further to a circular geodesic orbit with radius $r_{\rm p} = r_0 (= \text{const} > 2M)$, the coefficients on the left-hand side of (3.46)-(3.47) work out to be

$$\begin{aligned}
a_0 &= \frac{1}{2} r_0^4 f_0^2 \lambda(\lambda+2) \\
a_1 &= 2r_0^5 \left[\lambda - y(\lambda-3) - 2y^2(\lambda+5)\right]/\gamma_0, \\
a_2 &= 2r_0^6 f_0 (\lambda + 6y)/\gamma_0^2, \\
a_3 &= 16 M r_0^6/\gamma_0^3,
\end{aligned} \tag{4.5}$$

$$\begin{aligned}
b_0 &= 0 = b_2, \\
b_1 &= 4r_0^6 \left[\lambda - 2y(\lambda-1) - 6y^2\right]/\gamma_0, \\
b_3 &= 8 r_0^8/\gamma_0^3,
\end{aligned} \tag{4.6}$$

$$\begin{aligned}
c_0 &= r_0^3 f_0^2 (1-y)\lambda(\lambda+2), \\
c_1 &= f_0 r_0^4 \left[\lambda(\lambda+5) - 2(\lambda^2+2\lambda-6)y - 2(4\lambda+17)y^2 \right. \\
&\quad \left. + 12y^3\right]/\gamma_0, \\
c_2 &= 2r_0^5 \left[3\lambda + (15-7\lambda)y + 2(\lambda-23)y^2 + 24y^3\right]/\gamma_0^2, \\
c_3 &= 2 f_0 r_0^6 (\lambda + 22y)/\gamma_0^3, \\
c_4 &= 16 M r_0^6/\gamma_0^4,
\end{aligned} \tag{4.7}$$

$$
\begin{aligned}
d_0 &= \frac{1}{2} r_0^4 f_0^2 \lambda(\lambda+2), \\
d_1 &= 2 r_0^5 f_0 \left[3\lambda - 5(\lambda-1)y - 12y^2\right]/\gamma_0, \\
d_2 &= 2 r_0^6 \left[3\lambda + 2(5-3\lambda)y - 24y^2\right]/\gamma_0^2, \\
d_3 &= 16 f_0 r_0^7/\gamma_0^3, \\
d_4 &= 8 r_0^8/\gamma_0^4,
\end{aligned}
\tag{4.8}
$$

where

$$
y := \frac{M}{r_0}, \qquad f_0 := f(r_0), \qquad \gamma_0 := \left(1 - \frac{3M}{r_0}\right)^{-1/2}. \tag{4.9}
$$

We have used here the fact that, for circular geodesics, $\dot{u}_{\rm p} = \dot{v}_{\rm p} (= \gamma_0)$ and all higher-order τ derivatives of $u_{\rm p}$ and $v_{\rm p}$ vanish.

Furthermore, for a circular geodesic orbit we may assume that $[\phi_{\ell m}]$ depends on time solely via $e^{-im\Omega t}$, where

$$
\Omega := d\varphi_{\rm p}/dt = \sqrt{M/r_0^3} \tag{4.10}
$$

is the orbital angular velocity. Hence, in Eqs. (3.46)-(3.47) $d/d\tau$ may be replaced with $-im\Omega(dt_{\rm p}/d\tau) = -im\Omega\gamma_0$. These equations then become algebraic, taking the simple form

$$
\begin{aligned}
a_\Sigma\left[\phi\right] + b_\Sigma\left[\phi_{,v}\right] &= (-1)^m \left[\bar{\psi}_{2,\ell,-m}\right], \\
c_\Sigma\left[\phi\right] + d_\Sigma\left[\phi_{,v}\right] &= (-1)^m \left[\partial_v \bar{\psi}_{2,\ell,-m}\right],
\end{aligned}
\tag{4.11}
$$

where $a_\Sigma = \sum_{n=0}^{3} (-im\Omega\gamma_0)^n a_n$ and similarly for b_Σ, c_Σ and d_Σ. The solutions are

$$
\left[\phi^{\rm IRG}_{\ell m}\right] = \frac{(-1)^m}{\tilde{\Delta}} \left(d_\Sigma \left[\bar{\psi}_{2,\ell,-m}\right] - b_\Sigma \left[\partial_v \bar{\psi}_{2,\ell,-m}\right]\right), \tag{4.12}
$$

$$
\left[\partial_v \phi^{\rm IRG}_{\ell m}\right] = \frac{(-1)^m}{\tilde{\Delta}} \left(a_\Sigma \left[\partial_v \bar{\psi}_{2,\ell,-m}\right] - c_\Sigma \left[\bar{\psi}_{2,\ell,-m}\right]\right), \tag{4.13}
$$

where $\tilde{\Delta} := a_\Sigma d_\Sigma - b_\Sigma c_\Sigma$, and we have restored all labels. We find

$$
\tilde{\Delta} = \frac{1}{4} f_0^4 r_0^8 \left[\lambda^2(\lambda+2)^2 + (12mM\Omega)^2\right], \tag{4.14}
$$

which, we note, is positive definite.

Equations (4.12) and (4.13) give the desired jumps in the Hertz potential and its v

derivative in terms of the jumps in the Weyl scalar (Ψ_0) corresponding to the physical perturbation. The latter jumps are easily obtained from the distributional source of the Teukolsky equation satisfied by the Weyl scalar. In Appendix A we show how the jumps $\left[\partial_v \bar{\psi}_{2,\ell,-m}\right]$ and $\left[\bar{\psi}_{2,\ell,-m}\right]$ are derived, and give them explicitly for circular geodesic orbits in Schwarzschild. Once $[\phi]$ and $[\phi_{,v}]$ are known, the jumps in other derivatives of ϕ can be obtained iteratively, by means of the general procedure described in the previous chapter. For instance,

$$\begin{aligned}
[\phi_{,u}] &= -im\Omega\,[\phi] - [\phi_{,v}]\,, \\
[\phi_{,vu}] &= -U(r_0)\,[\phi_{,u}] - V(r_0)\,[\phi_{,v}] - W(r_0)\,[\phi]\,, \\
[\phi_{,uu}] &= -im\Omega\,[\phi_{,u}] - [\phi_{,vu}]\,, \\
[\phi_{,vv}] &= -im\Omega\,[\phi_{,v}] - [\phi_{,vu}]\,,
\end{aligned} \tag{4.15}$$

and so on.

4.1 Analytical solutions for $m = 0$

Axisymmetric modes (those with $m = 0$) are also stationary, and admit simple analytic solutions. We write these solutions here explicitly, as they will be useful in testing our numerical implementation in the next chapter.

For $m = 0$ we have $\phi^\ell_{,t} = 0$, and the homogeneous Teukolsky equation (4.1) reduces to

$$r\left[\left(r^3 f^2 \phi^\ell\right)' / (r^2 f)\right]' - \lambda\,\phi^\ell = 0, \tag{4.16}$$

where a prime denotes d/dr. Two linearly independent solutions are

$$\begin{aligned}
\phi^\ell &= \frac{\mathsf{P}^{m=2}_\ell(x)}{\sqrt{\lambda(\lambda+2)}(r-2M)} =: \phi^\ell_P(r), \\
\phi^\ell &= \frac{\mathsf{Q}^{m=2}_\ell(x)}{\sqrt{\lambda(\lambda+2)}(r-2M)} := \phi^\ell_Q(r),
\end{aligned} \tag{4.17}$$

where P^m_ℓ and Q^m_ℓ are associated Legendre functions of the first and second kinds, respectively, $x := (r-M)/M$, and the solutions have been normalized so as to render

the Wronskian ℓ independent:

$$(\phi_P^\ell)'\phi_Q^\ell - \phi_P^\ell(\phi_Q^\ell)' = \frac{M}{r^4 f^3}. \tag{4.18}$$

The solution ϕ_P^ℓ blows up as $\sim r^{\ell-1}$ at infinity but has a regular Taylor expansion at the event horizon. The solution ϕ_Q^ℓ is regular at infinity (where it falls off as $\sim r^{-\ell-2}$) but blows up as $\sim f^{-2}$ at the horizon.

Recalling Eqs. (3.33) and (3.34), we see that ϕ_P^ℓ satisfies physical boundary conditions on the horizon (but not at infinity), while ϕ_Q^ℓ satisfies physical boundary conditions at infinity (but not on the horizon). Therefore, a unique physical solution is given by

$$\begin{aligned} \phi^-_{-2\ell 0} &= C_\ell^-(r_0)\phi_P^\ell(r), \\ \phi^+_{-2\ell 0} &= C_\ell^+(r_0)\phi_Q^\ell(r). \end{aligned} \tag{4.19}$$

The coefficients $C_\ell^\pm(r_0)$ are determined from the two jump conditions $\phi^+_{\ell 0}(r_0) - \phi^-_{\ell 0}(r_0) = [\phi_{\ell 0}]$ and $(\phi^+_{\ell 0})'(r_0) - (\phi^-_{\ell 0})'(r_0) = [\phi'_{\ell 0}]$, giving

$$\begin{aligned} C_\ell^- &= r_0^4 f_0^3 \left([\phi_{\ell 0}]\, \phi'_Q(r_0) - [\phi'_{\ell 0}]\, \phi_Q^\ell(r_0) \right)/M, \\ C_\ell^+ &= r_0^4 f_0^3 \left([\phi_{\ell 0}]\, \phi'_P(r_0) - [\phi'_{\ell 0}]\, \phi_P^\ell(r_0) \right)/M, \end{aligned} \tag{4.20}$$

where we have substituted for the Wronskian from Eq. (4.18). The jumps $[\phi_{\ell 0}]$ and $[\phi'_{\ell 0}] = (2/f_0)\,[\phi_{\ell 0,v}]$ are calculated using Eq. (4.12) with Eqs. (A.16) and (A.17). For $m = 0$ we obtain the simple expressions

$$[\phi_{\ell 0}] = \frac{16\pi\mu\gamma_0}{r_0^2 f_0^2 \lambda(\lambda+2)} \left(y^2 \mathcal{Y}^\ell + i f_0 r_0 \Omega \mathcal{Y}^\ell_\theta \right), \tag{4.21}$$

$$\begin{aligned} [\phi'_{\ell 0}] = &-\frac{8\pi\mu\gamma_0}{r_0^3 f_0^3 \lambda(\lambda+2)} \Big\{ \left[2f_0(1-y)^2 + 4y^2 + y f_0 \lambda \right] \mathcal{Y}^\ell \\ &+ 2i f_0 (1+2y) r_0 \Omega \mathcal{Y}^\ell_\theta - f_0^2 \mathcal{Y}^\ell_{\theta\theta} \Big\}, \end{aligned} \tag{4.22}$$

where $\mathcal{Y}^\ell := {}_2\bar{Y}_{\ell 0}\left(\frac{\pi}{2}, 0\right)$, and $\mathcal{Y}^\ell_\theta$ and $\mathcal{Y}^\ell_{\theta\theta}$ are, respectively, the first and second derivatives of ${}_2\bar{Y}_{\ell m}(\theta, 0)$ with respect to θ, evaluated at $\theta = \pi/2$. We note that $\mathcal{Y}^\ell$ and $\mathcal{Y}^\ell_{\theta\theta}$ vanish for all odd values of ℓ, while $\mathcal{Y}^\ell_\theta$ vanishes for all even values of ℓ. Inspecting Eqs. (4.21) and (4.22) we consequently find that the jumps $[\phi_{\ell 0}]$ and $[\phi'_{\ell 0}]$ are real for even ℓ and imaginary for odd ℓ.

In summary, the axially symmetric piece of the IRG ℓ-mode Hertz potential in and out

of a circular geodesic orbit in Schwarzschild spacetime ($\phi^{-}_{-2\ell 0}$ and $\phi^{+}_{-2\ell 0}$, respectively) is given analytically by Eq. (4.19), with the coefficients $C^{\pm}_{\ell}(r_0)$ given in Eq. (4.20) [with Eqs. (4.21) and (4.22)]. The $m = 0$ solution is purely real for even ℓ and purely imaginary for odd ℓ. We have checked that our analytic solution (4.19) agrees with that obtained in Ref. [34] using a different method, namely starting with Ψ_4 and using the "angular" inversion formula (2.52).

Chapter 5

Circular orbits in Schwarzschild (numerical implementation)

In this chapter we present an illustrative numerical implementation of our method, specializing to circular geodesic orbits in Schwarzschild spacetime. Our goal here is twofold: First, we will be able to provide some test for our formulation by comparing numerical results with results obtained analytically or using other methods. Second, we aim to illustrate the kind of numerical implementation strategy we have in mind, which, we believe, can be used to tackle more general cases. Here we do not seek sophistication in our numerical technique, and we do not concern ourselves with questions of computational performance or code optimization. We leave such matters to future work.

5.1 Method

Our code solves for the IRG Hertz-potential modes $\phi^{\rm IRG}_{\ell m}(r,t)$ by evolving a finite-difference version of the hyperbolic equation (4.1) on a fixed 1+1D grid in double-null (u,v) coordinates, subject to the jump conditions (4.12) and (4.13). This double-null approach follows the general strategy set out in Refs. [50, 51, 38].

Such characteristic evolution has been successful in computing GSF for circular [51], eccentric [38] and generic orbits [100] in Schwarzschild. The major advantage comes from imposing only initial conditions on the null rays instead of conditions on the causal boundaries of the numerical domain needed in a standard Cauchy evolution. A careful implementation of the latter boundary conditions becomes difficult for high ℓ modes as

discussed in [101]. We avoid this problem altogether with a characteristic evolution. Moreover, we choose the 1+1D approach as it fits our setup, where the spacetime is separated in two halves and matched with a discontinuity at the particle location. A 2+1D approach would require a careful handling of a string-like discontinuity over the spacetime. Such procedure has not been implemented to the best of our knowledge and may need careful and non-trivial handling of such discontinuities. Additionally, the reduced dimension of the 1+1D scheme allows for a faster computation.

Our finite-difference method, detailed in Sec. 5.2, is a straightforward second-order convergent scheme. By this we mean that its *global* (time-accumulated) error scales as h^2, where $h \times h$ are the null-coordinate dimensions of a single grid cell. (To achieve this requires that the local finite-difference error at each grid cell scales with a higher power of h). Higher-order convergence may be desirable in future applications. It can be achieved in a straightforward manner, following, e.g., the methods of [103] or [38]. In practice, we compute finite-difference scheme with an error of $O(h^4)$ in the case of vacuum cells (since the total number of such cells scale as h^{-2}) and an error of $O(h^3)$ for the cells crossed by the particle (since the total number of such cells scale as h^{-1}), thus providing an accumulated error of $O(h^2)$.

The code, implemented in `Mathematica`, takes as input the orbital radius r_0 and the mode numbers ℓ, m, and returns the fields $\phi^{\pm\mathrm{IRG}}_{\ell m}(t, r)$. The evolution starts from initial data on two characteristic rays $v = r_*(r_0) =: v_0$ and $u = -r_*(r_0) =: u_0$, which intersect on the particle's orbit at $t = 0$. The numerical integration then proceeds along successive $v = \text{const} > v_0$ rays, with the jump conditions (4.12) and (4.13) imposed whenever the particle's worldline [represented by the line $v = u + 2r_*(r_0)$] is crossed. The future boundaries of the grid are taken at some large values of v and u (approximating null infinity and the event horizon, respectively), so the numerical domain has no timelike causal boundaries where boundary conditions would have been required. For initial data we take, for simplicity, $\phi^{\mathrm{IRG}}_{\ell m}(v = v_0) = 0 = \phi^{\mathrm{IRG}}_{\ell m}(u = u_0)$. This choice, which violates the jump conditions at $r = r_0$, produces an initial burst of nonphysical ("junk") radiation, which, however, dies out over time (with some ℓ-dependent inverse-power law). Non-zero values of the fields are provided by the jump conditions at the particle location. As shown in Fig. 5.9, the evolution proceeds until the level of junk radiation (as determined from the residual nonstationarity of the numerical solution) drops below a set threshold, and one then discards the early, junk-dominated part of the data.

How can one be sure that the late-time solution thus obtained is the physical, "retarded" solution sought for? Our artificial choice of characteristic initial data means that the early part of the evolution likely contains a nonphysical component that violates the retarded boundary condition (it would contain, in particular, radiation that comes in from past null infinity and out of the past horizon). Since the numerical solution satisfies the correct jump conditions on the particle (up to numerical error), this nonphysical component may be thought of as a homogeneous (vacuum) perturbation superposed on the true, inhomogeneous physical solution. With our choice of initial conditions, we also know that this vacuum perturbation has an initial compact support. It is a well known feature of the vacuum Teukolsky equation (see, e.g., [97]) that solutions of an initial compact support die off at late time and have no manifestation at timelike infinity. Thus, we expect the nonphysical component of the numerical solution to die off at late time, and the full solution to relax to its physical value.[1]

As discussed in Sec. 3.2, one can also check *a posteriori* whether the numerical solution is the physical one. For stationary ($m = 0$) modes, in our IRG case, all nonphysical solutions blow up either at infinity or at the horizon (or at both), so demonstrating boundedness of our solution (even in the limit of diminishing step size) should suffice to establish that the solution is indeed the physical one. For nonstationary ($m \neq 0$) modes, boundedness on the horizon implies that the internal solution ϕ^- is the physical one, though, in our IRG implementation, we have no such direct test for the external solution ϕ^+.

Our numerical experiments indeed suggest that the Hertz-potential field always settles down to the true, physical solution at late time (to within our controlled numerical accuracy). This is shown most convincingly by comparing with analytic results (for $m = 0$) and frequency-domain numerical calculations (for $m \neq 0$), in which the correct boundary conditions were explicitly imposed. We present some of this evidence below.

[1] In order to obtain a late-time solution other than the retarded one, one would need to adjust the form of characteristic initial data at late retarded and advanced times, so as to represent radiation coming out of past null infinity and/or out of the past horizon. Our argument is that whenever the initial data are compactly supported, as in our implementation, the solution will relax to the retarded one at late time.

5.2 Finite-difference scheme

In this section we describe the finite-difference scheme used in this chapter for numerically computing the Hertz-potential modes in the time domain. Our treatment is based on a characteristic evolution of the vacuum field equation (4.1) on a fixed 1+1D uniform mesh in double-null (v, u) coordinates. The numerical domain is depicted in Fig. 5.1. We start with initial conditions on the rays $v = v_0$ and $u = u_0$, and evolve along successive rows ("rays") of constant v. At each step of the integration, we approximate the value of the field at a grid point using the already-known values at a few grid points in its recent "causal past". The form of the finite-difference formula applied depends on the position of the grid point with respect to the particle's worldline (represented by the vertical line $v - v_0 = u - u_0$): For points that are sufficiently far from the worldline (those marked 'V' in Fig. 5.1) we apply a certain "vacuum" formula, whereas for points in the vicinity of the worldline ('L', 'R' or 'RR') or on it ('P') we apply modified formulas that involve the known jumps in the value of the field and its derivatives across the worldline. Below we shall describe the finite-difference schemes applied for each type of point.

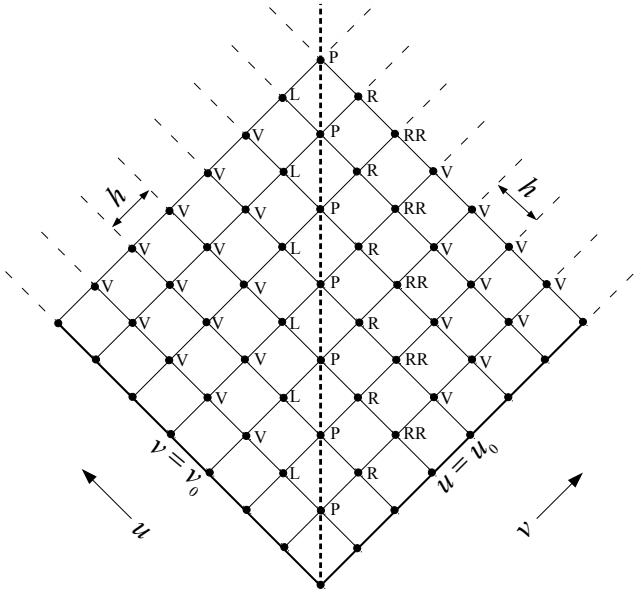

Figure 5.1: Our 1+1D double-null uniform grid in (u, v) coordinates. The numerical integration starts with characteristic initial conditions on $v = v_0$ and $u = u_0$ and proceeds along successive lines of constant v. The particle's worldline is represented by the vertical dashed line at $v - v_0 = u - u_0$, and grid points are labelled in accordance with their position with respect to it. In the text we describe the finite-difference formula applied for each type of grid point.

But first we introduce some notation. We let h denote the constant stepping interval

(in each of v and u), so that the u, v-coordinate dimensions of a single grid cell are $h \times h$. Consider an arbitrary grid point C at the coordinate position $(u, v) = (u_c, v_c)$, for some u_c and v_c. With reference to the point C, we denote by $\phi(n, k)$ (where $n, k \in \mathbb{N}$) our finite-difference approximant for the value of the field at the grid point with coordinates $(u, v) = (u_c - nh, v_c - kh)$. Our goal is to obtain, for each such point C, the value $\phi(0, 0)$ in terms of the values $\phi(n \geq 0, k \geq 0)$ (excluding $n = 0 = k$) that are computed in previous steps of the integration. For our second-order-convergence scheme it will prove sufficient to use the six values $\phi(1, 0)$, $\phi(0, 1)$, $\phi(1, 1)$, $\phi(2, 0)$, $\phi(0, 2)$ and $\phi(2, 2)$. This requires storing field values at three successive v=const rays at a time.

We note that the field value at a P-type point is ambiguous: the field there admits, in general, two different one-sided values ϕ^- and ϕ^+. We have found it convenient to assign to each P point a concrete one-sided value, and in practice we take it to be the left-hand value ϕ^-. (The choice of side here is arbitrary; assigning the value ϕ^+ would work just the same.) This amounts to taking the orbit to pass "just to the right" of the line of P points. Henceforth, whenever we refer to the value $\phi(n, k)$ at a P-type point, we mean $\phi^-(n, k)$. Of course, given ϕ^- at a P-type point, the right-hand value may be immediately recovered using

$$\phi^+ = \phi^- + [\phi], \tag{5.1}$$

where $[\phi]$ is the known jump in ϕ at that point.

5.2.1 V-type (vacuum) grid points

V-type points are those with coordinates (u, v) satisfying $\Delta v - \Delta u \geq 3h$ or $\Delta v - \Delta u \leq -2h$, where henceforth $\Delta v := v - v_0$ and $\Delta u := u - u_0$. Let us consider an arbitrary V-type grid point at $(u, v) = (u_c, v_c)$. To obtain a finite-difference expression for the field value at that point, it is convenient to consider the integral of both sides of the field equation (4.1) over the grid cell with vertices (u_c, v_c), $(u_c - h, v_c)$, $(u_c, v_c - h)$ and $(u_c - h, v_c - h)$ (i.e., the grid cell with our V-type point as its upper vertex). We represent that integral with the symbol $\int_\Diamond$.

Let us consider Eq. (4.1) term by term. First, we have

$$\int_\Diamond \phi_{,uv}\, du dv = \phi(0, 0) - \phi(1, 0) - \phi(0, 1) + \phi(1, 1), \tag{5.2}$$

which is *exact*, and does not involve any finite-difference approximation. Next, for the fourth term in (4.1) we obtain

$$\begin{aligned}\int_{\Diamond} W(r)\phi\, du dv &= \frac{1}{2}h^2 W(r_c)\left[\phi(1,0)+\phi(0,1)\right] \\ &\quad +O(h^4),\end{aligned} \tag{5.3}$$

where r_c is the value of r at the point (u_c, v_c). This finite-difference approximation suffices for our purpose: since the total number of V-type grid points scales as h^{-2}, the accumulated error from the omitted $O(h^4)$ terms should be of $O(h^2)$ at most, consistent with the sought-for quadratic convergence.

To obtain finite-difference approximations for the second and third terms in (4.1), we apply the following, more systematic procedure (following [38]). We first formally write ϕ as a double Taylor expansion in u and v about the point (u_c, v_c), keeping terms up to $O(h^2)$:

$$\phi(u,v) = \sum_{i,j=0}^{2} c_{ij}(u-u_c)^i (v-v_c)^j + O(h^3). \tag{5.4}$$

This should be valid in a vacuum neighborhood of (u_c, v_c). Taking (u_c, v_c) as our "$(0,0)$" point, we then apply Eq. (5.4) at each of the vacuum points $(1,0)$, $(0,1)$, $(1,1)$, $(2,0)$, $(0,2)$ and $(2,2)$. This yields six algebraic equations for the six coefficients c_{ij} $(0 \le i,j \le 2)$ in terms of the values $\phi(1,0)$, $\phi(0,1)$, $\phi(1,1)$, $\phi(2,0)$, $\phi(0,2)$ and $\phi(2,2)$, assumed known. We solve these equations and substitute the coefficient values back into Eq. (5.4), to obtain an approximation formula for $\phi(u,v)$ valid through $O(h^2)$ in the vicinity of (u_c, v_c). Using this formula with a Taylor expansion of the (smooth) potentials $U(r)$ and $V(r)$ about $r = r_c$, we obtain approximation formulas for the two terms $U(r)\phi_{,u}$ and $V(r)\phi_{,v}$, valid through $O(h)$ near (u_c, v_c). Finally, integrating over the grid cell, we obtain

$$\begin{aligned}\int_{\Diamond} U(r)\phi_{,u} du dv &= \frac{h}{24}\left\{(4U+hU_{,r_*})\left[\phi(1,0)-\phi(2,0)\right]\right. \\ &\quad +(28U-hU_{,r_*})\left[\phi(0,1)-\phi(1,1)\right] \\ &\quad \left.+4U\left[\phi(2,2)-\phi(0,2)\right]\right\}+O(h^4),\end{aligned} \tag{5.5}$$

$$\begin{aligned}\int_{\Diamond} V(r)\phi_{,v}dudv &= \frac{h}{24}\{(4V - hV_{,r_*})\,[\phi(0,1) - \phi(0,2)] \\ &\quad +(28V + hV_{r_*})\,[\phi(1,0) - \phi(1,1)] \\ &\quad +4V\,[\phi(2,2) - \phi(2,0)]\} + O(h^4),\end{aligned} \tag{5.6}$$

in which the radial functions U, $U_{,r_*}$, V and $V_{,r_*}$ are all evaluated at $r = r_c$.

Adding together the expressions (5.2)–(5.6) and equating to zero [the cell integral of the right-hand side of (4.1)], we obtain the desired finite-difference formula for $\phi(0,0)$ in the vacuum case:

$$\phi_{\rm Vac}(0,0) = \sum_{n,k} H_{nk}\,\phi(n,k) + O(h^4), \tag{5.7}$$

where the only nonvanishing coefficients are

$$\begin{aligned}H_{10} &= 1 - \frac{h}{6}(U + 7V) - \frac{h^2}{24}(U_{,r_*} + V_{,r_*} + 12W), \\ H_{01} &= 1 - \frac{h}{6}(V + 7U) + \frac{h^2}{24}(U_{,r_*} + V_{,r_*} - 12W), \\ H_{11} &= -1 + \frac{7h}{6}(U + V) - \frac{h^2}{24}(U_{,r_*} - V_{,r_*}), \\ H_{20} &= \frac{h}{6}(U + V) + \frac{h^2}{24}U_{,r_*}, \\ H_{02} &= \frac{h}{6}(U + V) - \frac{h^2}{24}V_{,r_*}, \\ H_{22} &= -\frac{h}{6}(U + V).\end{aligned} \tag{5.8}$$

Here, all radial functions are evaluated at $r = r_c$.

5.2.2 Near-particle grid points

RR, R, L and P-type points are those with coordinates (v,u) satisfying $\Delta v - \Delta u = +2h$, $+h$, $-h$ and 0, respectively. For such points, the above vacuum scheme (5.7) does not quite work as it stands, because it involves field values at points on both sides of the particle's worldline, where the field has a jump discontinuity.

To account for the discontinuity we apply the following procedure (again following [38]). For a given near-particle point (RR, R, L or P) with coordinates (u_c, v_c), we write

down two separate Taylor expansions,

$$\phi^{\pm}(u,v) = \sum_{i,j=0}^{2} c_{ij}^{\pm}(u-u_c)^i(v-v_c)^j + O(h^3), \tag{5.9}$$

each suitable for points on the corresponding side of the particle: ϕ^- for points on the "left" ($r \le r_0$) and ϕ^+ for points on the "right" ($r > r_0$). We apply the formula to the six points $(1,0)$, $(0,1)$, $(1,1)$, $(2,0)$, $(0,2)$ and $(2,2)$ as before. This now yields 6 equations for the 12 coefficients $c_{ij}^{\pm}$ ($0 \le i,j \le 2$), so the system is underdetermined. However, the known jump conditions across the particle's worldline provide additional constraints: we get 6 additional relations between the $c_{ij}^{\pm}$'s by imposing the known jumps $[\phi]$, $[\phi_{,u}]$, $[\phi_{,v}]$, $[\phi_{,uu}]$, $[\phi_{,uv}]$ and $[\phi_{,vv}]$ at some point along the worldline. We choose that point to be $(0,2)$ for the RR case, $(0,1)$ for the R case, $(1,0)$ for the L case, and $(0,0)$ for the P case. Solving the resulting set of 12 equations, we obtain the 12 coefficients $c_{ij}^{\pm}$ in terms of the field values at the above six points and the above 6 jumps. Substituting back into (5.9) again gives an approximation formula for $\phi^{\pm}$ in the vicinity of (u_c, v_c), which can be used to construct approximate expressions for each of the terms in the field equation (4.1) near (u_c, v_c). Finally, we integrate these expressions over the grid cell, using either '+' or '−' values, as appropriate (the former for cases RR and R and the latter for case L; for P points we use ϕ^+ on the right-hand half of the cell and ϕ^- on its left).

Following this procedure, and collecting all terms, we arrive at the near-particle finite-difference formula

$$\phi_{\rm X}(0,0) = \phi_{\rm Vac}(0,0) + J_{\rm X} + O(h^3), \tag{5.10}$$

in which $X \in \{RR, R, L, P\}$, $\phi_{\rm Vac}(0,0)$ is the vacuum expression given in Eq. (5.7), and the form of the jump terms $J_{\rm X}$ depends on the point type in question:

$$\begin{aligned}
J_{\rm RR} &= \left(\frac{1}{6}h(U+V) - \frac{1}{24}h^2 V_{,r_*}\right)[\phi]_{(0,2)}, \\
J_{\rm R} &= \left(1 - hU - \frac{1}{2}h^2 W + \frac{1}{24}h^2 U_{,r_*}\right)[\phi]_{(0,1)} \\
&\quad -\frac{1}{6}h^2(U+V)[\phi_{,v}]_{(0,1)}, \\
J_{\rm L} &= -\left(\frac{1}{6}h(U+V) + \frac{1}{24}h^2 U_{,r_*}\right)[\phi]_{(1,0)} \\
&\quad +\frac{1}{6}h^2(U+V)[\phi_{,u}]_{(1,0)}, \\
J_{\rm P} &= -\left(1 - hV - \frac{1}{24}h^2 V_{,r_*}\right)[\phi]_{(0,0)} - \frac{1}{2}h^2 V[\phi_{,v}]_{(0,0)} \\
&\quad +\left(h - \frac{1}{3}h^2 U - \frac{5}{6}h^2 V\right)[\phi_{,u}]_{(0,0)} \\
&\quad -\frac{1}{2}h^2\left([\phi_{,uv}]_{(0,0)} + [\phi_{,uu}]_{(0,0)}\right).
\end{aligned} \tag{5.11}$$

Here, all radial functions are evaluated at the point $(0,0)$ under consideration, while the jumps are evaluated at the appropriate worldline point, indicated in subscript. Note that we have truncated the expressions at $O(h^2)$, leaving an $O(h^3)$ error in Eq. (5.10). We allow ourselves to do so because the total number of near-particle (RR, R, L and P-type) points scales only like $1/h$, so the accumulated error from the omitted $O(h^3)$ local term should scale as h^2 at most, consistent with quadratic convergence. We also note that $J_{\rm P}$ may be written, through the relevant $O(h^2)$, in the alternative form

$$\begin{aligned}
J_{\rm P} &= -\frac{1}{2}\left([\phi]_{(0,0)} + [\phi]_{(1,1)}\right) - \frac{1}{4}h\left([\phi_{,r_*}]_{(0,0)} + [\phi_{,r_*}]_{(1,1)}\right) \\
&\quad +\left(hV + \frac{1}{24}h^2 V_{,r_*}\right)[\phi]_{(0,0)} - \frac{1}{2}h^2 V[\phi_{,v}]_{(0,0)} \\
&\quad -\left(\frac{1}{3}h^2 U + \frac{5}{6}h^2 V\right)[\phi_{,u}]_{(0,0)},
\end{aligned} \tag{5.12}$$

which involves jumps in the field and its first derivatives only [at the expense of requiring the jumps at the point $(1,1)$ as well]. This form may be simpler to use in practice.

Equations (5.7) and (5.10) constitute our finite-difference scheme. We see that, at the required order, the implementation of our scheme requires knowledge of the jumps in the field and its first derivatives only. Jumps in higher derivatives may be required for scheme with convergence faster than quadratic.

5.3 Sample results: Circular orbits in Swarzshild spacetime

Table 5.1 compares our TD values of the fields $|\phi^-_{l,m}|$ with the respective FD values [104]. Figure 5.2 shows sample results for $(\ell, m) = (2, 0)$, demonstrating the relaxation of the numerical solution towards the analytically known solution (4.19) at late time. The figure displays the behavior of the fields ϕ^+_{20} and ϕ^-_{20} on the particle (fixed on a circular geodesic orbit at $r_0 = 7M$), as a function of time. The inset illustrates how the asymptotic agreement with the analytical solution improves with decreasing grid size. Our highest-resolution run in this case (with $h = M/8$) took about 3 minutes on a modest laptop.

Table 5.1: Our time-domain numerical results for $|\phi^-(r_p)|$ (upper values) compared with frequency-domain results [104] (lower values). Here $r_p = 7M$ and $h = M/8$.

(l, m)	$\lvert\phi^-(r_p)\rvert$
2,0	0.01210855 0.01210815
2,1	0.00305721 0.00305704
2,2	0.00172599 0.00172575

We tested convergence for a single (l, m)-mode and found the expected quadratic convergence for all modes as shown in Fig. 5.8. The convergence results both for static and non-static modes are positive and provide a convergence ratio approaching the value of 4 (as confirmation of quadratic convergence). If we use as a rough measure of numerical error the difference between the highest-resolution value and the value obtained via a Richardson extrapolation to $h \to 0$ (assuming quadratic convergence), we see that the extrapolated value is consistent with the analytical result to within the estimated error. As can be seen from Table 5.1 the accuracy of our results is good, as relative errors show (for our highest-resolution run $h = M/8$) a mere $\sim 5 \times 10^{-5}$ relative error.

Figures 5.3 and 5.4 further test the $m = 0$ solution for a variety of ℓ values, again comparing with the analytical solution (4.19). Higher multipoles exhibit smaller-scale features, the resolution of which demands smaller step sizes and hence extra computational resources. On the other hand, higher multipoles also relax faster at late time, allowing a shorter evolution, which somewhat alleviates the computational burden.

Figures 5.5 and 5.6 display numerical results for a nonaxisymmetric mode of the Hertz

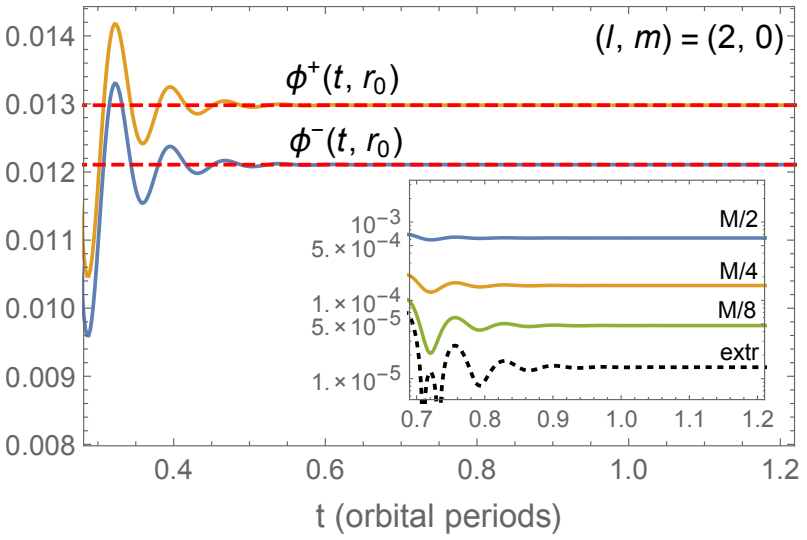

Figure 5.2: Relaxation of the numerical solution at late time. Shown here are numerical results for $\phi^{\pm}_{20}(t, r_0)$ (divided by μ/M^2), i.e. the $(\ell, m) = (2, 0)$ mode of the IRG Hertz potential along the particle's orbit (where it is discontinuous), as a function of time. The orbit is a circular geodesic with $r_0 = 7M$. The early part of the solution is dominated by nonphysical junk radiation. The solution relaxes at late time to a stationary value, shown to be in agreement with that of the analytical solution (4.19), indicated as a dashed line. The inset shows, for ϕ^{-}_{20}, how the agreement with the analytical solution improves with increasing numerical resolution: shown, on a semilogarithmic scale, is the magnitude of *relative* difference between the numerical data and the analytic value for each of $h = \{\frac{1}{2}, \frac{1}{4}, \frac{1}{8}\}M$, along with (in the dashed line) a Richardson extrapolation to $h \to 0$, which assumes quadratic convergence in h. As a rough error bar on the extrapolated value one may take the magnitude of its difference with the $h = M/8$ result, which in relative terms is $\sim 3 \times 10^{-5}$. We see that the extrapolated value agrees with the analytical result to within that error bar.

potential ($m = 1$). In this case we do not have analytical results, but we can compare with numerical solutions obtained using the frequency-domain approach of Merlin and Shah [68], who kindly provided us with numerical data generated by their code. As demonstrated in Fig. 5.5, our results agree with theirs to within our (small) estimated numerical error. Figure 5.6 illustrates the behavior of the $m = 1$ solution on a t=const slice, showing waves away from the particle and a discontinuity on it. In Fig. 5.9 we show the real part of the Hertz field on the full (u, v)-grid.

Once we have at hand the Hertz potential, reconstruction of the IRG metric perturbation becomes straightforward, through a mode-by-mode application of Eq. (2.75). Figure 5.7 shows, as an illustration, some of the components of the $(\ell, m) = (2, 0)$ mode of reconstructed perturbation in the vicinity of the particle. The analytical solution is also shown, for comparison. We observe $h^{\mathrm{rec}+}_{\alpha\beta} \neq h^{\mathrm{rec}-}_{\alpha\beta}$ on the particle, as expected.

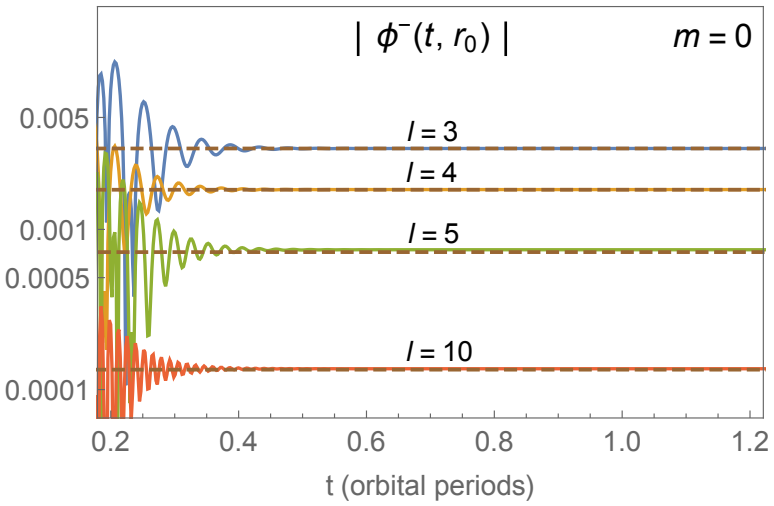

Figure 5.3: The axisymmetric piece of the Hertz potential on the particle, for different ℓ values. We show here $|\phi^{-}_{\ell 0}(t, r_0)|$ (divided by μ/M^2) for $\ell = 3, 4, 5, 10$ and $r_0 = 7M$. The corresponding known analytic values are shown in dashed lines, for comparison. Note how modes of higher ℓ relax faster, as expected.

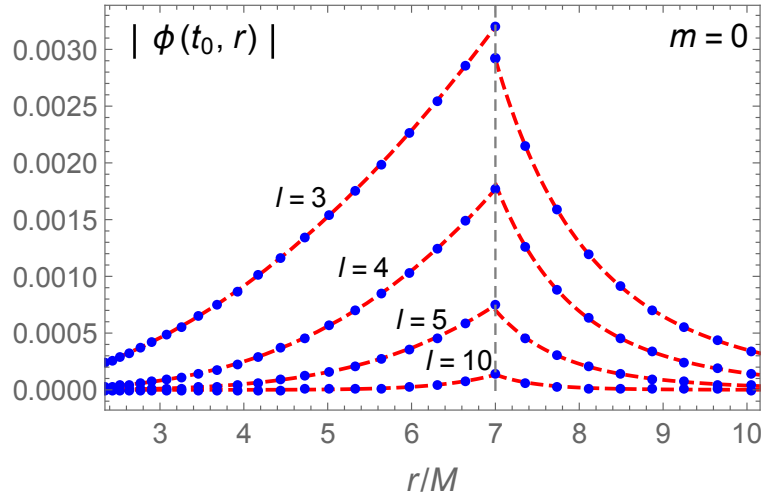

Figure 5.4: Same as in Fig. 5.3, this time showing the behavior of $|\phi^{\pm}_{\ell 0}|$ as a function of r at some fixed (late) time $t = t_0$. We show individual numerical data points, with the analytic solutions (dashed lines) displayed for comparison. The fields $\phi^{-}_{\ell 0}$ and $\phi^{+}_{\ell 0}$ do not agree on the particle [recall Eq. (4.21)], which is clearly manifest in the $\ell = 3$ case; higher-ℓ modes have smaller jumps, which are harder to resolve by eye in this figure.

We remind that the components on the metric perturbation shown in Figure 5.7 are given in a particular gauge (the IRG). It is useful to consider gauge-invariant quantities constructed from the perturbation, as these have a more solid physical interpretation, and they can be used to compare with results obtained in other gauges. One such gauge-invariant quantity (for circular orbits) was first introduced by S. Detweiler in [55]: it is the contraction $h_{\mu\nu}u^\mu u^\nu$. It can be shown that each of its ℓ, m modes is

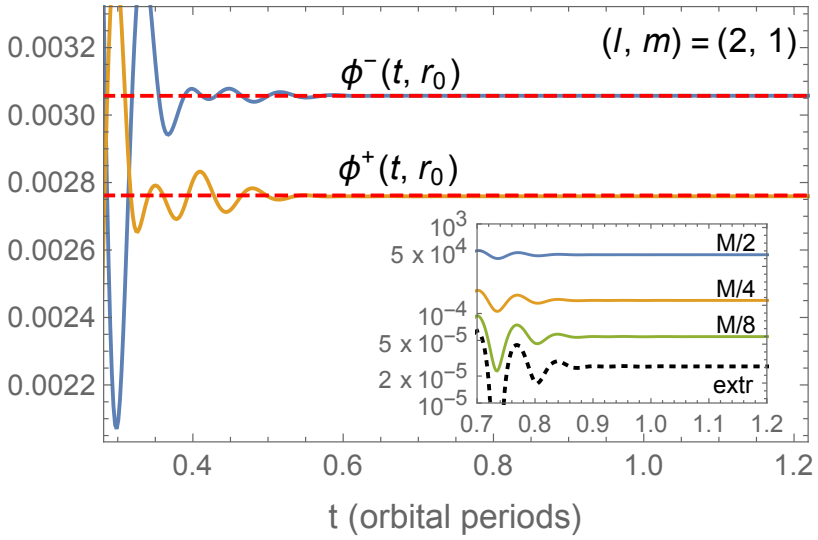

Figure 5.5: Results for $(\ell, m) = (2, 1)$. This figure is organized the same as Fig. 5.2, but for convenience we show here the quantities $|\phi^{\pm}_{21}(t, r_0)\ {}_{-2}Y_{21}(\pi/2, \varphi_{\rm p}(t))|$ (divided by μ/M^2), which are t independent in the physical solution. Again, $r_0 = 7M$. Each one-sided numerical solution settles down to a constant value, which appears to be in agreement with solutions obtained using the frequency-domain approach of Ref. [68] (dashed line). The inset explores the agreement for ϕ^{-}_{21} in more detail: it shows the *relative* difference between our numerical results and the frequency-domain ones for three choices of step size h, with a Richardson extrapolation to $h \to 0$ (dashed line). As a rough error bar on the extrapolated value we take the magnitude of its difference with the $h = M/8$ result, which in relative terms is $\sim 3 \times 10^{-5}$. We see that the extrapolated value agrees with the frequency-domain result to within that error bar (the numerical error of the frequency-domain value is known to be much smaller).

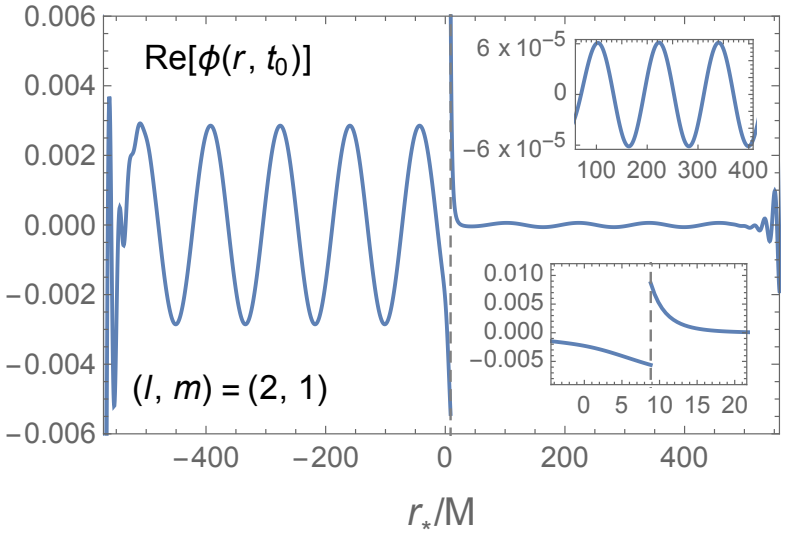

Figure 5.6: A t=const slice of the same solution shown in Fig. 5.5. We show the real part of the IRG field ϕ_{21} as a function of r_* on some (late) time slice. The noisy features at both extremes are remnants of initial junk radiation, to be discarded.

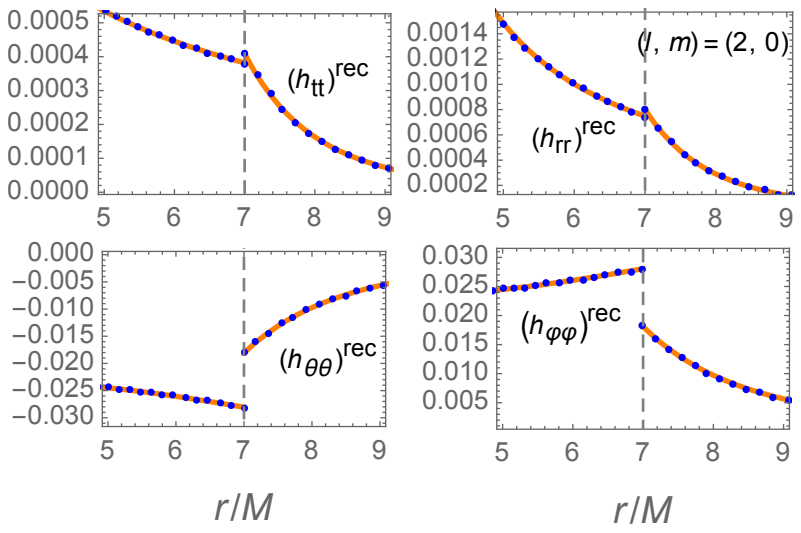

Figure 5.7: The $(\ell, m) = (2, 0)$ mode of the time-domain reconstructed IRG metric perturbation $h^{\mathrm{rec}\pm}_{\alpha\beta}$, in the vicinity of the orbit (a circular geodesic at $r_0 = 7M$). We show, for illustration, only four of the components (with h_{tt} and h_{rr} divided by μ/M and $h_{\theta\theta}$ and $h_{\varphi\varphi}$ divided by μM), on a t=const slice. Data points correspond to numerical data, and the solid lines come from applying the reconstruction formula (2.75) to the analytical solution (4.19). This reconstructed perturbation can be used directly as input for a SF calculation, using the mode-sum procedure reviewed in Sec. 2.6.1.

individually gauge invariant. Here we compare the value reconstructed from the static mode $(\ell, m) = (2, 0)$ of the Hertz potential ($r_0 = 10M$):

$$(h_{\mu\nu}u^\mu u^\nu)^{FD}_{20} = 0.0784077, \qquad (h_{\mu\nu}u^\mu u^\nu)^{TD}_{20} = 0.0784074. \tag{5.13}$$

These values show a relative error of $\sim 3 \times 10^{-6}$ for our highest resolution ($h = M/8$), below our estimated error (see [105] for a discussion on similar overestimated errors in the scalar case). The surprisingly good match may relate to the comparison of static modes, where the evolution is particularly stable and the rate of convergence behave marginally better then a second order one (notice inset in Fig. 5.8 (a), where the convergence ratio sits above the value of 4).

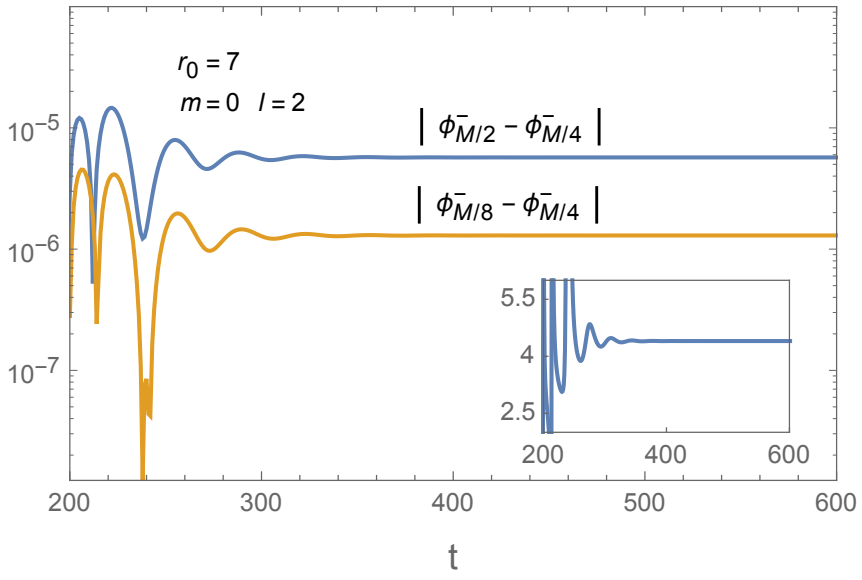

(a)

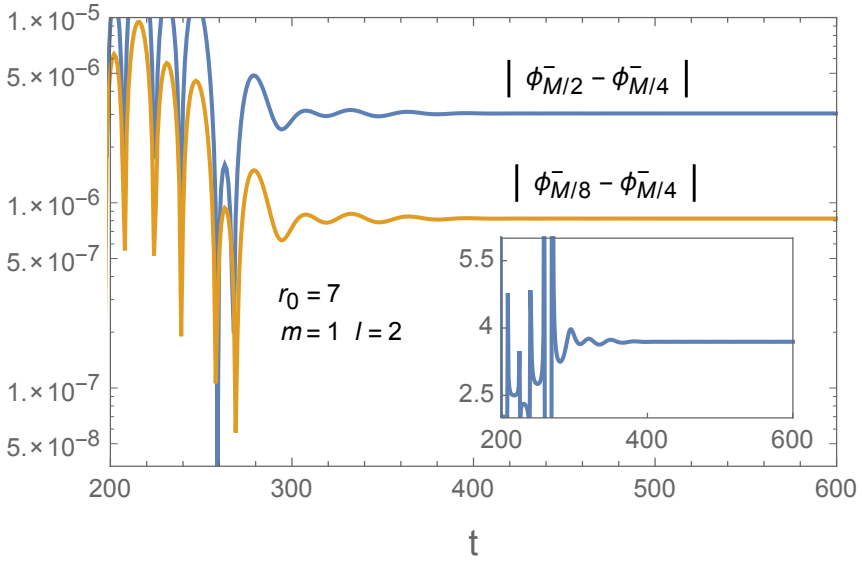

(b)

Figure 5.8: Convergence test in semi-Log scale for $r_0 = 7M$, $m = \{0, 1\}$, $M = 1$ and grid-step $h = \{M/2, M/4, M/8\}$. Here we show the test for $\ell = 2$ for static case (up) and non-static case (down). Similar results are found for different values of ℓ. The insets show the absolute value of the convergence ratio $(\phi_{M/2} - \phi_{M/4})/(\phi_{M/4} - \phi_{M/8})$ where the subscript denotes the grid-step size h. We find quadratic convergence for static modes and non-static modes for the field values near the particle.

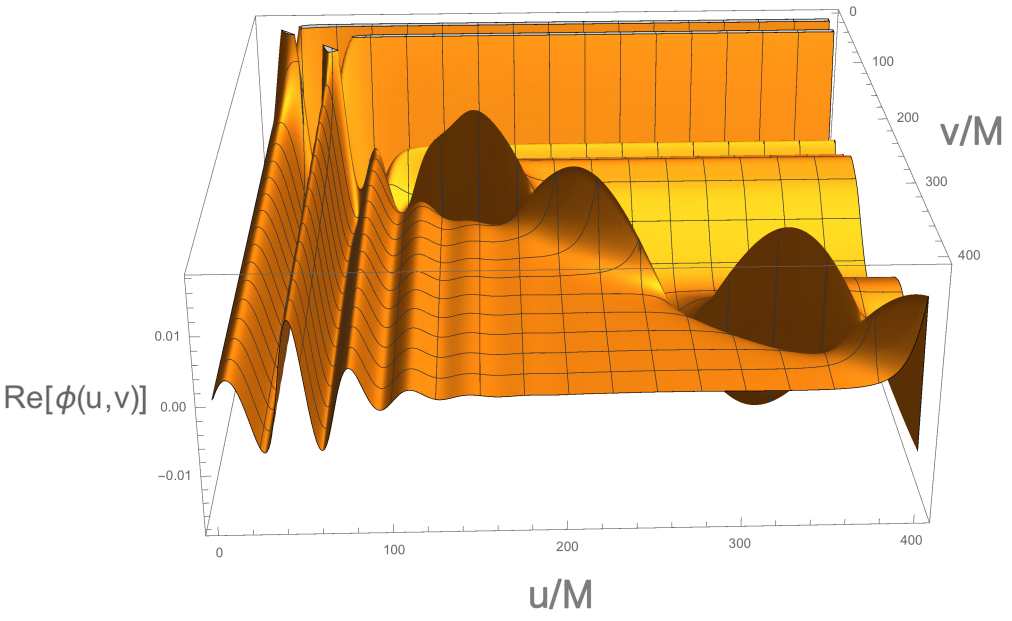

Figure 5.9: Here we show $\mu/M^2 Re[\phi_{21}^{-}(u,v)]$ for $r_0 = 6M$, $M = 1$, $\mu = 1$ on the full (u,v) grid. The initial noise clearly falls off at late time and the discontinuity at the particle (diagonal of the grid) is visible.

Chapter 6

Circular orbits in Kerr (formulation)

In this chapter we extend the application of our method to circular orbits in Kerr spacetime. The Teukolsky equation for $a \neq 0$ cannot be fully separated into multipole modes in the time domain. Nevertheless, we choose to decompose the Hertz field Φ in (spin-weighted) spherical-harmonic ℓ-modes and solve Teukolsky equation as a set of coupled equations. We compute the jumps needed for the numerical implementation by solving the system of equations (3.46) and (3.47). In this system, the coupling terms are dealt with using an iterative scheme to be described below. The Teukolsky equation (3.23) contains new types of terms (involving first and second time derivatives), necessitating significant modification to our finite-difference scheme. Similarly to the Schwarzschild case, the solution for the axisymmetric modes ($m = 0$) is obtained analytically. We derive this solution here and compare it with our numerical results in Chapter 7.

Here we specialize to a circular geodesic orbits with radius $r_0 = \text{const} > 2M$ in Kerr spacetime. Thus, we assume that $[\phi_{\ell m}]$ depends on time solely via $e^{-im\Omega t}$, where Ω is the orbital angular velocity. This is explicitly

$$\Omega := d\varphi_{\rm p}/dt = \frac{1}{\sqrt{r_0^3/M} + a}. \tag{6.1}$$

Hence, in Eqs. (3.46)-(3.47), the derivatives $d/d\tau$ may be replaced with $-im\Omega(dt_{\rm p}/d\tau) = -im\Omega\gamma_0$, where

$$\gamma_0 = \frac{(1+\frac{a}{M}v^3)}{\sqrt{1-3v^2+2\frac{a}{M}v^3}}, \tag{6.2}$$

with $v=\sqrt{r_0/M}$. Thus, we write the system (3.46)-(3.47) as

$$\begin{aligned} a_\Sigma[\phi] + b_\Sigma[\phi_{,v}] &= (-1)^m\left[\bar{\psi}_{2,\ell,-m}\right] - \mathcal{I}\text{-terms} =: S_1, \\ c_\Sigma[\phi] + d_\Sigma[\phi_{,v}] &= (-1)^m\left[\partial_v\bar{\psi}_{2,\ell,-m}\right] - \mathcal{I}\text{-terms} =: S_2, \end{aligned} \tag{6.3}$$

where $a_\Sigma = \sum_{n=0}^{3}(-im\Omega\gamma_0)^n a_n$ and similarly for b_Σ, c_Σ and d_Σ. We recall that the terms collected under '$\mathcal{I}$-terms' are certain linear combinations of the coupling term $\mathcal{I}(\phi^{\ell\pm1},\phi^{\ell\pm2})$ and its $\tilde{v}$ and $\tilde{u}$ derivatives (up to third derivatives), which have entered the relations via our use of the Teukolsky equation (3.23). The $\mathcal{I}$-terms are taken to the RHS and considered as sources for the set of equations. To write explicitly S_1 and S_2 as functions of $\left[\bar{\psi}_{2,\ell,-m}\right]$ and $\left[\partial_v\bar{\psi}_{2,\ell,-m}\right]$ we impose the circular orbits condition for the $\mathcal{I}$-terms. The time derivatives in $\left[\mathcal{I}(\phi^{\ell\pm1},\phi^{\ell\pm2})\right]$ can be written in terms of $[\phi_{\ell m}]$ using $d\phi_{\ell m}/dt = -im\Omega\phi_{\ell m}$, resulting in

$$\begin{aligned} [\mathcal{I}] = -a^2(-im\Omega/2)^2\left(C^\ell_{++}\left[\phi^{\ell+2}_{sm}\right] + C^\ell_{+}\left[\phi^{\ell+1}_{sm}\right] + C^\ell_{-}\left[\phi^{\ell-1}_{sm}\right] + C^\ell_{--}\left[\phi^{\ell-2}_{sm}\right]\right) \\ +2ias(-im\Omega/2)\left(c^\ell_{+}\left[\phi^{\ell+1}_{sm}\right] + c^\ell_{-}\left[\phi^{\ell-1}_{sm}\right]\right), \end{aligned} \tag{6.4}$$

where the constant coefficients are given by (3.11) and (3.12). We are now ready to implement an iterative scheme over the $\mathcal{I}$-terms in the equations (6.3).

6.1 Iterative scheme for coupling terms

The equation (6.4) shows that all interaction terms are proportional to at least one power of $a\Omega$. In Fig. 6.1 we plotted $a\Omega$ for a particle orbiting at the ISCO (the Innermost Stable Circular Orbit). We see that $a\Omega_{\rm ISCO}$ is bounded from above by $1/2$, and it is usually quite a bit smaller than $1/2$ (except for prograde orbits around a near-extremal hole). Since $a\Omega < a\Omega_{\rm ISCO}$, this suggests that the dimensionless quantity $a\Omega$ may serve as a perturbative parameter in Eq. (6.3). With this in mind, we impose at zero-th order the following:

$$\left[\mathcal{I}^{(0)}\right] = 0 \quad \Rightarrow \quad \mathcal{I}\text{-terms}^{(0)} = 0, \tag{6.5}$$

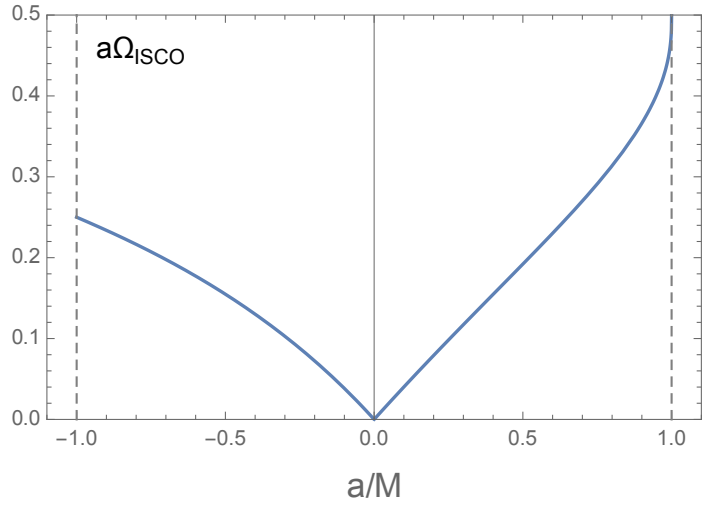

Figure 6.1: The dimensionless parameter $a\Omega_{\rm ISCO}$ as a function of black-hole spin. Note this parameter is bounded from above by 1/2, and it is usually quite a bit smaller than 1/2.

where the subscript indicates the order of the iteration. Then, the jumps for the Hertz potential are computed following the procedure used in the Schwarzschild case (see Chapter 4). These are given explicitly by

$$\left[\phi^{\rm IRG(0)}_{\ell m}\right] = \frac{(-1)^m}{\tilde{\Delta}}\left(d_\Sigma\left[\bar{\psi}_{2,\ell,-m}\right] - b_\Sigma\left[\partial_v\bar{\psi}_{2,\ell,-m}\right]\right), \tag{6.6}$$

$$\left[\partial_v\phi^{\rm IRG(0)}_{\ell m}\right] = \frac{(-1)^m}{\tilde{\Delta}}\left(a_\Sigma\left[\partial_v\bar{\psi}_{2,\ell,-m}\right] - c_\Sigma\left[\bar{\psi}_{2,\ell,-m}\right]\right). \tag{6.7}$$

Here the coefficients $(a_\Sigma, b_\Sigma, c_\Sigma, d_\Sigma)$ will hold a less simple form than the Schwarzschild case. We compute each (ℓ, m)-mode separately, as no general expression takes a meaningful and readable form.

At the first order, we write explicitly the coupling terms substituting the zero-th order jumps from equations (6.6) and (6.7). Recalling equation (6.4), the first-order jumps for the coupling terms take the form

$$\begin{aligned}\left[\mathcal{I}^{(1)}\right] = -a^2(-im\Omega/2)^2\left(C^\ell_{++}\left[\phi^{\ell+2(0)}_{sm}\right] + C^\ell_{+}\left[\phi^{\ell+1(0)}_{sm}\right] + C^\ell_{-}\left[\phi^{\ell-1(0)}_{sm}\right] + C^\ell_{--}\left[\phi^{\ell-2(0)}_{sm}\right]\right)\\ +2ias(-im\Omega/2)\left(c^\ell_{+}\left[\phi^{\ell+1(0)}_{sm}\right] + c^\ell_{-}\left[\phi^{\ell-1(0)}_{sm}\right]\right).\end{aligned} \tag{6.8}$$

Using equations (4.15), we write all u-derivatives acting on $\left[\mathcal{I}^{(1)}\right]$ as v-derivatives. Then, the zero-th order jumps $\left[\partial^{(n)}_v\phi^{\rm IRG(0)}_{\ell m}\right]$ can be substituted into $\mathcal{I}$-terms$^{(1)}$. Notice that the jumps $\left[\partial^{(n)}_v\phi^{\rm IRG}_{\ell m}\right]$, for any n, can be written solely in terms of $\left[\partial_v\phi^{\rm IRG(0)}_{\ell m}\right]$ and $\left[\phi^{\rm IRG(0)}_{\ell m}\right]$.

Furthermore, the latter are computed at the zeroth order and explicitly written only in terms of $\left[\bar{\psi}_{2,\ell,-m}\right]$ and $\left[\partial_v\bar{\psi}_{2,\ell,-m}\right]$ as in (6.6)-(6.7). Thus, substituting (6.8) into the $\mathcal{I}$-terms$^{(1)}$ and making explicit the $\left[\bar{\psi}_{2,\ell,-m}\right]$ and $\left[\partial_v\bar{\psi}_{2,\ell,-m}\right]$ dependence, we conclude that

$$\mathcal{I}\text{-terms}^{(1)} = \alpha_0\left[\partial_v\bar{\psi}_{2,\ell,-m}\right] + \beta_0\left[\bar{\psi}_{2,\ell,-m}\right], \tag{6.9}$$

where (α_0, β_0) are constants. In this form, we consider $\mathcal{I}$-terms$^{(1)}$ as part of the source for the set of equations (6.3). Thus, the solutions for the latter are

$$\left[\phi^{\text{IRG}}_{\ell m}\right] = \frac{1}{\tilde{\Delta}}\left(d_\Sigma S_1 - b_\Sigma S_2\right), \tag{6.10}$$

$$\left[\partial_v\phi^{\text{IRG}}_{\ell m}\right] = \frac{1}{\tilde{\Delta}}\left(a_\Sigma S_2 - c_\Sigma S_1\right), \tag{6.11}$$

where $\tilde{\Delta} := a_\Sigma d_\Sigma - b_\Sigma c_\Sigma$.

This scheme can be implemented iteratively. For the n-th order, $\mathcal{I}$-terms$^{(n)}$ will be written explicitly in terms of the jumps $\left[\phi^{\text{IRG}(n-1)}_{\ell m}\right]$ and $\left[\partial_v\phi^{\text{IRG}(n-1)}_{\ell m}\right]$ that are consequently written only in terms of $\left[\bar{\psi}_{2,\ell,-m}\right]$ and $\left[\partial_v\bar{\psi}_{2,\ell,-m}\right]$. The iteration can be cut when the solution reaches the precision desired. We tested the convergence of such iteration and encouraging results are given in the next numerical chapter.

6.2 Analytical solution for $m = 0$

Similarly to the $a = 0$ case, the analytical solution of Teukolsky equation (3.23) can be computed for the static case $m = 0$. For this mode, we have $\phi^{\ell}_{,t} = 0$. Hence, Teukolsky

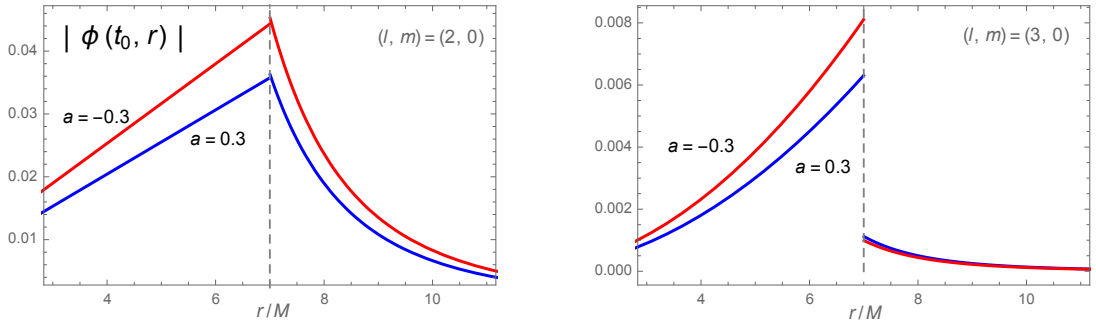

Figure 6.2: A time-slice of the static inhomogeneous physical-solution of Teukolsky equation. Here $a = \{-0.3M, 0.3M\}$, $r_0 = 7M$, $\ell = 2$ on the left and $\ell = 3$ on the right. The dashed vertical line indicates the particle location. The discontinuity at r_0 is present for both modes.

equation reduces to [Eq.(A13) of [91]]

$$\Delta^{-s}(\Delta^{s+1}(\phi_{s\ell})_{,r})_{,r} - \lambda_{s\ell}\phi_{s\ell} = 0, \tag{6.12}$$

where $\lambda_{s\ell} = \ell(\ell+1) - s(s+1)$. In our implementation we will use IRG, which corresponds to $s = -2$. Thus, two linearly independent solutions are

$$\phi^{\ell}_{P}(r) = \Delta \mathsf{P}^{-2}_{\ell}(x), \tag{6.13}$$

$$\phi^{\ell}_{Q}(r) = \Delta \mathsf{Q}^{-2}_{\ell}(x), \tag{6.14}$$

where $x = (r-M)/\sqrt{M^2-a^2}$ and $(\mathsf{P}^{-2}_{\ell}(x), \mathsf{Q}^{-2}_{\ell}(x))$ are associated Legendre functions of the first and second kinds, respectively. The boundary conditions analysis and the derivation of the jumps for the phyisical solution hold as in the case $a = 0$. The $\phi^{\ell}_{P}(r)$ satisfies physical boundary conditions on the horizon (but not at infinity), while $\phi^{\ell}_{Q}(r)$ satisfies physical boundary conditions at infinity (but not on the horizon). Therefore, a unique physical solution is given by

$$\begin{aligned} \phi^{-}_{-2\ell 0} &= C^{-}_{\ell}(r_0)\phi^{\ell}_{P}(r), \\ \phi^{+}_{-2\ell 0} &= C^{+}_{\ell}(r_0)\phi^{\ell}_{Q}(r). \end{aligned} \tag{6.15}$$

The coefficients $C^{\pm}_{\ell}(r_0)$ are determined from the two jump conditions $\phi^{+}_{\ell 0}(r_0) - \phi^{-}_{\ell 0}(r_0) = [\phi_{\ell 0}]$ and $(\phi^{+}_{\ell 0})'(r_0) - (\phi^{-}_{\ell 0})'(r_0) = [\phi'_{\ell 0}]$, giving

$$\begin{aligned} C^{-}_{\ell} &= \frac{[\phi_{\ell 0}]\,\phi'_{Q}(r_0) - [\phi'_{\ell 0}]\,\phi^{\ell}_{Q}(r_0)}{\phi'_{P}(r_0)\phi_{Q}(r_0) - \phi'_{Q}(r_0)\phi^{\ell}_{P}(r_0)}, \\ C^{+}_{\ell} &= \frac{[\phi_{\ell 0}]\,\phi'_{P}(r_0) - [\phi'_{\ell 0}]\,\phi^{\ell}_{P}(r_0)}{\phi'_{P}(r_0)\phi_{Q}(r_0) - \phi'_{Q}(r_0)\phi^{\ell}_{P}(r_0)}. \end{aligned} \tag{6.16}$$

where $[\phi'_{\ell 0}] = (2/f_0)\,[\phi_{\ell 0,v}]$ and

$$f_0 = \frac{\Delta_0}{r_0^2 + a^2}, \qquad \Delta_0 = r_0^2 - 2Mr_0 + a^2. \tag{6.17}$$

The coupling terms for $m = 0$ vanish [see equation (6.4)]. Then, the jumps $[\phi_{\ell 0}]$ and $[\phi_{\ell 0,v}]$ are computed using equations (6.6) and (6.7). For the static case, only the

coefficients (a_0, b_0, c_0, d_0) are needed and these are for $a \neq 0$

$$a_0 = \frac{1}{2}\lambda_2 \Delta^2, \tag{6.18}$$

$$b_0 = 0, \tag{6.19}$$

$$c_0 = \frac{1}{2}\lambda_2 \Delta^2 \frac{(M - r_0)}{a^2 + r_0^2}, \tag{6.20}$$

$$d_0 = \frac{1}{2}\lambda_2 \Delta^2, \tag{6.21}$$

where $\lambda_2 = (\ell - 1)\ell(\ell + 1)(\ell + 2)$. Thus, we find

$$\tilde{\Delta} = (\frac{1}{2}\lambda_2 \Delta^2)^2. \tag{6.22}$$

Then, the jumps are readily derived as

$$[\phi_{\ell 0}] = \frac{2}{\lambda_2 \Delta^2} [\psi_{0,\ell 0}], \tag{6.23}$$

$$[\partial_v \phi_{\ell 0}] = \frac{2}{\lambda_2 \Delta} [\partial_v \psi_{0,\ell 0}] + \frac{2(M - r_0)}{\lambda_2 \Delta (a^2 + r_0^2)} [\psi_{0,\ell 0}]. \tag{6.24}$$

These can be compared with equation (40) in [91], where the angular inversion formula is used to derive $[\phi_{\ell 0}]$ from the $s = -2$ Weyl scalar $\psi_{4,\ell 0}$.

In summary, we substitute (6.23) and (6.24) into (6.16). The coefficients are then substituted into the unique solution (6.15). We provide in Fig. 6.2 the plot of this solution for some values of ℓ and a.

Chapter 7

Circular orbits in Kerr (numerical implementation)

In this chapter we present an illustrative numerical implementation of our method, specialising to circular geodesic orbits in Kerr spacetime. The methodology and the code implementation setup follow to the previously discussed Schwarzschild case (see Chapter 5). However, after mode decomposition, the Teukolsky equation is a set of coupled equations that we solve as a matrix equation. Additionally, time derivatives are now present in the Teukolsky equation and need to be expressed within our finite-difference scheme. Similarly to Chapter 5 we do not concern ourselves with questions of computational performance or code optimisation.

7.1 Method

Our code solves for the IRG Hertz-potential modes $\phi^{\mathrm{IRG}}_{\ell m}(r,t)$ by evolving a finite-difference version of (3.23) on a fixed 1+1D grid in double-null $(\tilde{u},\tilde{v})$ coordinates, subject to the jump conditions derived from the iterative scheme described in Sec. 6.1.

The evolution here presented is not a characteristic one, as for the Schwarzschild case. The normals to the surfaces $\tilde{u} = const$ or $\tilde{v} = const$ are spacelike (see [106] for a discussion on light cones in Kerr). This ensure us with a causal evolution, once the values of the field is set on both initial rays. This kind of evolution is similar to the one given (for the scalar case) in [73], where the author successfully compared a 2+1D code with a 1+1D code, testing the validity of such scheme. Here we set our code to solve a

1+1D evolution in Kerr for the gravitational case. The motivation behind this choice is strongly related with the simplicity of the extension of our tested Schwarzschild code. Additionally, as discussed in Chapter 5, our method relies on a clear separation of the space-time into two separate regions where the vacuum equation are solved and matched via junction conditions. Such simplification would break down in a 2+1D approach, where the major complication of dealing with a string-like discontinuity would arise. Here we aim to test for the first time such evolution, providing a first insight to the validity and stability of the method.

Our finite-difference method is a straightforward second-order convergent scheme as described in Sec. 7.3 and integration of the time derivatives will be given in the finite-difference form. Higher-order convergence can be achieved in a straightforward manner, following, e.g., the methods of [103] or [38]. The set of coupled equations is solved for a set $\{\phi^{\rm IRG}_{\ell_{min}m}(r,t),\dots,\phi^{\rm IRG}_{\ell_{max}m}(r,t)\}$. This means that we compute the value of the field for each point C with coordinates $(\tilde{u},\tilde{v}) = (\tilde{u}_c,\tilde{v}_c)$ for all the ℓ-modes within our set simultaneously. The set of equations must be cut at a chosen ℓ_{max}, and the missing field values ℓ_{max+1} and ℓ_{max+2} necessary to solve for ℓ_{max-1} and ℓ_{max} are set to zero. The accuracy of such cut-off can be tested by comparing a fixed field mode for different cut-offs ℓ_{max}. We run such a test and we provide the results in Sec. 7.3. The convergence may differ for different kind of orbits as higher ℓ-modes may be dominant.

The code presents the same implementation strategy described in Sec. 5.1. The initial conditions on the $(\tilde{u},\tilde{v})$-axis are set to zero for all modes within our set, producing an initial junk radiation that we discard. The particle location is set on the grid diagonal defined by $\tilde{v} = \tilde{u} + 2r_*(r_0)$. The jump conditions are imposed each time the particle location is crossed. As discussed in Sec. 3.2, one checks *a posteriori* whether the numerical solution is the physical one. Our tests suggest that, also for Kerr, the numerical solution settle to the physical solution. We provide evidence of this in Sec. 7.3.

7.2 Finite-difference scheme: Coupling terms

In the case of Kerr, the coupling terms between different ℓ-modes must be added to our finite-difference scheme described in Sec. 5.2. These are first and second derivatives in time of the neighbouring ℓ-modes (recall, Teukolsky equation (3.23)). To write the time

derivatives within our $(\tilde{u},\tilde{v})$ scheme we use

$$\int_{\Diamond} F(r)\phi_{,t}\, d\tilde{u}d\tilde{v} = \int_{\Diamond} F(r)\phi_{,\tilde{v}}\, d\tilde{u}d\tilde{v} + \int_{\Diamond} F(r)\phi_{,\tilde{u}}\, d\tilde{u}d\tilde{v}, \tag{7.1}$$

$$\int_{\Diamond} F(r)\phi_{,tt}\, d\tilde{u}d\tilde{v} = \int_{\Diamond} F(r)\phi_{,\tilde{v}\tilde{v}}\, d\tilde{u}d\tilde{v} + \int_{\Diamond} F(r)\phi_{,\tilde{u}\tilde{u}}\, d\tilde{u}d\tilde{v} + 2\int_{\Diamond} F(r)\phi_{,\tilde{u}\tilde{v}}\, d\tilde{u}d\tilde{v}, \tag{7.2}$$

where $F(r)$ is a generic function of r. The first derivatives can be written using (5.6) and (5.5). Explicitly we find for the terms in (3.23)

$$\begin{aligned}\int_{\Diamond}(2iasc_{\pm}^{\ell})\tilde{K}(r)\phi_{,t}^{\ell\pm1}\, d\tilde{u}d\tilde{v} \;=\; & \frac{(iasc_{\pm}^{\ell})h}{12}\Big\{(4\tilde{K}(r)-h\tilde{K}(r)_{,r_*})\Big[\phi^{\ell\pm1}(0,1)-\phi^{\ell\pm1}(0,2)\Big]\\ & +(4\tilde{K}(r)+h\tilde{K}(r)_{,r_*})\Big[\phi^{\ell\pm1}(1,0)-\phi^{\ell\pm1}(2,0)\Big]\\ & +(\tilde{K}(r)+h\tilde{K}(r)_{,r_*})\Big[\phi^{\ell\pm1}(1,0)-\phi^{\ell\pm1}(1,1)\Big]\\ & +(\tilde{K}(r)-h\tilde{K}(r)_{,r_*})\Big[\phi^{\ell\pm1}(0,1)-\phi^{\ell\pm1}(1,1)\Big]\\ & +4\tilde{K}(r)\Big[2\phi(2,2)-\phi^{\ell\pm1}(2,0)-\phi^{\ell\pm1}(0,2)\Big]\Big\}+O(h^4).\end{aligned} \tag{7.3}$$

where $\tilde{K}(r)$ and $c_{\pm}^{\ell}$ are given in (3.24) and (3.12), respectively. The second derivative terms can we written using and expansion with additional grid points. For our second-order-convergence scheme we add to the previous set six values $\phi(0,3)$, $\phi(1,3)$, $\phi(3,0)$, $\phi(3,1)$ and $\phi(3,3)$. This requires storing field values at five successive $\tilde{v}$=const rays at a time. We compute each term in Eq. (7.2) and find for the sum:

$$\begin{aligned}\int_{\Diamond}\tilde{K}(r)\phi_{,tt}^{\ell\pm1}\, d\tilde{u}d\tilde{v} \;=\; & \frac{\tilde{K}(r)}{2}\Big[-\phi^{\ell\pm1}(3,0)-8\phi^{\ell\pm1}(3,3)+8\phi^{\ell\pm1}(0,1)\\ & +8\phi^{\ell\pm1}(1,0)-32\phi^{\ell\pm1}(2,2)-4\phi^{\ell\pm1}(2,0)-4\phi^{\ell\pm1}(2,0)\\ & -\phi^{\ell\pm1}(0,3)+17\phi^{\ell\pm1}(1,2)+17\phi^{\ell\pm1}(2,1)\Big]+\\ & -\frac{h}{24}\tilde{K}_{,r_*}(r)\Big[-\phi^{\ell\pm1}(3,0)+4\phi^{\ell\pm1}(0,1)-4\phi^{\ell\pm1}(1,0)-4\phi^{\ell\pm1}(2,0)\\ & +4\phi^{\ell\pm1}(2,0)+\phi^{\ell\pm1}(0,3)+\phi^{\ell\pm1}(1,2)-\phi^{\ell\pm1}(2,1)\Big]+\\ & +\frac{h^2}{96}\tilde{K}_{,r_*r_*}(r)\Big[-\phi^{\ell\pm1}(3,0)-8\phi^{\ell\pm1}(3,3)+8\phi^{\ell\pm1}(0,1)\\ & +8\phi^{\ell\pm1}(1,0)-32\phi^{\ell\pm1}(2,2)-4\phi^{\ell\pm1}(2,0)-4\phi^{\ell\pm1}(2,0)\\ & -\phi^{\ell\pm1}(0,3)+17\phi^{\ell\pm1}(1,2)+17\phi^{\ell\pm1}(2,1)\Big]+O(h^4).\end{aligned} \tag{7.4}$$

Similarly we write the coupling terms for $\ell\pm2$.

These terms will be added to the scheme given in Eq. (5.10) effectively modifying the vacuum term $\phi_{\rm Vac}(0,0)$ as follow:

$$\phi_{\rm Vac-Coup}(0,0) = \phi_{\rm Vac}(0,0) + \phi_{\rm d1}(0,0) + \phi_{\rm d2}(0,0), \tag{7.5}$$

where we defined

$$\phi_{\rm d1}(0,0) := \int_{\Diamond} [(2iasc_{-}^{\ell})\tilde{K}(r)\phi_{,t}^{\ell-1} + (2iasc_{+}^{\ell})\tilde{K}(r)\phi_{,t}^{\ell+1}]\, d\tilde{u}d\tilde{v}, \tag{7.6}$$

$$\phi_{\rm d2}(0,0) := \int_{\Diamond} a^2\tilde{K}(r)(C_{++}^{\ell}\phi_{,tt}^{\ell+2} + C_{+}^{\ell}\phi_{,tt}^{\ell+1} + C_{-}^{\ell}\phi_{,tt}^{\ell-1} + C_{--}^{\ell}\phi_{,tt}^{\ell-2})\, d\tilde{u}d\tilde{v}. \tag{7.7}$$

Thus, the finite-difference scheme for Kerr is defined by

$$\phi_{\rm X}(0,0) = \phi_{\rm Vac-Coup}(0,0) + J_{\rm X} + O(h^3), \tag{7.8}$$

in which $X \in \{RR, R, L, P\}$ as described in Sec. 5.2.2.

7.3 Sample results: Kerr Case

7.3.1 Vacuum test

As a first test of our code implementation, we have run it without a source, using compact pulse as initial data. Fig. 7.1 displays a sample of results from our vacuum runs. We imposed a pulse at $r = 7M$ as initial condition (in practice setting the value of the first grid element to 1). The typical features of solutions to the Teukolsky equation in vacuum are present: the quasinormal-mode oscillations at early times and the inverse-power-law tails at late time. The slope of the tails, for all ℓ-modes is $\propto t^{-7}$ as expected, since the $\ell = 2$ tail is known to dominate the late time behaviour of all $\ell \geq 2$ modes through coupling [97].

7.3.2 Static modes: Comparison with analytic solutions

Similarly to the Schwarzschild case, we can compare the particle static axial-symmetric modes with the analytical solution given in Sec. 6.2. In Fig. 7.2 we present the comparison for two values of a and several values of ℓ.

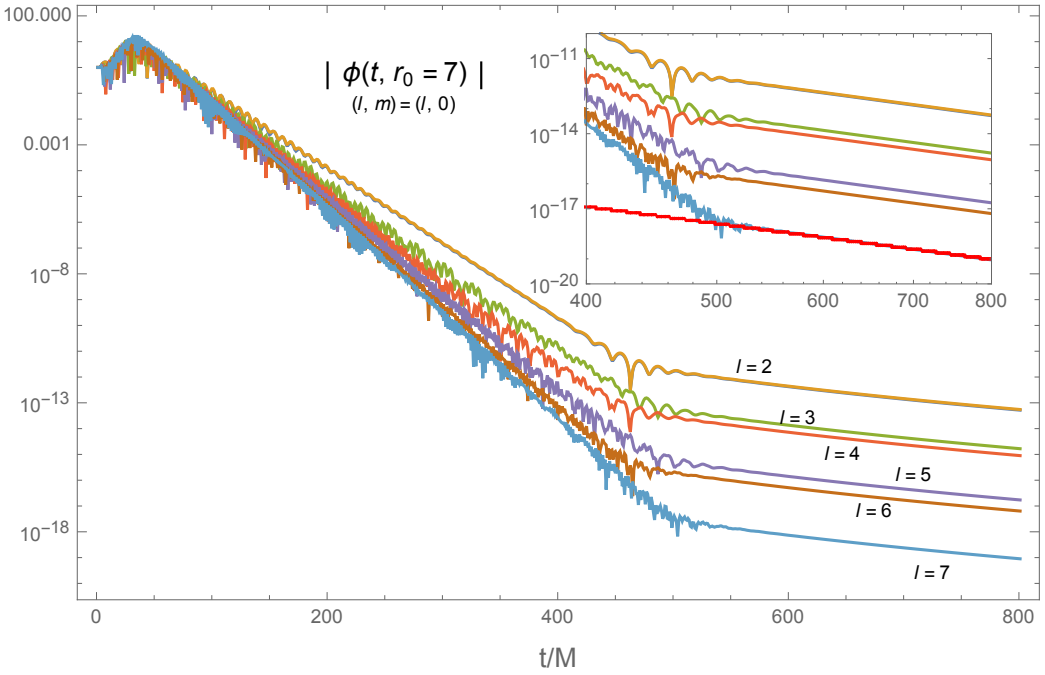

Figure 7.1: The vacuum Hertz field for $a = 10/11M$, $M = 1$, $m = 0$, $\ell = (2, 3, 4, 5, 6, 7)$ and $\ell_{max} = 7$ in a semi-log scale. The inset shows the late time tails in a Log-Log scale compared with a t^{-7} fall off (red line). The tails, for all ℓ-modes, present a fall off $\propto t^{-7}$ as the late time behaviour is dominated by the $\ell = 2$ mode.

7.3.3 Sample results for non-static modes

A set of non-static modes are shown for two values of a in Fig. 7.3. Additionally, we show a time slice of $Im[\phi_{21}]$ for two different spins in Fig. 7.4. The discontinuity at the particle is clear for both spins and the initial condition noise have been discarded. For a view of the field on the full $(\tilde{u}, \tilde{v})$-grid, we refer to Fig. 7.5.

7.3.4 Convergence of iteration scheme for jump calculation

In Sec. 6.1 we described how we compute the jumps for the Hertz potential, starting from the jumps $[\psi_{0\ell m}]$. Here we tested the iteration procedure for the coupling terms, by computing numerically the jumps for a fixed (ℓ, m)-mode of the Hertz potential Φ for different number of iterations. Figure 7.6 shows the results of our convergence test for a sample of a values. The convergence improves strongly with smaller spin, but even for spin as high as $a = 0.99M$ only 3-4 iterations are needed in practice.

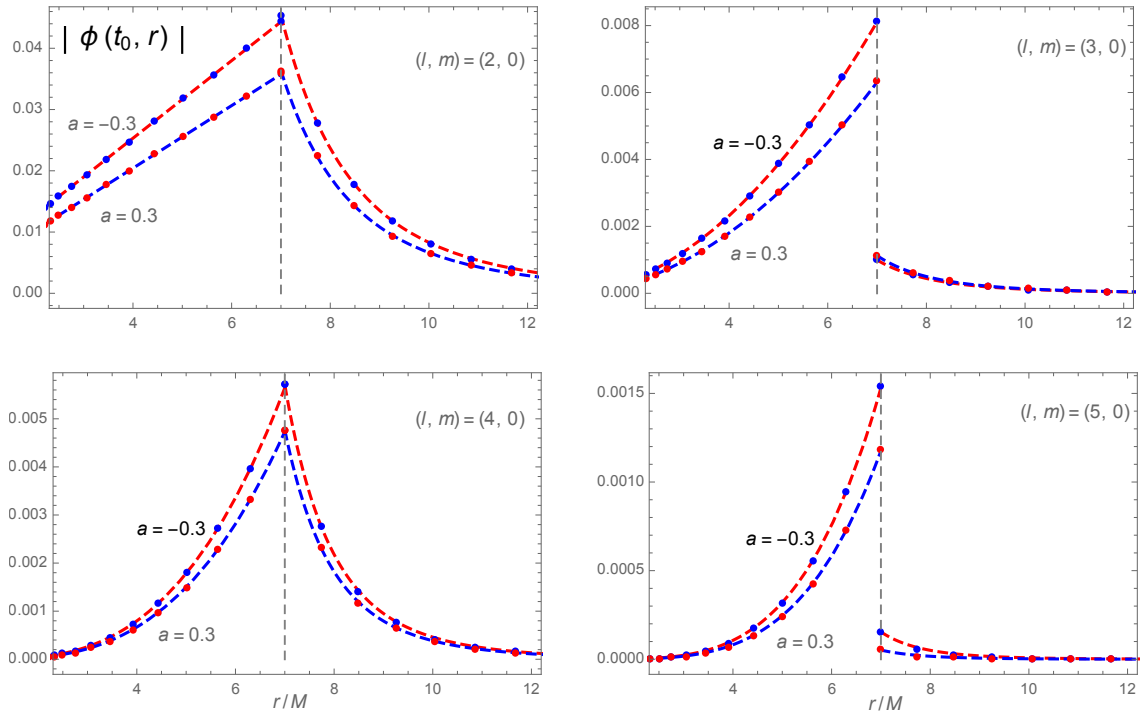

Figure 7.2: The plots show the behavior of $|\phi^{\pm}_{\ell 0}|$ as a function of r at some fixed (late) time $t = t_0$. Here $a = \{-0.3M, 0.3M\}$, $r_0 = 7M$, $M = 1$ and $\ell_{max} = 5$. We show individual numerical data points, with the analytic solutions (dashed lines) displayed for comparison. The dashed vertical line defines the particle location. The fields $\phi^{-}_{\ell 0}$ and $\phi^{+}_{\ell 0}$ do not agree on the particle, which is clearly manifest in the cases of $\ell = \{3, 5\}$.

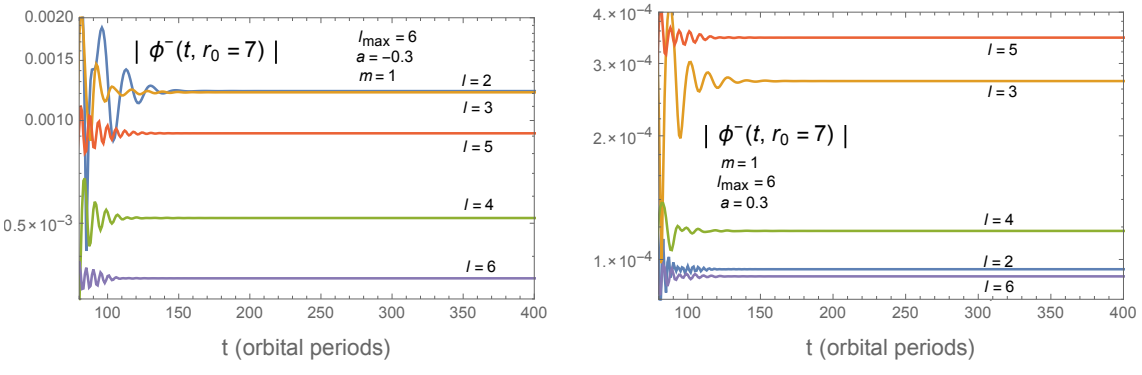

(a) (b)

Figure 7.3: The plots show in a semi-log scale some non-static modes of $|\phi^{\pm}_{\ell m}|$ ($m = 1$ and $\ell = \{2, 3, 4, 5, 6\}$) for a fixed cutoff of $\ell_{max} = 6$. Here $r_0 = 7M$, $M = 1$ and $a = (-0.3M, 0.3M)$ for figure ((a),(b)), respectively,. Similarly to the Schwarzschild case, an initial noise is present. This fall off rapidly in the evolution and the field settle to its physical value.

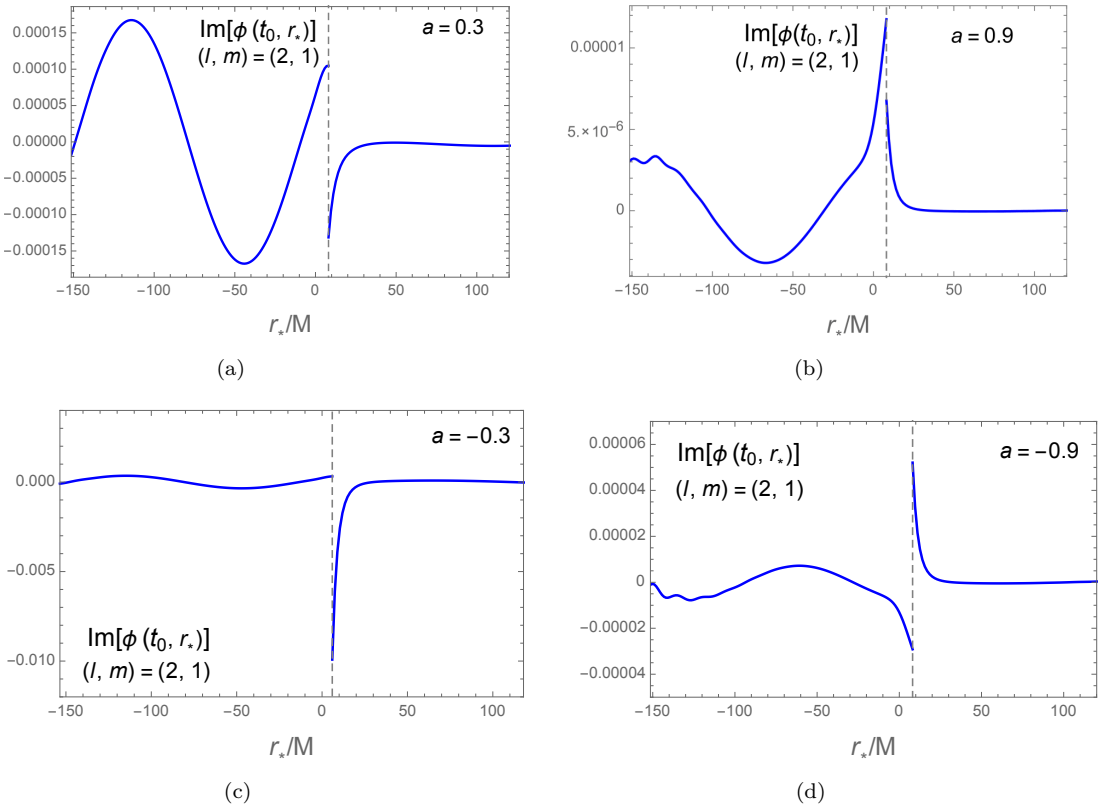

Figure 7.4: We show the imaginary part of the IRG Hertz potential for $(\ell, m) = (2, 1)$, $r_0 = 7M$, $M = 1$, $\ell_{max} = 4$, $t = constant$ as a function of r_*. The discontinuity at the particle location (dashed vertical-line) is clear for both spins. The noisy features at the extremes have been discarded.

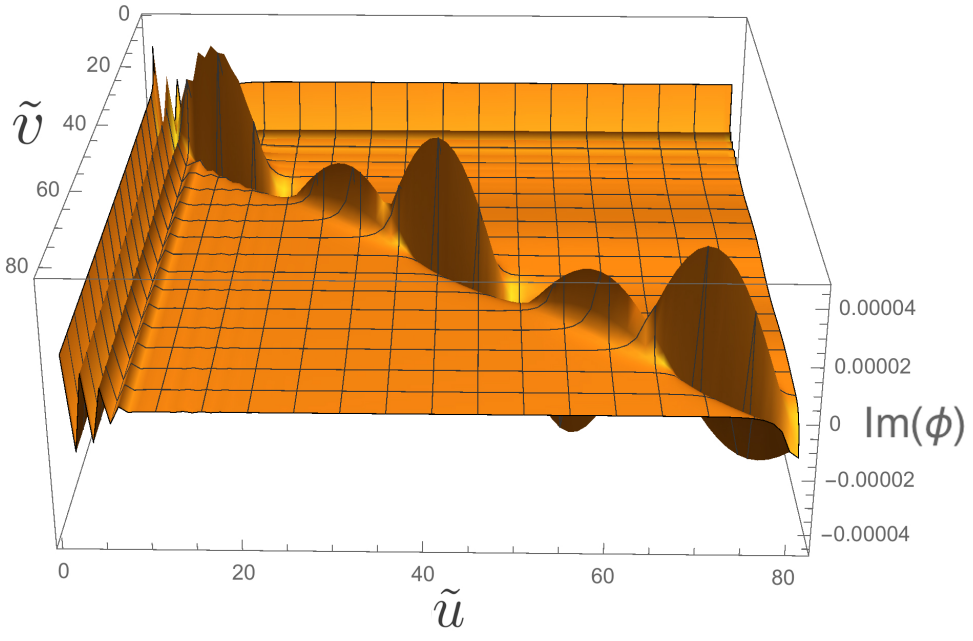

Figure 7.5: The imaginary part of the Hertz field on the full $(\tilde{u}, \tilde{v})$-grid. Here $a = 0.3M$, $M = 1$, $m = 1$, $\ell = 3$. The initial noise decays rapidly and the jump at the particle (diagonal of the grid) is clearly visible.

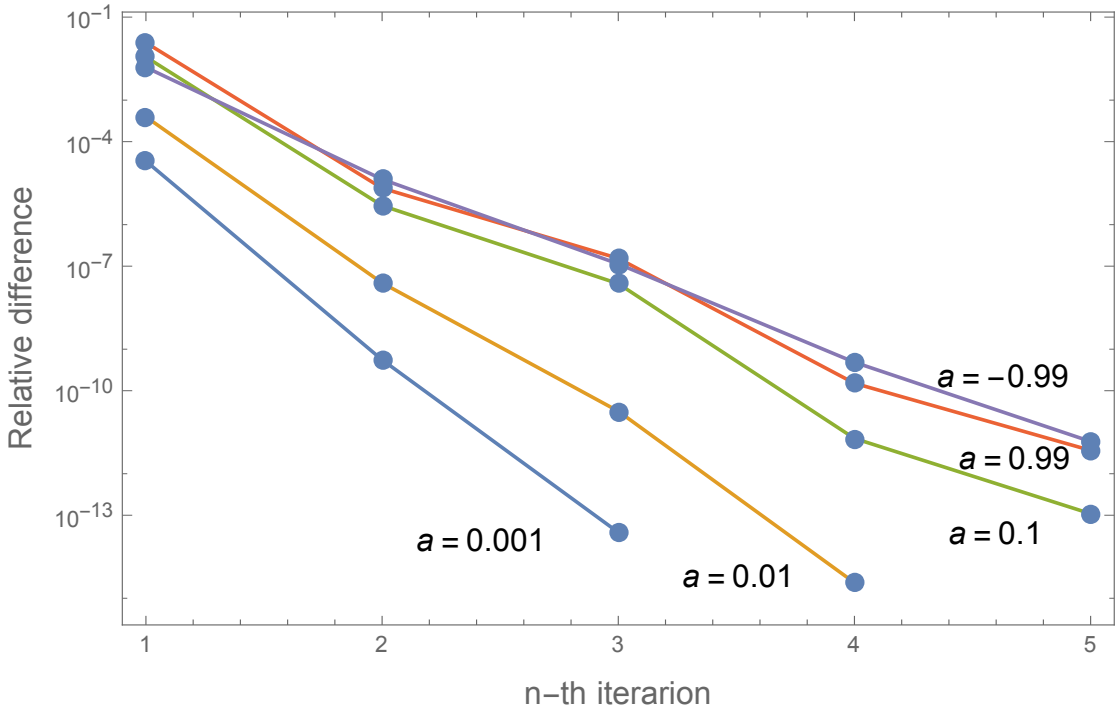

Figure 7.6: The plot presents the convergence test for the Hertz jumps over the $\mathcal{I}$-terms iteration for a set of values of a. Here $r_0 = 7M$, $M = 1$, $(\ell, m) = (2, 1)$ and $a = \{-0.99M, 0.99M, 0.1M, 0.01M, 0.001M\}$. The relative difference for the Hertz jump of two subsequents iterations (namely $(\left[\phi^{\mathrm{IRG}(n-1)}_{\ell m}\right] - \left[\phi^{\mathrm{IRG}(n)}_{\ell m}\right])/(\left[\phi^{\mathrm{IRG}(n-1)}_{\ell m}\right])$) is plotted in a semi-logarithmic scale. The convergence clearly improves for smaller values of a.

7.3.5 Numerical convergence

We tested convergence for a single (ℓ, m)-mode and found the expected quadratic convergence for static modes. The tests for non-static modes show a linear convergence, in disagreement with our expected quadratic result. We show in Fig. 7.7 the convergence results both for static and non-static modes. Additionally, we observe for some ℓ-modes that the convergence ratio deviate marginally from 4 and 2, for the stationary and non-stationary modes respectively. An estimate for the error can be taken to be of the order of the relative difference of our best two resolutions. By use of Fig. 7.7 and normalising to the field value we find a relative error of $\sim 8 \times 10^{-3}$ for non static modes and $\sim 2 \times 10^{-5}$ for static modes.

The incorrect convergence for the non-static case can arise from different factors in the code. Firstly, the junction conditions may play a role in the convergence rate. Our method is the first to explicitly compute the jumps at the particle for the Hertz potential in IRG, so we have not been able to compare our numerical jumps with other

existing codes. Here we used as jump values numerical result from a 3-loop iteration of our iterative scheme. Higher precision on our jumps may resolve the issue. We ran an additional test actively removing the coupling terms from the finite-difference scheme, without improvement in the convergence rate. For the scope of this work, linear convergence is a good enough result as we are not looking for high precision nor highly efficient computation. Future work would aim to improve efficiency and convergence of the method. These technical issues should not hold major difficulties.

7.3.6 ℓ-mode truncation

As discussed in Chapter 6, in order to compute the field values, we need to choose a cut-off for the ℓ modes to have a finite dimensional matrix-system. We can test the convergence of a fixed mode by comparing the values for different cut-offs $\ell_{\max}$. Figure 7.8 shows the field for different values of $\ell_{\max}$. We fitted the late time field values with a function of the type $f(\ell_{\max}) = A + B/\ell_{\max}^{C}$ and we found $C \sim 0.759$. This convergence test is specific for our setup of circular orbits. For some general orbits, a higher cut-off could be needed to reach the desired precision, as higher modes will contribute more strongly.

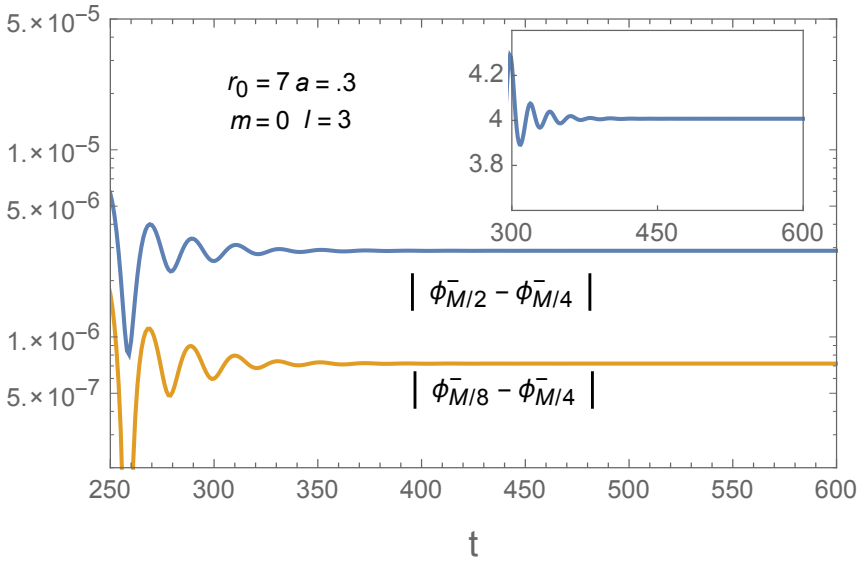

(a)

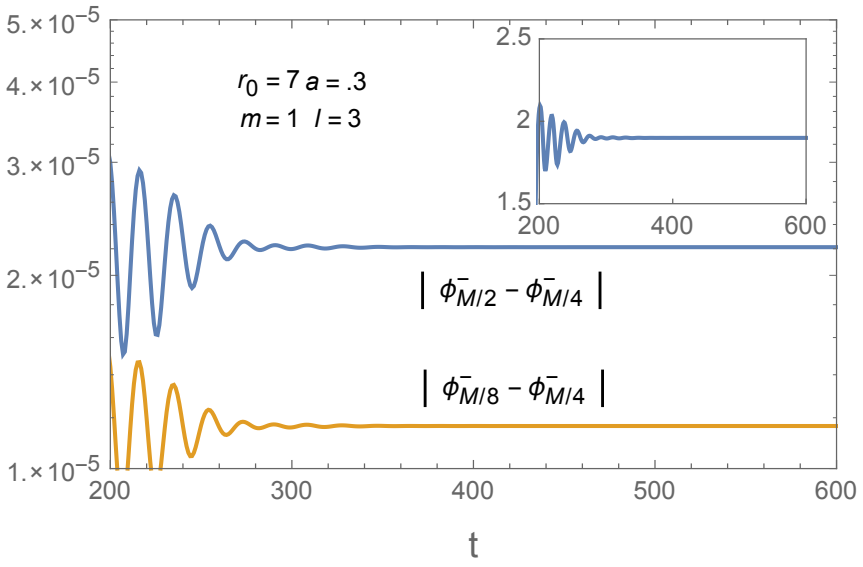

(b)

Figure 7.7: Convergence test for $a = 0.3M$, $r_0 = 7M$, $m = \{0, 1\}$, $M = 1$ and grid-step $h = \{M/2, M/4, M/8\}$. Here we show the test for $\ell = 3$ for static case (up) and non-static case (down). Similar results are found for different values of ℓ. The insets show the absolute value of the convergence ratio $(\phi_{M/2} - \phi_{M/4})/(\phi_{M/4} - \phi_{M/8})$ where the subscript denotes the grid-step size h. We find quadratic convergence for static modes and linear convergence for non-static modes the for the field values near the particle. We observe that for some ℓ-modes the convergence ratio deviate marginally from 4 and 2, for the stationary and non-stationary modes respectively.

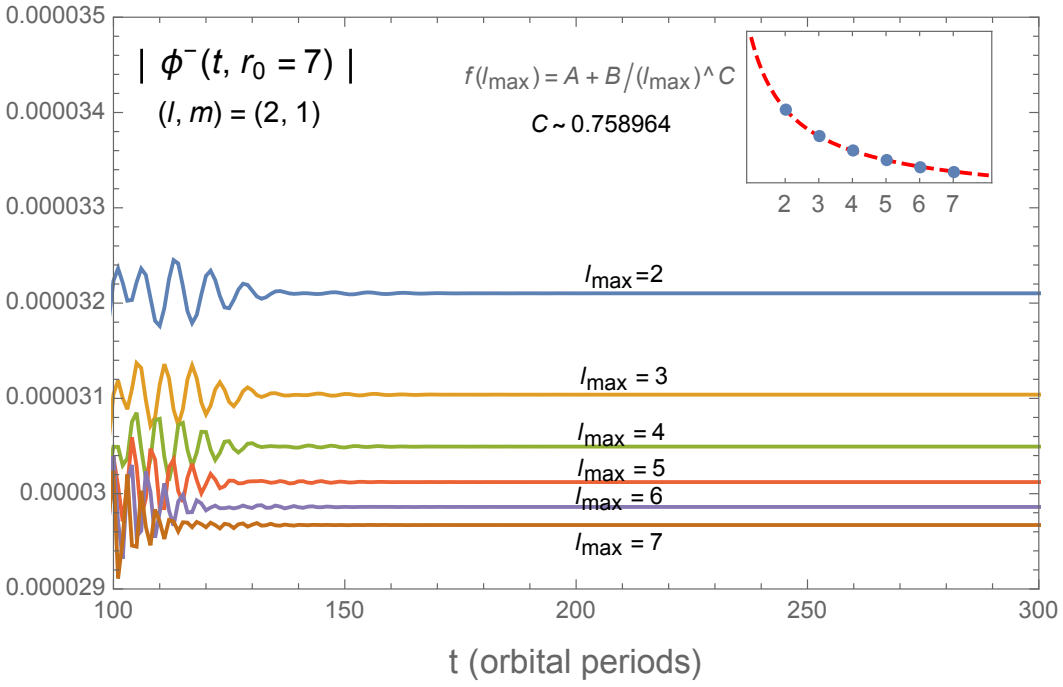

Figure 7.8: Convergence test for the iteration over the ℓ_{max} cut-off for the coupling terms. The plot shows the absolute value of the Hertz field on the grid diagonal ($r_0 = 7M$) for $(\ell, m) = (2, 1)$, $a = 0.3M$, $M = 1$ and $\ell_{max} = (2, 3, 4, 5, 6, 7)$. The inset shows the rate of convergence of the late-time field with respect to ℓ_{max}.

Chapter 8

Conclusions

A recent body of work [61, 59, 62, 68, 92, 40, 41, 34, 90] showed how the gravitational self-force experienced by a point particle in orbit around a Kerr black hole can be calculated from a reconstructed metric perturbation, starting from frequency-domain solutions of the fully separated Teukolsky equations. In this approach, a suitable version of the metric perturbation is reconstructed as a sum over frequency-harmonic modes (subject to a certain regularization procedure). This thesis develops a time-domain version of that approach, which circumvents the need to calculate individual frequency modes of the perturbation. Instead, each multipole [(ℓ, m) mode] of the perturbation is reconstructed (numerically) directly as a function of time. This should enable tackling some SF problems that are not directly amenable to a frequency-domain treatment, including the very important problem of self-consistently evolving the orbit under backreaction from the SF.

The new method, developed in Chapter 3, has the metric perturbation reconstructed multipole by multipole from scalarlike potentials $\phi^{+}_{\ell m}(t, r)$ and $\phi^{-}_{\ell m}(t, r)$ defined in the vacuum regions $r > r_{\rm p}(t)$ and $r < r_{\rm p}(t)$, respectively. Each of these fields is a solution of a 1+1D version of the vacuum Teukolsky equation [Eq. (3.17), or its alternative form (3.23)], which, for $a \neq 0$, exhibits coupling between different ℓ modes. The crucial and most difficult step in the method is the determination of jump conditions that relate between $\phi^{+}_{\ell m}$ and $\phi^{-}_{\ell m}$ across the particle's trajectory $r = r_{\rm p}(t)$ in the 1+1D domain. A general method for doing so, for arbitrary motion in Kerr, was developed in Sec. 3.3. The jump conditions were derived explicitly, first for the example of circular geodesic orbits in Schwarzschild and then for the example of circular equatorial geodesic orbits

in Kerr. Chapters 5 and 7, respectively, presented full numerical implementations for these two cases.

Looking ahead, let us first consider the extension of our treatment in Chapters 4 and 5 to an arbitrary motion in Schwarzschild spacetime. The most nontrivial aspect of the extension concerns the explicit determination of jump conditions for $\phi^{\pm}_{\ell m}$. For this, one needs to refer back to the general jump equations (3.46) and (3.47), which are a coupled set of fourth-order ODEs along the orbit. Strategies for solving this set were discussed in Sec. 3.3. For strictly periodic orbits (including any bound geodesic orbit), one can decompose the jumps by means of a discrete Fourier series, and solve the resulting ODEs frequency mode by frequency mode. But the main potential of the method is its ability to tackle non-periodic setups, including the problem of parabolic/hyperbolic flybys or captures, and the problem of self-consistent evolution. In such cases, the jump equations may have to be solved as ODEs, with suitable initial conditions. For orbits that start or end at infinity, such conditions may most conveniently be imposed there. In the case of self-consistent evolution, initial values for the jump conditions could be well approximated by assuming exact orbital periodicity at an initial moment where the evolution is strongly adiabatic. In both cases, it remains necessary to explore the numerical stability of the set of ODEs and develop a robust and efficient method for solving them along the orbit.

Moving on to implementation in Kerr, the main additional complication comes from ℓ-mode coupling. The 1+1D Teukolsky equation (3.17) [or its alternative version (3.23)] couples between each ℓ mode and its nearest and next-to-nearest neighbours, so the numerical evolution problem needs to be recast in a matrix form, with "all" ℓ modes solved for simultaneously. In practice, a large-ℓ cutoff must be introduced, and its error controlled. As already mentioned, the narrow band-diagonal form of the matrix operator is computationally advantageous. Chapter 6 formulated the case of circular equatorial geodesic motion in Kerr spacetime and introduced an iterative scheme needed to derive the jump conditions at the particle. The system of equations was then written as an algebraic set of equations with a source modified at each step of the iteration. Chapter 7 gives the results evolving our 1+1D Teukolsky equation both in vacuum and with a particle in Kerr explicitly. We explored the dependence of the numerical solution on the multipole cutoff and quantified the convergence. The iterative scheme proposed in Chapter 6 was tested for different spin values. As expected, the iteration converge faster

for smaller values of a. The analytical solution for static modes is successfully compared with the numerical solution. Some issue of numerical convergence is present and would have to be addressed for a higher precision computation.

The next necessary step in the development of the method is to address the problem for generic orbits in Kerr. A first step to such extension is to consider eccentric orbits. The major changes from the discussed circular orbit case would be in the computation of the jump condition. The set of equations (3.46) and (3.47) will now need to be solved as a set of ODEs. Nevertheless, the iteration procedure proposed would not significantly change. For highly eccentric orbits, a slower convergence as higher l-modes contribute more strongly is expected. In the Kerr case for generic orbits, this additional hurdle is not expected to present a major difficulty in practice.

Finally, the most inspiring extension of our method lies on self-consistent evolution. The numerical method must be cast in such a way that at each time step (or several-time steps) the trajectory of the particle is corrected by the SF computed from the metric reconstruction. The method is particularly well suited for such implementation as the field can be updated at each time-slice with new initial conditions matching the correct (updated) field values. The numerics involved will need to be efficiently implemented to make such evolution computationally appealing.

The method developed in this thesis is the only method thus far proposed capable of fully tackling the problem of time-domain calculations of metric perturbations from a point particle in Kerr spacetime. (The Lorenz-gauge approach of Dolan and Barack [66] is hampered by gauge-instability problems.) We are therefore looking forward for its further development.

Appendix A

Calculating the discontinuity in the Weyl scalar and its derivative

In Chapter 4 we described the derivation of the (IRG) Hertz potential for circular geodesic orbits around a Schwarzschild black hole. Equations (4.12) and (4.13) therein gave necessary jump conditions for the ℓ-mode Hertz potential across the particle's orbit in the $1+1$D domain. These jumps were expressed in terms of the jumps in the corresponding ℓ mode of the Weyl scalar Ψ_0 associated with the physical perturbation—more precisely, in terms of $[\psi_{s=2,\ell,m}]$ and $[\partial_v \psi_{s=2,\ell,m}]$. In this appendix we show how the latter jumps are derived directly from the source of the $s=2$ Teukolsky equation, and provide explicit expressions for them.

Let $\Psi_0 \equiv \Psi_{s=2}$ be the Weyl scalar associated with the physical metric perturbation sourced by the point particle. We expand it in $s=2$ spherical harmonics, as in Eq. (3.36):

$$\Psi_{s=2} = (r\Delta^2)^{-1} \sum_{\ell=2}^{\infty} \sum_{m=-\ell}^{\ell} \psi_{2\ell m}(t,r)\, {}_2Y_{\ell m}(\theta,\varphi). \tag{A.1}$$

Thus $\psi_{2\ell m} \equiv \psi^{+}_{2\ell m}$ for $r > r_0$ and $\psi_{2\ell m} \equiv \psi^{-}_{2\ell m}$ for $r < r_0$, where $\psi^{\pm}_{2\ell m}$ are the "homogeneous" ℓ-mode fields featured in Eq. (3.36). The field $\psi_{2\ell m}$ satisfies the $1+1$D $s=2$ inhomogeneous Teukolsky equation (here specialized to $a=0$ and $s=2$) with a suitable distributional source term T corresponding to the energy-momentum of our geodesic pointlike particle:

$$\psi_{,uv} + U_2(r)\psi_{,u} + V_2(r)\psi_{,v} + W_2(r)\psi = T, \tag{A.2}$$

where hereafter indices $s\ell m$ are dropped for brevity, and the potentials are

$$U_2(r) = -\frac{2M}{r^2}, \qquad V_2(r) = \frac{2f}{r}, \tag{A.3}$$

$$W_2(r) = \frac{f}{4}\left(\frac{(\ell+3)(\ell-2)}{r^2} + \frac{6M}{r^3}\right). \tag{A.4}$$

We now need the explicit form of the ℓ-mode source T, for the case of a point particle in a circular geodesic orbit. This can be worked out as explained (e.g.) in Sec. III.A of Ref. [34] (where T was derived for $s=-2$ and $m=0$), by using Eq. (A10) therein with the energy-momentum tensor (21) therein, and then decomposing into spin-2 spherical harmonics. We obtain the distributional form

$$\begin{aligned} T(t,r;r_0) = s_0(t,r_0)\delta(r-r_0) + s_1(t,r_0)\delta'(r-r_0) \\ +s_2(t,r_0)\delta''(r-r_0), \end{aligned} \tag{A.5}$$

where the coefficients are given by

$$s_n = \mu\gamma_0\pi\tilde{s}_n, \tag{A.6}$$

with

$$\begin{aligned} \tilde{s}_0 \;=\; & f_0 r_0\left[2(1-4y+10y^2) - 2i\tilde{m}\Omega r_0(1+3y) - \tilde{m}^2\right]\mathcal{Y}(t) \\ & -2f_0^2 r_0\left[i\Omega r_0(1+4y)+\tilde{m}\right]\mathcal{Y}_\theta(t) \\ & -f_0^3 r_0 \mathcal{Y}_{\theta\theta}(t), \end{aligned} \tag{A.7}$$

$$\begin{aligned} \tilde{s}_1 \;=\; & 2f_0^2 r_0\left[-2M(1+y) + i\tilde{m}\Omega r_0^2\right]\mathcal{Y}(t) \\ & +2if_0^3 r_0^3\Omega\mathcal{Y}_\theta(t), \end{aligned} \tag{A.8}$$

$$\tilde{s}_2 = M f_0^3 r_0^2 \mathcal{Y}(t). \tag{A.9}$$

We recall $y = M/r_0$ and $f_0 = 1-2M/r_0$, and we have further introduced here

$$\tilde{m} := m\gamma_0^{-2} = m(1-3M/r_0) \tag{A.10}$$

and

$$\mathcal{Y}(t) := {}_2\bar{Y}_{\ell m}\left(\frac{\pi}{2}, \Omega t\right), \tag{A.11}$$

with $\mathcal{Y}_\theta$ and $\mathcal{Y}_{\theta\theta}$ being, respectively, the first and second derivatives of ${}_2\bar{Y}_{\ell m}(\theta, \Omega t)$ with respect to θ, evaluated at $\theta = \pi/2$. We have taken $\varphi_{\rm p}(t) = \Omega t$, with Ω being the orbital angular velocity, and used $d\mathcal{Y}/dt = -im\Omega\mathcal{Y}$ and $d^2\mathcal{Y}/dt^2 = -m^2\Omega^2\mathcal{Y} = -m^2(M/r_0^3)\mathcal{Y}$.

Next, we substitute the *Ansatz*

$$\psi = \psi^+(t,r)\Theta(r-r_0) + \psi^-(t,r)\Theta(r_0-r) \tag{A.12}$$

$$+\psi_\delta(t,r_0)\delta(r-r_0), \tag{A.13}$$

where $\Theta(\cdot)$ is the standard Heaviside step function, into the field equation (A.2). We note all resulting terms that are proportional to $\Theta(r-r_0)$ or to $\Theta(r_0-r)$ vanish, by virtue of $\psi^\pm(t,r)$ being homogeneous solutions. The remaining terms are supported on $r = r_0$ only, and are each proportional to δ, δ' or δ''. We use the distributional identities

$$\begin{aligned}
F(r)\delta(r-r_0) &= F(r_0)\delta(r-r_0), \\
F(r)\delta'(r-r_0) &= F(r_0)\delta'(r-r_0) - F'(r_0)\delta(r-r_0), \\
F(r)\delta''(r-r_0) &= F(r_0)\delta''(r-r_0) - 2F'(r_0)\delta'(r-r_0) \\
&\quad + F''(r_0)\delta(r-r_0)
\end{aligned} \tag{A.14}$$

[valid for any smooth function $F(r)$] to reexpress the coefficients of δ, δ' and δ'' in terms of r_0 (and t) only, and then compare the values of these coefficients across both sides of Eq. (A.2), recalling the form of T in Eq. (A.5). From the coefficient of δ'' one immediately obtains

$$\psi_\delta(t,r_0) = -4f_0^{-2}s_2(t,r_0), \tag{A.15}$$

and subsequently comparing the coefficients of δ' and δ uniquely determines the jumps $[\psi] = \psi^+(r_0) - \psi^-(r_0)$ and $[\psi'] = (\psi^+)'(r_0) - (\psi^-)'(r_0)$. We obtain

$$[\psi] = 8\pi\mu\gamma_0 r_0^2\left[\left(y^2 - i\tilde{m}\Omega r_0\right)\mathcal{Y}(t) - if_0 r_0\Omega\mathcal{Y}_\theta(t)\right], \tag{A.16}$$

$$
\begin{aligned}
[\psi'] \;=\; & 4\pi\mu\gamma_0 r_0 \Big\{ \Big[2y^2 - 2 - y(\lambda-4) + \tilde{m}^2 f_0^{-1}(1+y^2\gamma_0^4) \\
& -2i\tilde{m} r_0 \Omega f_0^{-1}(3-7y) \Big] \mathcal{Y}(t) \\
& +2\left(-3i f_0 r_0 \Omega + \tilde{m}\right) \mathcal{Y}_\theta(t) + f_0 \mathcal{Y}_{\theta\theta}(t) \Big\} \,. \qquad \text{(A.17)}
\end{aligned}
$$

We recall $\lambda = (\ell+2)(\ell-1)$.

In summary, and restoring all suppressed indices, Eqs. (A.16) and (A.17) give the desired jumps $[\psi_{s=2,\ell,m}]$ and $\left[\psi'_{s=2,\ell,m}\right]$ in explicit form. The jump in the v derivative, needed as input for Eqs. (4.12) and (4.13), is obtained via

$$
\begin{aligned}
[\partial_v \psi] \;&=\; \frac{1}{2} f_0 \left[\psi'\right] + \frac{1}{2} \left[\partial_t \psi\right] \\
&=\; \frac{1}{2} f_0 \left[\psi'\right] - \frac{1}{2} i m \Omega \left[\psi\right] . \qquad \text{(A.18)}
\end{aligned}
$$

The above computation can be repeated in Kerr, with no substantial changes. The final expressions for the jumps in Kerr are not as compact as for the case $a = 0$ and are not of particular insight, so we avoid printing them explicitly.

Appendix B

Regularization paramenter B_α

For completeness we give here the values of the regularization paramenter. This can be expressed in a compact form as [44]

$$B_\alpha = \mu^2 (2\pi)^{-1} g_{\alpha\beta} P^{\beta}_{\ abcd} I^{abcd}, \tag{B.1}$$

where hereafter roman indices $(a, b, c, ...)$ run over the two Boyer–Lindquist angular coordinates θ, φ. The coefficients $P^{\alpha}_{\ abcd}$ are given by

$$\begin{aligned} P^{\alpha}_{\ abcd} &= \frac{1}{2}[P^{\alpha}_{\ d}(3P_{abc} + 2P_{ab}P_c) - P^{\alpha\lambda}(2P_{\lambda ab} + P_{ab\lambda})P_{cd}] \\ &\quad + (3P^{\alpha}_{\ a}P_{be} - P^{\alpha}_{\ e}P_{ab})C^{e}_{cd}, \end{aligned} \tag{B.2}$$

where

$$P_\alpha \equiv u^\lambda u^\rho g_{\lambda\rho,\alpha}, \qquad P_{\alpha\beta} \equiv g_{\alpha\beta} + u_\alpha u_\beta, \qquad P_{\alpha\beta\gamma} \equiv \Gamma^{\lambda}_{\alpha\beta} P_{\lambda\gamma}, \tag{B.3}$$

and

$$C^{\theta}_{\varphi\varphi} = \frac{1}{2}\sin\theta_0 \cos\theta_0, \qquad C^{\varphi}_{\theta\varphi} = C^{\varphi}_{\varphi\theta} = -\frac{1}{2}\cot\theta_0, \tag{B.4}$$

with all other coefficients $C^{\gamma}_{\alpha\beta}$ vanishing, and with $\Gamma^{\lambda}_{\alpha\beta}$ being the background connection coefficients at z. The quantities I^{abcd} are

$$I^{abcd} = (\sin\theta_0)^{-N} \int_0^{2\pi} G(\chi)^{-5/2} (\sin\chi)^N (\cos\chi)^{4-N}\, d\chi, \tag{B.5}$$

where

$$G(\chi) = P_{\theta\theta}\cos^2\chi + 2P_{\theta\varphi}\sin\chi\cos\chi/\sin\theta_p + P_{\varphi\varphi}\sin^2\chi/\sin^2\theta_p, \tag{B.6}$$

and $N \equiv N(abcd)$ is the number of times the index φ occurs in the combination (a, b, c, d), namely

$$N = \delta^a_\varphi + \delta^b_\varphi + \delta^c_\varphi + \delta^d_\varphi. \tag{B.7}$$

We may write I^{abcd} explicitly in terms of standard complete Elliptic integrals. Introducing the short-hand notation

$$\alpha \equiv \sin^2\theta_p\, P_{\theta\theta}/P_{\varphi\varphi} - 1, \qquad \beta \equiv 2\sin\theta_p\, P_{\theta\varphi}/P_{\varphi\varphi}, \tag{B.8}$$

we have

$$I^{abcd} = \frac{(\sin\theta_0)^{-N}}{d}[QI_K^{(N)}\hat{K}(w) + I_E^{(N)}\hat{E}(w)], \tag{B.9}$$

where

$$Q = \alpha + 2 - (\alpha^2+\beta^2)^{1/2}, \tag{B.10}$$

$$d = 3P_{\varphi\varphi}^{5/2}(\sin\theta_p)^{-5}(\alpha^2+\beta^2)^2(4\alpha+4-\beta^2)^{3/2}(Q/2)^{1/2}, \tag{B.11}$$

$\hat{K}(w) \equiv \int_0^{\pi/2}(1 - w\sin^2 x)^{-1/2}dx$ and $\hat{E}(w) \equiv \int_0^{\pi/2}(1 - w\sin^2 x)^{1/2}dx$ are complete Elliptic integrals of the 1st and 2nd kinds, respectively, and the argument is

$$w = \frac{2(\alpha^2+\beta^2)^{1/2}}{\alpha + 2 + (\alpha^2+\beta^2)^{1/2}}. \tag{B.12}$$

The ten coefficients $I_K^{(N)}, I_E^{(N)}$ in Eq. (B.9) are given by

$$\begin{aligned} I_K^{(0)} &= 4[12\alpha^3 + \alpha^2(8-3\beta^2) - 4\alpha\beta^2 + \beta^2(\beta^2-8)], \\ I_E^{(0)} &= -16[8\alpha^3 + \alpha^2(4-7\beta^2) + \alpha\beta^2(\beta^2-4) - \beta^2(\beta^2+4)], \end{aligned} \tag{B.13}$$

$$\begin{aligned} I_K^{(1)} &= 8\beta[9\alpha^2 - 2\alpha(\beta^2-4) + \beta^2], \\ I_E^{(1)} &= -4\beta[12\alpha^3 - \alpha^2(\beta^2-52) + \alpha(32-12\beta^2) + \beta^2(3\beta^2+4)], \end{aligned} \tag{B.14}$$

$$\begin{aligned} I_K^{(2)} &= -4[8\alpha^3 - \alpha^2(\beta^2-8) - 8\alpha\beta^2 + \beta^2(3\beta^2-8)], \\ I_E^{(2)} &= 8[4\alpha^4 + \alpha^3(\beta^2+12) - 2\alpha^2(\beta^2-4) \\ &\quad +3\alpha\beta^2(\beta^2-4) + 2\beta^2(3\beta^2-4)], \end{aligned} \tag{B.15}$$

$$
\begin{aligned}
I_K^{(3)} &= 8\beta[\alpha^3 - 7\alpha^2 + \alpha(3\beta^2 - 8) + \beta^2], \\
I_E^{(3)} &= -4\beta[8\alpha^4 - 4\alpha^3 + \alpha^2(15\beta^2 - 44) + 4\alpha(5\beta^2 - 8) \\
&\quad +\beta^2(3\beta^2 + 4)],
\end{aligned} \tag{B.16}
$$

$$
\begin{aligned}
I_K^{(4)} &= -4[4\alpha^4 - 4\alpha^3 + \alpha^2(7\beta^2 - 8) + 12\alpha\beta^2 - \beta^2(\beta^2 - 8)], \\
I_E^{(4)} &= 16[4\alpha^5 + 4\alpha^4 + \alpha^3(7\beta^2 - 4) + \alpha^2(11\beta^2 - 4) \\
&\quad +(2\alpha + 1)\beta^2(\beta^2 + 4)].
\end{aligned} \tag{B.17}
$$

Appendix C

Solving for $[\Psi]$ and $[\Psi_{,v}]$ for periodic orbits in Schwarzschild

When solving the set of equations (3.46) and (3.47) we want to keep the solution non-periodic to allow a self consistent evolution. For generic (bound) orbits, we can solve the equation for a periodic case and use the solution as initial condition, thus evolve the system numerically without imposing periodicity. An error in the initial conditions will be present but it will only negligibly affect the full evolution if enough orbits are computed.

Looking at the fourth order ODEs (3.46) and (3.47), it is possible to show that there is no periodic solution for the homogeneous case, and then find a specific periodic solution of the inhomogeneous case. Thus, this solution will be unique as the only one periodic. In this section we will explicitly find a periodic solution of the inhomogeneous equation imposing periodicity via Fourier decomposition.

If we specialize to the Schwarzschild case, we aim to solve a set of equations of the kind

$$\sum_{n=0}^{4} A^n(\tau)\frac{d^n}{d\tau^n}[\Psi](\tau) + \sum_{n=0}^{3} B^n(\tau)\frac{d^n}{d\tau^n}[\Psi_{,v}](\tau) = [\psi_0](\tau), \tag{C.1}$$

$$\sum_{n=0}^{4} \tilde{A}^n(\tau)\frac{d^n}{d\tau^n}[\Psi](\tau) + \sum_{n=0}^{3} \tilde{B}^n(\tau)\frac{d^n}{d\tau^n}[\Psi_{,v}](\tau) = [\psi_{0,v}](\tau). \tag{C.2}$$

Let's first look at the simple case of a single ODE with non-constant coefficients

$$\sum_{n=0}^{4} A^n(\tau)\frac{d^n}{d\tau^n}y(\tau) = f(\tau), \tag{C.3}$$

where for periodic orbits we will have both $f(\tau)$ and $A^n(\tau)$ to be periodic. When searching for periodic solutions of this equation we can decompose $y(\tau)$ in a Fourier series

$$y(\tau) = \sum_{q,p=0}^{\infty} y_{qp} e^{i\Omega_r p\tau} e^{i\Omega_\varphi q\tau}, \tag{C.4}$$

where Ω_r is the libration of epicyclic frequency of the orbit and Ω_φ the angular frequency. Lets impose periodicity also for the solution and the coefficients and decompose both with a Fourier series as

$$f(\tau) = \sum_{q,p=0}^{\infty} f_{qp} e^{i\Omega_r q\tau} e^{i\Omega_\varphi p\tau}, \qquad A^n(\tau) = \sum_{l,k=0}^{\infty} A^n_{lk} e^{i\Omega_r q\tau} e^{i\Omega_\varphi p\tau}. \tag{C.5}$$

Substituting we obtain

$$\begin{aligned}
&\sum_{q,p=0}^{\infty} f_{qp} e^{i\Omega_r q\tau} e^{i\Omega_\varphi p\tau} = \\
&= \sum_{l,k=0}^{\infty}\sum_{q,p=1}^{\infty}[\sum_{n=0}^{4} A^n_{lk} \sum \binom{n}{h} (i\Omega_r q)^{n-h} (i\Omega_\varphi p)^h y_{qp}] e^{i\Omega_r (q+l)\tau} e^{i\Omega_\varphi (p+k)\tau} \\
&+ \sum_{l,k=0}^{\infty} A^0_{lk} y_{00} e^{i\Omega_r l\tau} e^{i\Omega_\varphi k\tau} + \sum_{l,k=0}^{\infty}\sum_{n=0}^{4} A^n_{lk}\left[(i\Omega_\varphi)^n y_{10} e^{i\Omega_r l\tau} e^{i\Omega_\varphi (k+1)\tau} + (i\Omega_r)^n y_{01} e^{i\Omega_r (l+1)\tau} e^{i\Omega_\varphi k\tau}\right].
\end{aligned} \tag{C.6}$$

Equating coefficients, we obtain an equation for each coefficient y_{qp}. For instance, we find for the $(0,0)$-coefficient of $y(\tau)$ expansion

$$y_{00} A^0_{00} = f_{00} \qquad \rightarrow \quad y_{00} = f_{00}/A^0_{00} \quad for \quad A^0_{00} \neq 0. \tag{C.7}$$

Similarly we derive for the $(1,0)$-coefficient, by substituting (C.7), that

$$A^0_{10} y_{00} + \sum_{n=0}^{4} y_{10} A^n_{00} (i\Omega_\varphi)^n = f_{10} \quad \rightarrow \quad y_{10} = \frac{f_{10} + f_{00} A^0_{10}/A^0_{00}}{\sum_{n=0}^{4} A^n_{00}(i\Omega_\varphi)^n}, \tag{C.8}$$

when $\left[\sum_{n=0}^{4} A^n_{00}(i\Omega_\varphi)^n\right] \neq 0$. This procedure can be iterated to find the (n,m)-th coefficient for the expantion of $y(\tau)$.

The equations for the Hertz jumps (C.1) and (C.2) are a set of coupled equations of the same kind we just solved above. Extending this method to the full system is straightforward. We expand the fields ψ_0 and Ψ as in (C.4) and equate the coefficients. For instance, the first coefficient is derived from

$$A^0_{00}[\Psi]_{00} + B^0_{00}[\Psi_{,v}]_{00} = [\psi_0]_{00}, \tag{C.9}$$

$$\tilde{A}^0_{00}[\Psi]_{00} + \tilde{B}^0_{00}[\Psi_{,v}]_{00} = [\psi_{0,v}]_{00}, \tag{C.10}$$

that gives

$$[\Psi]_{00} = (\frac{[\psi_0]_{00}}{B^0_{00}} - \frac{[\psi_{0,v}]_{00}}{\tilde{B}^0_{00}})(\frac{A^0_{00}}{B^0_{00}} - \frac{\tilde{A}^0_{00}}{\tilde{B}^0_{00}})^{-1}, \tag{C.11}$$

$$[\Psi_{,v}]_{00} = (\frac{[\psi_0]_{00}}{A^0_{00}} - \frac{[\psi_{0,v}]_{00}}{\tilde{A}^0_{00}})(\frac{B^0_{00}}{A^0_{00}} - \frac{\tilde{B}^0_{00}}{\tilde{A}^0_{00}})^{-1}. \tag{C.12}$$

Similar equations hold for higher coefficients of the expansion.

This method can be extended to the Kerr case, where we would impose a 3-frequency expansion for the fields and the sources. In order to write the system of equations as in (C.1) and (C.2), the source must be modified accordingly to our iteration procedure described in Sec. 6.1.

Bibliography

[1] B. P. Abbott et al. Observation of Gravitational Waves from a Binary Black Hole Merger. *Phys. Rev. Lett.*, 116(6):061102, 2016.

[2] B. P. Abbott et al. GW151226: Observation of Gravitational Waves from a 22-Solar-Mass Binary Black Hole Coalescence. *Phys. Rev. Lett.*, 116(24):241103, 2016.

[3] Benjamin P. Abbott et al. GW170104: Observation of a 50-Solar-Mass Binary Black Hole Coalescence at Redshift 0.2. *Phys. Rev. Lett.*, 118(22):221101, 2017.

[4] Benjamin P. Abbott et al. GW170817: Observation of Gravitational Waves from a Binary Neutron Star Inspiral. *Phys. Rev. Lett.*, 119(16):161101, 2017.

[5] Clifford M. Will. The Confrontation between general relativity and experiment. *Living Rev. Rel.*, 9:3, 2006.

[6] Curt Cutler and Eanna E. Flanagan. Gravitational waves from merging compact binaries: How accurately can one extract the binary's parameters from the inspiral wave form? *Phys. Rev.*, D49:2658–2697, 1994.

[7] Eanna E. Flanagan and Scott A. Hughes. Measuring gravitational waves from binary black hole coalescences: 1. Signal-to-noise for inspiral, merger, and ringdown. *Phys. Rev.*, D57:4535–4565, 1998.

[8] LISA mission website: http://lisa.nasa.gov/.

[9] Drew Keppel and P. Ajith. Constraining the mass of the graviton using coalescing black-hole binaries. *Phys. Rev.*, D82:122001, 2010.

[10] Scott A. Hughes and Kristen Menou. Golden binaries for LISA: Robust probes of strong-field gravity. *Astrophys. J.*, 623:689–699, 2005.

[11] Leor Barack and Curt Cutler. LISA capture sources: Approximate waveforms, signal-to-noise ratios, and parameter estimation accuracy. *Phys. Rev.*, D69:082005, 2004.

[12] S Chandrasekhar. *The mathematical theory of black holes*. Oxford classic texts in the physical sciences. Oxford Univ. Press, Oxford, 2002.

[13] Frans Pretorius. Evolution of binary black hole spacetimes. *Phys. Rev. Lett.*, 95:121101, 2005.

[14] Mark Hannam. Status of black-hole-binary simulations for gravitational-wave detection. *Class. Quant. Grav.*, 26:114001, 2009.

[15] Luis Lehner and Frans Pretorius. Numerical Relativity and Astrophysics. *Ann. Rev. Astron. Astrophys.*, 52:661–694, 2014.

[16] Alessandra Buonanno, Gregory B. Cook, and Frans Pretorius. Inspiral, merger and ring-down of equal-mass black-hole binaries. *Phys. Rev.*, D75:124018, 2007.

[17] Jose A. Gonzalez, Ulrich Sperhake, and Bernd Bruegmann. Black-hole binary simulations: The Mass ratio 10:1. *Phys. Rev.*, D79:124006, 2009.

[18] J. Droste. The field of a single centre in Einstein's theory of gravitation, and the motion of a particle in that field. *Koninklijke Nederlandse Akademie van Wetenschappen Proceedings Series B Physical Sciences*, 19,:197–215, 1917,.

[19] Luc Blanchet. Gravitational radiation from post-Newtonian sources and inspiralling compact binaries. *Living Rev. Rel.*, 9:4, 2006.

[20] Luc Blanchet. Gravitational Radiation from Post-Newtonian Sources and Inspiralling Compact Binaries. *Living Rev. Rel.*, 17:2, 2014.

[21] Samuel E. Gralla and Robert M. Wald. A Rigorous Derivation of Gravitational Self-force. *Class. Quant. Grav.*, 25:205009, 2008. [Erratum: Class. Quant. Grav.28,159501(2011)].

[22] Samuel E. Gralla. Second Order Gravitational Self Force. *Phys. Rev.*, D85:124011, 2012.

[23] Eric Poisson, Adam Pound, and Ian Vega. The Motion of point particles in curved spacetime. *Living Rev. Rel.*, 14:7, 2011.

[24] Steven Detweiler. Gravitational radiation reaction and second order perturbation theory. *Phys. Rev.*, D85:044048, 2012.

[25] Adam Pound. Second-order gravitational self-force. *Phys. Rev. Lett.*, 109:051101, 2012.

[26] Theodore C. Quinn and Robert M. Wald. An Axiomatic approach to electromagnetic and gravitational radiation reaction of particles in curved space-time. *Phys. Rev.*, D56:3381–3394, 1997.

[27] Yasushi Mino, Misao Sasaki, and Takahiro Tanaka. Gravitational radiation reaction to a particle motion. *Phys. Rev.*, D55:3457–3476, 1997.

[28] Paul A. M. Dirac. Classical theory of radiating electrons. *Proc. Roy. Soc. Lond.*, A167:148–169, 1938.

[29] Bryce S. DeWitt and Robert W. Brehme. Radiation damping in a gravitational field. *Annals Phys.*, 9:220–259, 1960.

[30] Steven L. Detweiler and Bernard F. Whiting. Selfforce via a Green's function decomposition. *Phys. Rev.*, D67:024025, 2003.

[31] Leor Barack and Amos Ori. Mode sum regularization approach for the selfforce in black hole space-time. *Phys. Rev.*, D61:061502, 2000.

[32] Leor Barack, Darren A. Golbourn, and Norichika Sago. m-Mode Regularization Scheme for the Self Force in Kerr Spacetime. *Phys. Rev.*, D76:124036, 2007.

[33] Ian Vega and Steven L. Detweiler. Regularization of fields for self-force problems in curved spacetime: Foundations and a time-domain application. *Phys. Rev.*, D77:084008, 2008.

[34] Cesar Merlin, Amos Ori, Leor Barack, Adam Pound, and Maarten van de Meent. Completion of metric reconstruction for a particle orbiting a Kerr black hole. *Phys. Rev.*, D94(10):104066, 2016.

[35] Anna Heffernan, Adrian Ottewill, and Barry Wardell. High-order expansions of the Detweiler-Whiting singular field in Kerr spacetime. *Phys. Rev.*, D89(2):024030, 2014.

[36] Anna Heffernan, Adrian Ottewill, and Barry Wardell. High-order expansions of the Detweiler-Whiting singular field in Schwarzschild spacetime. *Phys. Rev.*, D86:104023, 2012.

[37] Leor Barack and Norichika Sago. Gravitational self-force correction to the innermost stable circular orbit of a Schwarzschild black hole. *Phys. Rev. Lett.*, 102:191101, 2009.

[38] Leor Barack and Norichika Sago. Gravitational self-force on a particle in eccentric orbit around a Schwarzschild black hole. *Phys. Rev.*, D81:084021, 2010.

[39] Maarten van de Meent. Gravitational self-force on generic bound geodesics in Kerr spacetime. 2017.

[40] Maarten van de Meent and Abhay G. Shah. Metric perturbations produced by eccentric equatorial orbits around a Kerr black hole. *Phys. Rev.*, D92(6):064025, 2015.

[41] Maarten van de Meent. Gravitational self-force on eccentric equatorial orbits around a Kerr black hole. *Phys. Rev.*, D94(4):044034, 2016.

[42] Leor Barack and Darren A. Golbourn. Scalar-field perturbations from a particle orbiting a black hole using numerical evolution in 2+1 dimensions. *Phys. Rev.*, D76:044020, 2007.

[43] Barry Wardell and Niels Warburton. Applying the effective-source approach to frequency-domain self-force calculations: Lorenz-gauge gravitational perturbations. *Phys. Rev.*, D92(8):084019, 2015.

[44] Leor Barack. Gravitational self force in extreme mass-ratio inspirals. *Class. Quant. Grav.*, 26:213001, 2009.

[45] Barry Wardell and Achamveedu Gopakumar. Self-force: Computational Strategies. *Fund. Theor. Phys.*, 179:487–522, 2015.

[46] Adam Pound and Jeremy Miller. Practical, covariant puncture for second-order self-force calculations. *Phys. Rev.*, D89(10):104020, 2014.

[47] Adam Pound. Conservative effect of the second-order gravitational self-force on quasicircular orbits in Schwarzschild spacetime. *Phys. Rev.*, D90(8):084039, 2014.

[48] Adam Pound. Second-order perturbation theory: problems on large scales. *Phys. Rev.*, D92(10):104047, 2015.

[49] Jeremy Miller, Barry Wardell, and Adam Pound. Second-order perturbation theory: the problem of infinite mode coupling. *Phys. Rev.*, D94(10):104018, 2016.

[50] Leor Barack and Carlos O. Lousto. Perturbations of Schwarzschild black holes in the Lorenz gauge: Formulation and numerical implementation. *Phys. Rev.*, D72:104026, 2005.

[51] Leor Barack and Norichika Sago. Gravitational self force on a particle in circular orbit around a Schwarzschild black hole. *Phys. Rev.*, D75:064021, 2007.

[52] Sam R. Dolan and Leor Barack. Self force via m-mode regularization and 2+1D evolution: Foundations and a scalar-field implementation on Schwarzschild. *Phys. Rev.*, D83:024019, 2011.

[53] Tullio Regge and John A. Wheeler. Stability of a Schwarzschild singularity. *Phys. Rev.*, 108:1063–1069, 1957.

[54] Leor Barack and Carlos O. Lousto. Computing the gravitational selfforce on a compact object plunging into a Schwarzschild black hole. *Phys. Rev.*, D66:061502, 2002.

[55] Steven L. Detweiler. A Consequence of the gravitational self-force for circular orbits of the Schwarzschild geometry. *Phys. Rev.*, D77:124026, 2008.

[56] Seth Hopper, Erik Forseth, Thomas Osburn, and Charles R. Evans. Fast spectral source integration in black hole perturbation calculations. *Phys. Rev.*, D92:044048, 2015.

[57] Leor Barack and Amos Ori. Gravitational selfforce and gauge transformations. *Phys. Rev.*, D64:124003, 2001.

[58] Samuel E. Gralla. Gauge and Averaging in Gravitational Self-force. *Phys. Rev.*, D84:084050, 2011.

[59] Tobias S. Keidl, Abhay G. Shah, John L. Friedman, Dong-Hoon Kim, and Larry R. Price. Gravitational Self-force in a Radiation Gauge. *Phys. Rev.*, D82(12):124012, 2010. [Erratum: Phys. Rev.D90,no.10,109902(2014)].

[60] Abhay G. Shah, Tobias S. Keidl, John L. Friedman, Dong-Hoon Kim, and Larry R. Price. Conservative, gravitational self-force for a particle in circular orbit around a Schwarzschild black hole in a Radiation Gauge. *Phys. Rev.*, D83:064018, 2011.

[61] Tobias S. Keidl, John L. Friedman, and Alan G. Wiseman. On finding fields and self-force in a gauge appropriate to separable wave equations. *Phys. Rev.*, D75:124009, 2007.

[62] Adam Pound, Cesar Merlin, and Leor Barack. Gravitational self-force from radiation-gauge metric perturbations. *Phys. Rev.*, D89(2):024009, 2014.

[63] Sarp Akcay. A Fast Frequency-Domain Algorithm for Gravitational Self-Force: I. Circular Orbits in Schwarzschild Spacetime. *Phys. Rev.*, D83:124026, 2011.

[64] Thomas Osburn, Erik Forseth, Charles R. Evans, and Seth Hopper. Lorenz gauge gravitational self-force calculations of eccentric binaries using a frequency domain procedure. *Phys. Rev.*, D90(10):104031, 2014.

[65] Sarp Akcay, Niels Warburton, and Leor Barack. Frequency-domain algorithm for the Lorenz-gauge gravitational self-force. *Phys. Rev.*, D88(10):104009, 2013.

[66] Sam R. Dolan and Leor Barack. Self-force via m-mode regularization and 2+1D evolution: III. Gravitational field on Schwarzschild spacetime. *Phys. Rev.*, D87:084066, 2013.

[67] Leor Barack and Paco Giudice. Time-domain metric reconstruction for self-force applications. *Phys. Rev.*, D95(10):104033, 2017.

[68] Cesar Merlin and Abhay G. Shah. Self-force from reconstructed metric perturbations: numerical implementation in Schwarzschild spacetime. *Phys. Rev.*, D91(2):024005, 2015.

[69] Ramon Lopez-Aleman, Gaurav Khanna, and Jorge Pullin. Perturbative evolution of particle orbits around Kerr black holes: Time domain calculation. *Class. Quant. Grav.*, 20:3259–3268, 2003.

[70] Lior M. Burko and Gaurav Khanna. Mode coupling mechanism for late-time Kerr tails. *Phys. Rev.*, D89(4):044037, 2014.

[71] Lior M. Burko, Gaurav Khanna, and Anil Zenginoglu. Cauchy-horizon singularity inside perturbed Kerr black holes. *Phys. Rev.*, D93(4):041501, 2016.

[72] Andrea Taracchini, Alessandra Buonanno, Gaurav Khanna, and Scott A. Hughes. Small mass plunging into a Kerr black hole: Anatomy of the inspiral-merger-ringdown waveforms. *Phys. Rev.*, D90(8):084025, 2014.

[73] Sam R. Dolan. Superradiant instabilities of rotating black holes in the time domain. *Phys. Rev.*, D87(12):124026, 2013.

[74] Eric Poisson. The Motion of point particles in curved space-time. *Living Rev. Rel.*, 7:6, 2004.

[75] Norichika Sago, Leor Barack, and Steven L. Detweiler. Two approaches for the gravitational self force in black hole spacetime: Comparison of numerical results. *Phys. Rev.*, D78:124024, 2008.

[76] Samuel E. Gralla and Robert M. Wald. A Note on the Coordinate Freedom in Describing the Motion of Particles in General Relativity. *Class. Quant. Grav.*, 28:177001, 2011.

[77] Ezra Newman and Roger Penrose. An Approach to gravitational radiation by a method of spin coefficients. *J. Math. Phys.*, 3:566–578, 1962.

[78] Saul A. Teukolsky. Perturbations of a rotating black hole. 1. Fundamental equations for gravitational electromagnetic and neutrino field perturbations. *Astrophys. J.*, 185:635–647, 1973.

[79] P. L. Chrzanowski. Vector Potential and Metric Perturbations of a Rotating Black Hole. *Phys. Rev.*, D11:2042–2062, 1975.

[80] L. S. Kegeles and J. M. Cohen. CONSTRUCTIVE PROCEDURE FOR PERTURBATIONS OF SPACE-TIMES. *Phys. Rev.*, D19:1641–1664, 1979.

[81] R. M. Wald. Construction of solutions of gravitational, electromagnetic, or other perturbation equations from solutions of decoupled equations. *Physical Review Letters*, 41:203–206, July 1978.

[82] John M. Stewart. Hertz-Bromwich-Debye-Whittaker-Penrose Potentials in General Relativity. *Proc. Roy. Soc. Lond.*, A367:527–538, 1979.

[83] Carlos O. Lousto and Bernard F. Whiting. Reconstruction of black hole metric perturbations from Weyl curvature. *Phys. Rev.*, D66:024026, 2002.

[84] Robert M. Wald. On perturbations of a kerr black hole. *Journal of Mathematical Physics*, 14(10):1453, 1973.

[85] Robert M. Wald. Construction of Solutions of Gravitational, Electromagnetic, Or Other Perturbation Equations from Solutions of Decoupled Equations. *Phys. Rev. Lett.*, 41:203–206, 1978.

[86] Robert M Wald. On perturbations of a kerr black hole. *Journal of Mathematical Physics*, 14(10):1453–1461, 1973.

[87] B. F. Whiting and L. R. Price. Metric reconstruction from Weyl scalars. *Class. Quant. Grav.*, 22:S589–S604, 2005.

[88] Larry R. Price, Karthik Shankar, and Bernard F. Whiting. On the existence of radiation gauges in Petrov type II spacetimes. *Class. Quant. Grav.*, 24:2367–2388, 2007.

[89] Amos Ori. Reconstruction of inhomogeneous metric perturbations and electromagnetic four potential in Kerr space-time. *Phys. Rev.*, D67:124010, 2003.

[90] Maarten van de Meent. The mass and angular momentum of reconstructed metric perturbations. 2017.

[91] Cesar Merlin, Amos Ori, Leor Barack, Adam Pound, and Maarten van de Meent. Completion of metric reconstruction for a particle orbiting a Kerr black hole. 2016.

[92] Abhay G. Shah and Adam Pound. Linear-in-mass-ratio contribution to spin precession and tidal invariants in Schwarzschild spacetime at very high post-Newtonian order. *Phys. Rev.*, D91(12):124022, 2015.

[93] Maarten van de Meent. Self-force corrections to the periapsis advance around a spinning black hole. *Phys. Rev. Lett.*, 118(1):011101, 2017.

[94] Leor Barack and Amos Ori. Gravitational selfforce on a particle orbiting a Kerr black hole. *Phys. Rev. Lett.*, 90:111101, 2003.

[95] J. N. Goldberg, A. J. Macfarlane, E. T. Newman, F. Rohrlich, and E. C. G. Sudarshan. Spin-s Spherical Harmonics and ð. *Journal of Mathematical Physics*, 8:2155–2161, November 1967.

[96] S. A. Teukolsky. Rotating black holes - separable wave equations for gravitational and electromagnetic perturbations. *Phys. Rev. Lett.*, 29:1114–1118, 1972.

[97] Leor Barack. Late time decay of scalar, electromagnetic, and gravitational perturbations outside rotating black holes. *Phys. Rev.*, D61:024026, 2000.

[98] Samuel E. Gralla, Scott A. Hughes, and Niels Warburton. Inspiral into Gargantua. *Class. Quant. Grav.*, 33(15):155002, 2016.

[99] Leor Barack and Amos Ori. Late time decay of gravitational and electromagnetic perturbations along the event horizon. *Phys. Rev.*, D60:124005, 1999.

[100] Marta Colleoni, Leor Barack, Abhay G. Shah, and Maarten van de Meent. Self-force as a cosmic censor in the Kerr overspinning problem. *Phys. Rev.*, D92(8):084044, 2015.

[101] Scott A. Hughes. The Evolution of circular, nonequatorial orbits of Kerr black holes due to gravitational wave emission. *Phys. Rev.*, D61(8):084004, 2000. [Erratum: Phys. Rev.D90,no.10,109904(2014)].

[102] Carlos O. Lousto and Richard H. Price. Understanding initial data for black hole collisions. *Phys. Rev.*, D56:6439–6457, 1997.

[103] Carlos O. Lousto. A time-domain fourth-order-convergent numerical algorithm to integrate black hole perturbations in the extreme-mass-ratio limit. *Class. Quant. Grav.*, 22:S543–S568, 2005.

[104] Frequency domain data kindly provided by Dr. van de Meent.

[105] Roland Haas. Time domain calculation of the electromagnetic self-force on eccentric geodesics in Schwarzschild spacetime. 2011.

[106] Frans Pretorius and Werner Israel. Quasispherical light cones of the Kerr geometry. *Class. Quant. Grav.*, 15:2289–2301, 1998.